LASER BRAIN SURGERY WITH NEAR INFRARED LASERS: INVESTIGATION OF THE OPTIMAL PARAMETERS BY REAL-TIME TEMPERATURE MONITORING

by

Burcu Tunç Çamlıbel

B.S, in Physics, Boğaziçi University, 2006

M.S, in Biomedical Engineering, Boğaziçi University, 2009

Submitted to the Institute of Biomedical Engineering

in partial fulfillment of the requirements

for the degree of

Doctor

of

Philosophy

Boğaziçi University

2016

To my beloved ones; my little brother, my grandmother and my mother-in-law. I am sure that they would have been very happy to see my graduation. They will be missed forever.

ACKNOWLEDGMENTS

I would like to offer my sincerest gratitude to my thesis advisor, Prof. Dr. Murat Gülsoy for his continuous support and guidance. It was great to work with you, you always inspired me in every aspect of my life. I am grateful to Prof. Dr. Ata Akın for his valuable insights, contributions and suggestions as a member of my thesis committee. I would like to thank Assoc. Prof. Dr. Burak Güçlü as well as his encouragement and his existence in my thesis committee. I would like to thank Prof. Dr. İnci Çilesiz, I feel very lucky to meet such a woman in academy, who will inspire me in my whole academic life. And finally Assoc. Prof. Dr. Mehmet Burçin Ünlü, your encouragement since we met, never ended, never fall away, thank you. I would also like to thank Assist. Prof. Dr. Esin Öztürk Işık for her valuable comments.

I need to open another parenthesis for my friends, but first I have to start with my university. I am very proud of being a part of such a great institution. This university gave me the chance to meet lots of inspiring people and to work with very enthusiastic team. I would like to thank my friends, without them this overwhelming PhD period cannot be such a joyful experience. We had great times, I am sure that I am going to miss those years. I want to start with my friends from Medical Lasers Laboratory; Ercan, Hakan, Heba, Melike, Meral, Mustafa Kemal and Özgür, thank you for being part of this period, your friendship and partnership was very valuable for me. I was really lucky that I had a chance to work such an amazing group. And my dear friends from Biomedical Engineering Institute; Ahu, Engin, Esin, Fatma, Murat and Neslihan, I am very thankful to every single one of you. And Finally Bora, Cemile, Didar, Gamze and Nermin; your friendship is priceless, you were always with me in every struggle of my life.

Ayfer, Uğur, and Onur, my lovely family. I cannot imagine a life without your support. And finally my love, my family, Kazım, thank you for your endless support, and love.

ACADEMIC ETHICS AND INTEGRITY STATEMENT

I, Burcu Tunç Çamlıbel, hereby certify that I am aware of the Academic Ethics and Integrity Policy issued by the Council of Higher Education (YÖK) and I fully acknowledge all the consequences due to its violation by plagiarism or any other way.

Name :

Signature:

Date:

ABSTRACT

LASER BRAIN SURGERY WITH NEAR INFRARED LASERS: INVESTIGATION OF THE OPTIMAL PARAMETERS BY REAL-TIME TEMPERATURE MONITORING

The thermal damage of the surrounding tissue can be an unwanted result of continuous-wave laser irradiation. In order to propose an effective way alternative to conventional surgical techniques, photothermal damage must be taken under control by a detailed dose study. Real-time temperature monitoring can be also an effective way to get rid of these side effects. The aim of this study was to overcome the side effects of photothermal interactions with a better establishment of experiments for investigating the photothermal effects of lasers and to specify optimal laser parameters in order to propose lasers in clinical use. In the present study, ablation/vaporization capability of three different infrared lasers operating at 980-nm, 1070-nm and 1940-nm were investigated through comparative experiments. All studies were performed *ex vivo* followed by *in vivo* with real-time temperature monitoring and male Wistar rats were used as an animal model. Animals were sacrificed immediately after the stereotaxic surgery for histological examinations. Sections were stained with Cresyl Fast Violet in order to measure the thermally altered areas.

The relation between laser parameters, temperature changes and ablation efficiency were determined. The correlations between rate of temperature change and ablation efficiency were calculated. In conclusion, this comparative study showed that the change in temperature in the tissue during laser irradiation, even though the laser source is different in terms of wavelength, can be a good indicator for the characteristics of lesion created by the laser.

Keywords: Laser, Brain Surgery, Temperature Monitoring, Thermal Effects, Ablation, Coagulation, Ablation Efficiency, Reversible and Irreversible Damage.

ÖZET

YAKIN KIZILALTI LASERLERLE BEYİN CERRAHİSİ: GERÇEK ZAMANLI SICAKLIK MONİTORİZASYONU İLE OPTİMAL PARAMETRELERİN BELİRLENMESİ

Sürekli-dalga laser uygulamaları çevre dokularda istenmeyen ısıl hasara neden olabilmektedir. Laser uygulamalarının konvansiyonel cerrahi tekniklere alternatif olabilmesi için bu ısıl hasarların detaylı bir doz çalışması ile kontrol altına alınabilmesi gerekir. Isıl hasarları düşük bir seviyeye indirgemede gerçek zamanlı sıcaklık monitorizasyonu da etkin bir yol olabilir. Bu çalışmanın amacı, fototermal etkileşimin istenmeyen etkilerinin daha iyi bir deney düzeneğiyle üstesinden gelmek ve laserlerin klinik uygulamlarda kullanılabilmesi için optimal laser parametrelerini belirlemektir. Çalışmada, 980-nm, 1070-nm ve 1940-nm olmak üzere, üç farklı kızılaltı laser karşılaştırmalı deneylerle incelenmiştir. *ex vivo* çalışmaların ardından *in vivo* çalışmalar yapılmıştır. Bütün deneylerde dokudaki sıcaklığın gerçek zamanlı olarak ölçümü yapılmıştır. Deneylerde hayvan modeli olarak erkek Wistar sıçanları kullanılmıştır. Stereotaktik cerrahileri takiben hayvanlar sakrifiye edilmiş ve histolojik incelemeler için hazırlanmıştır. Hayvanlardan alınan dokular Cresyl Fast Violet ile boyanarak ısıl değişim gösteren bölgeler ölçülmüştür.

Uygulanan laser parametreleri ile ablasyon verimlilikleri ve sıcaklık değişimleri arasındaki ilişki incelenmiştir. Sıcaklık değişim hızı ile ablasyon verimlilikleri arasındaki korelasyonlar hesaplanmıştır. Sonuç olarak bu çalışma sıcaklık monitorizasyonunun dalgaboyundan bağımsız olarak oluşan lezyonların özellikleri yönünden önemli bir gösterge olduğunu ortaya koymuştur.

Anahtar Sözcükler: Laser, Beyin Cerrahisi, Sıcaklık Monitorizasyonu, Isıl Etkiler, Ablasyon, Koagülasyon, Ablasyon Verimliliği, Tersinebilir ve Tersinemez Hasarlar.

TABLE OF CONTENTS

LIST OF FIGURES

LIST OF TABLES

LIST OF SYMBOLS

g	Anisotropy factor
I	Intensity
I_0	Initial intensity
l	Distance
N_a	Concentration of the absorbent molecule
r	Pearson's correlation coefficient
t	Time
T	Temperature
μ_a	Absorption coefficient
μ_s	Scattering coefficient
ρ	Spearman's rank correlation coefficient
σ_a	Interaction cross section

LIST OF ABBREVIATIONS

AA	Ablated Area
AD	Ablation Diameter
AE	Ablation Efficiency
ANOVA	Analysis of Variance
CA	Coagulated Area
CD	Coagulation Diameter
CFV	Cresyl Fast Violet
CW	Continuous Wave
c-m	continuous mode
DNA	Deoxyribonucleic Acid
EA	Edematous Area
Er:YAG	Erbium-doped Yttrium Aluminium Garnet
IR	Infrared
KTP	Potassium Titanyl Phosphate
LITT	Laser Induced Interstitial Therapy
NA	Numerical Aperture
NEA	Normalized Edematous Area
Nd:YAG	Neodymium-doped Yttrium Aluminium Garnet
NIR	Near Infrared
PB	Phosphate Buffer
p-m-m	pulsed modulated mode
RNA	Ribonucleic Acid
Tm:fiber	Thulium Fiber
Tm:YAP	Thulium Yttrium Aluminium Perovskite
UV	Ultraviolet
YLF	Yttrium Lithium Fluoride

1. INTRODUCTION

1.1 Motivation

The motivation for the work that is described in this dissertation originated from the lecture “Laser-tissue interactions", in which we discussed the mechanisms behind these interactions in detail. Direct electric current and radiofrequency energies have been used for neurosurgery as ablators and coagulators for decades [1–3]. Besides those conventional techniques, different types of lasers, which are high intensity light sources and capable of penetrating tissue have been under investigation since the first lasers became available. The promise of coagulation (irreversible thermal damage), and ablation (thermally removed tissue) with or without mechanical contact still attracts researchers and clinicians for laser studies [4]. Optical transmission of energy with fibers allows minimally invasive surgery for the near infrared wavelengths and this advantage is the main motivation of laser studies. In neurosurgery, laser ablation can be used for removing tumors or certain parts of the brain tissue for the treatment of epilepsy or Parkinson’s disease [5]. However, the probable photothermal damage given to surrounding healthy tissue is the bottleneck of surgical lasers. Thermal damage is unavoidable but can be minimized by selecting the right laser wavelength and by estimating the safe dose parameters [4]. Resulting damage may be sensitive to laser dose and estimating the proper laser parameters is crucial before taking the system to the clinic.

In order to propose an effective alternative to conventional surgical techniques, photothermal damage must be taken under control by a detailed dose study. Laser power, energy delivered to target tissue, spot size, power density, exposure time, mode of operation can be tested and resulting effect can be defined in terms of the amount of ablation, coagulation, and carbonization. Real-time temperature measurements can also be very helpful for describing the photothermal effect and also for controlling the laser parameters. In the present study a laser-thermoprobe was designed in order to measure the near-by temperature during laser application.

The underlying motivation for the research described in the subsequent chapters is that with a comprehensive comparison of ablation capabilities of infrared lasers operating with different wavelengths and temperature monitoring of the tissue during lasing, it may be possible to specify optimal laser parameters for laser brain surgery.

1.2 Objectives

The main goal of the present study is to investigate the potential of a new laser-thermoprobe, which consists of a laser and a real-time thermocouple measurement system for brain surgery. Specifically, different parameters (laser power, energy density, exposure time, continuous-mode or pulsed-modulated-mode) were tested and the ablation efficiency (the amount of removed tissue with respect to the total photothermal damage) was investigated with reference to the real-time temperature measurements of nearby tissue in an *ex vivo* and *in vivo* study. Relationship between rate of temperature change over time and the thermal effects of the laser application was investigated.

Other than that; the research comprises the following specific aims:

- to investigate the thermal effects of laser brain ablation of infrared 980-nm, 1070-nm and 1940-nm lasers on viability of different sections of brain *in vivo*.
- to find out optimum parameters of laser brain ablation for least thermal damage to the surrounding healthy tissue for lasers operating at 1940-nm, 980-nm and 1070-nm.
- to compare the thermal effects of 1940-nm Tm:fiber, 980-nm diode lasers and 1070-nm fiber laser on the brain tissue.
- to analyze laser irradiated tissue thermographically and histologically to correlate thermal events and tissue damage to laser irradiation parameters.

1.3 Overview

Following this introduction, this manuscript includes five chapters.

In Chapter 2, a detailed historic background of use of lasers in medicine with literature review of laser brain ablation with different laser types is given. The laser mechanism and the characteristics of lasers, which were used in this study, are explained.

In Chapter 3; Materials and Methods; *ex vivo* and *in vivo* experiments are described in detail. Preparation of brain samples and animals, laser delivery, temperature measurement, histology (Cresyl Fast Violet (CFV), Hematoxylin and Eosin (H&E) staining, tissue sectioning) and the way data are quantified and analyzed are explained.

In Chapter 4, results for *ex vivo* and *in vivo* studies are represented. Ablation efficiencies and rate of temperature increased of three different lasers are compared. Results are discussed in macroscopic and microscopic scales accordingly.

In Chapter 5, overall study is evaluated. The summary of the study is given comprehensively.

2. BACKGROUND

Over 40 years, lasers have been widely studied and are being used in local hospitals and specialized clinical centers for many surgical applications. Laser is an acronym of Light Amplification by Stimulated Emission of Radiation. Laser light is produced by stimulated emission and optical feedback mechanisms. It consists of a laser medium, excitation source for pumping energy and mirrors as a resonator. The laser medium can be solid, liquid or gas. The excitation source can be electrical discharge, a flash lamp or another laser. The pumping energy injects light into the laser medium, where the electrons of outermost layers of the atoms excite. Some of the excited electrons will return to lower energy level with photon emissions. These emitted photons will be reflected in the resonator in order to increase population of stimulated electrons to undergo stimulated emission. Electrons surrounding an atom or a molecule even though they are found at their lowest energy level (resting state), can exist at more than one energy level. When an electron absorbs a photon, it rises to higher energy level, which is called excited state. This excited electron will emit a photon identical to the photon that was initially absorbed. This phenomena is called spontaneous emission. On the other hand, if another photon of appropriate energy collides with this excited electron, the electron will return to its resting state by emitting two photons which are synchronized in space and time called stimulated emission. But a population inversion which is a state in which the number of excited electrons are higher than the number of electrons in lower states is required for laser operation. As it is stated population inversion is necessary for laser operation, when population inversion is achieved the photons have a higher probability of colliding excited electrons and stimulating further emission of photons with the same energy and wavelength. An electrical, chemical or light energy as an external source is required to provide excitation process which is called pumping [6–8].

Lasers can be classified as three main categories in its time domain: (1) continuous wave (CW), (2) quasi-continuous (modulated) wave, and (3) pulsed wave. Continuous wave lasers produce continuous output beam at constant power. Quasi-continuous lasers

emit pulses of light on the order of microseconds to milliseconds width at a constant power. Pulsed lasers emit light in the form of optical pulses on the order of nanoseconds to femtoseconds rather than continuous mode. Pulsed lasers achieve extremely short emissions of high power peak with a sudden population inversion in the lasing medium.

Stimulation emission was first theorized by Einstein in 1917, but it took almost 10 years to find experimentally and took over 30 years just predict the possibility of laser. Then in 1960 a simple form of laser was developed. Thereafter, with large numbers of modifications and developments, today various lasers with different wavelength are available for medical applications [9–13]. The main differences of laser light from visible light can be listed as below:

1. It is monochromatic, that is only a single wavelength of light is produced. All light waves are of the same wavelength.
2. It is coherent, that is, all photons are in the same phase and have the same polarization.
3. It is collimated, that is the coherent waves are in parallel. Laser light goes through in one direction with infinitesimal divergence.

These properties listed above, make the lasers useful in medical applications [14,15]. To find appropriate laser for medical and surgical applications, the laser-tissue interactions should be understood comprehensively.

2.1 Laser-Tissue Interactions

The physical events that can occur when light interacts with tissue were described in this section.

Tissue is treated as scattering and absorbing medium where reflection and transmission also take place when interacts with light. When light interacts with the tissue

either absorption will takes place or it may be scattered according to the probability function expressed as anisotropy factor. In Figure 2.1 the behavior of light when interacts with tissue is represented schematically [16].

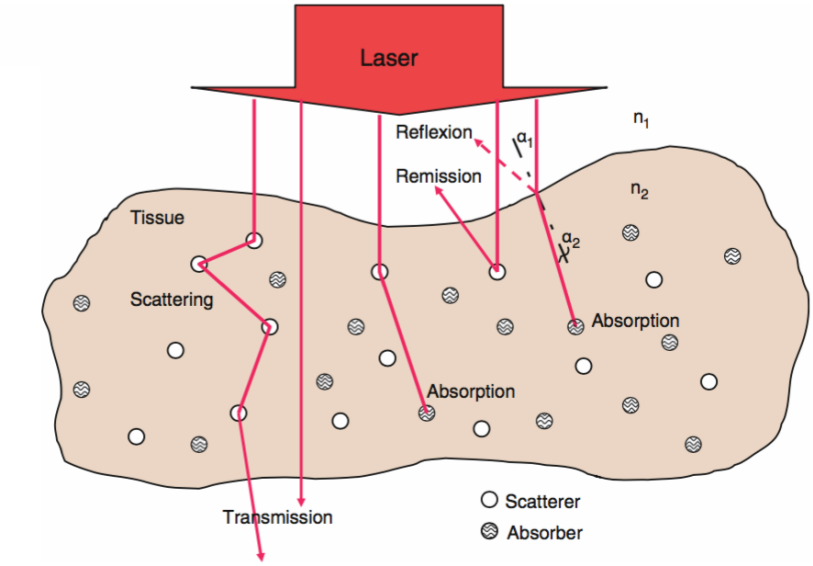

Figure 2.1 Optical behaviour of a tissue layer during irradiation with laser light [16].

Scattering, which determines the volumetric distribution of light in the tissue is the primary step for light-tissue interaction, which is followed by absorption, heat generation and heat conduction. Scattering structure of the tissue can be macroscopic, microscopic and submicroscopic structures [16].

Tissue components that absorb light are called chromophores. Chromophores; absorbing molecular components of the tissue can be listed as; porphyrin, haemoglobin, melanin, flavin, retinol, nuclear acids, deoxyribonucleic acid (DNA)/ribonucleic acid (RNA) and water. The absorption of light by any chromophore in the tissue is highly dependent on the wavelength of the light. For example for UV wavelengths amino acids are the main absorber while water is the main absorber for IR wavelengths [6]. Figure 2.2 represents the absorption spectra of different chromophores of biological tissue and water.

The optical and thermal responses of the tissue to laser irradiation are highly dependent on the wavelength of the laser source [6, 14, 16]. Heat is generated when a collimated or diffused light interacts with the tissue, but for low irradiance that do not

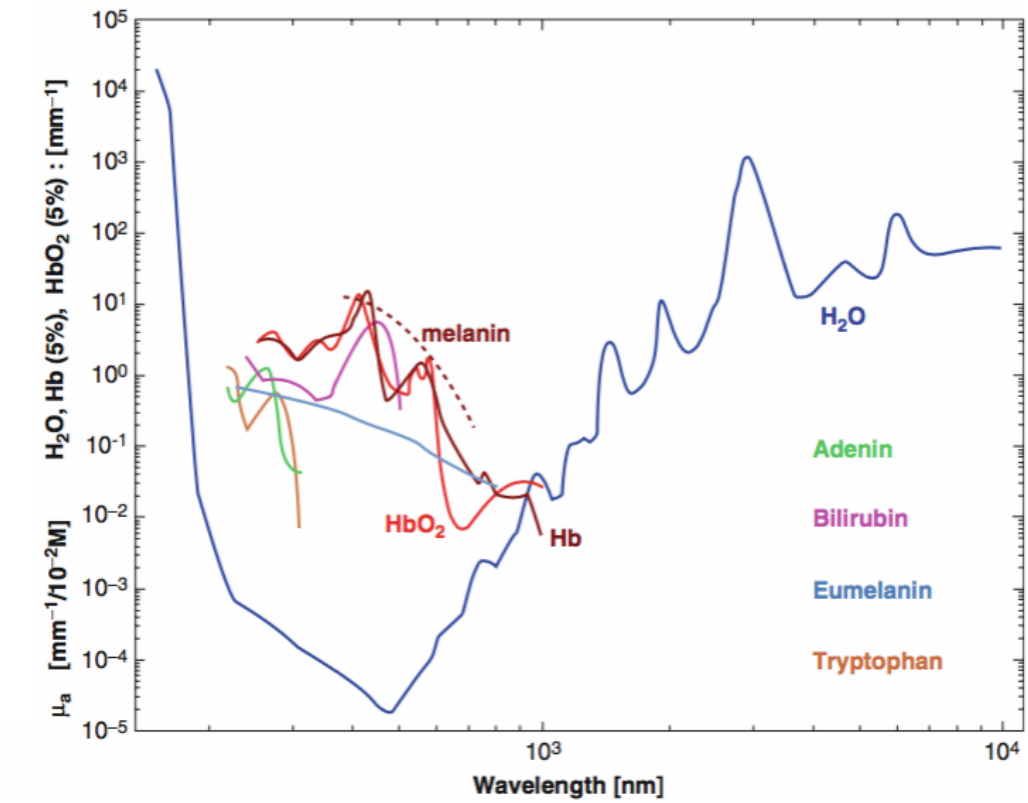

Figure 2.2 Absorption spectra of chromophores in biological soft tissue [16].

increase the temperature of the tissue significantly diagnostic, photochemical or biostimulative applications are general applications, whereas high irradiance that increase tissue temperature to high levels can ablate tissue or create mechanical and thermal damage [16].

2.1.1 Laser-tissue Interaction Mechanisms

Above, the behavior of laser light in the tissue is described and important phenomena are listed. In this section, the laser-tissue interaction mechanisms will be described. The first systematic description of the laser-tissue reaction mechanisms were presented by Boulnois in 1986 [16, 17] (Figure 2.3).

We can divide laser-tissue interaction mechanisms into two categories as non-thermal and thermal reactions. Non-thermal reactions occur at low-dose irradiation of the living tissues. Low-dose irradiation may result with proliferation of cells. Those

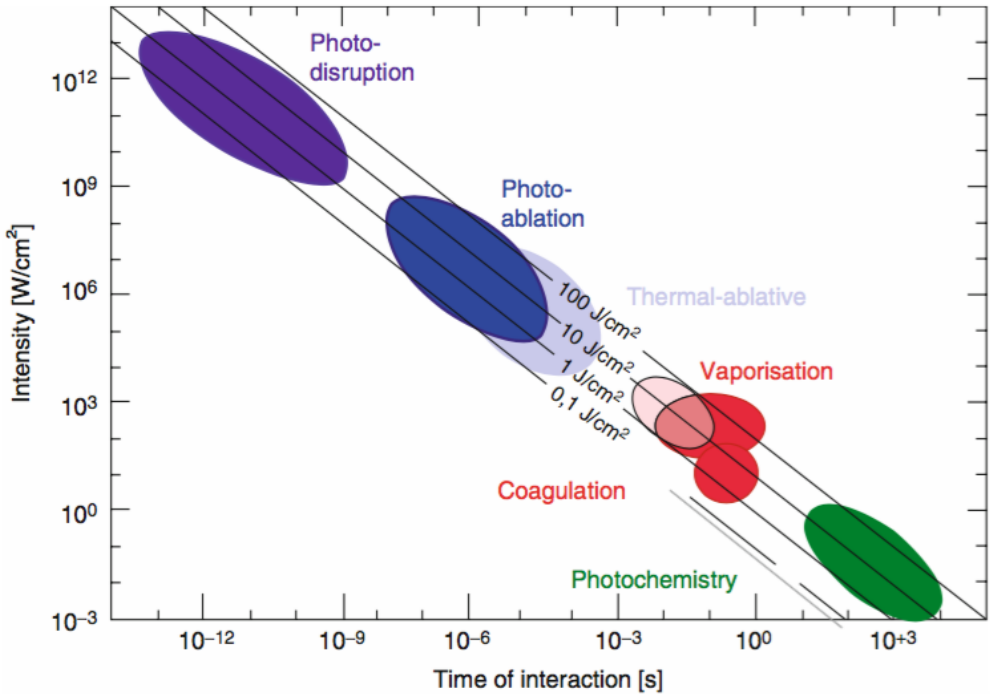

Figure 2.3 Plot of laser-tissue interaction mechanisms over time of interaction. Modified by [16] from [17].

non-thermal reactions can be listed as biostimulation and photodynamic therapy (PDT), which are out of scope of this thesis [16]. In this thesis we are going to focus on thermal reactions that is thermal effects of laser irradiation on biological tissues.

2.1.1.1 Photothermal reactions. Photothermal reactions occur when the tissue is heated due to the absorption of the photons by tissue components, DNA, RNA, chromophores, water, protein or enzymes [6]. The photothermal effects due to change in the temperature of the tissue are summarized in Table 2.1.

Usually, several thermal effects take place simultaneously in the tissue, depending on the temperature gradient. Figure 2.4 schematically represents several thermal effects on laser irradiated biological tissue [14]. The aim in medical procedures is to have one of those thermal effects, avoiding others, therefore laser parameters must be chosen very carefully. Another important aim is to give minimum thermal damage to the surrounding tissues.

Table 2.1
Photothermal effects due to the temperature of the tissue [14]

Temperature	Molecular and tissue reactions
42-45°C	Hyperthermia leading to protein structural changes
45-50°C	Drastic conformational changes, enzyme inactivation, edema
50-60°C	Coagulation, protein denaturation
80°C	Collagen denaturation, permeabilization of membranes
80-100°C	Dehydration, formation of extracellular vacuoles, vaporization
>100°C	Boiling, streaming, breaking of the vacuoles
100-300°C	Vaporaziation, tissue ablation
>300°C	Carbonization

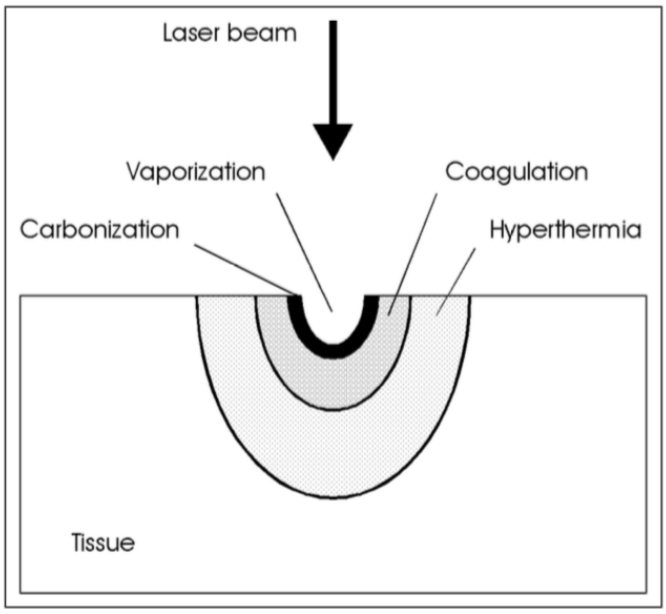

Figure 2.4 Location of Thermal Effects Inside Biological Tissue [14].

Temperature is the most important parameter in photothermal interactions. The maximum temperature reached within the tissue and its spatial distribution basically define the thermal effects in the tissue and the thermal damage nearby. So, monitoring temperature as a function of time during laser application gives very useful information on laser settings increasing the effectiveness of the procedure and helping to avoid possible unwanted damages.

The photothermal interaction is the conversion of laser energy to heat within the tissue. Absorption and scattering of photons by the macromolecules determine the interaction process. The absorption and scattering behavior of biological tissue are very important phenomena, because they play an important role on the response of biological tissue to the laser irradiation. Absorption behavior of the tissue gives a clue on the ablative effect of the responsive laser light, whereas scattering behavior of the tissue defines volumetric distribution of laser light in the tissue [6, 16].

In biological tissues water, hemoglobin, lipids, and other proteins are the main macromolecules (water is the most crucial one, e.g. 72% and 82% of subcortical and cortical tissues consists of water respectively [18]) [6, 14, 19, 20]. Heat deposition in tissue causes temperature increase and depending on the temperature gradient occurred vaporization could be succeeded, whereas heat loss occurs immediately by conduction to all adjacent tissues. Heat transfer depends on the following properties; geometry of the organism, heat capacity of the organism, thermophysical and physiological properties of organs and tissues (thermal conductivity, specific heat, density, blood perfusion rate and their spatial and thermal dependencies, heat production via radiative absorption, conduction of heat, heat transfer due to blood flow, heat exchange with the environment and heat production due to metabolic processes).

The relation between the thermal diffusion and the extent of the tissue necrosis can be summarized as follows: Thermal necrosis increases with increasing irradiation time for low laser power. Time for thermal diffusion reduces with reduced laser application time, resulting in smaller necrosis zone. If the irradiation time is equal to thermal diffusion or relaxation time, thermal necrosis is minimized. This minimum value cannot be less than the penetration depth of the laser light. Figure 2.5 shows the threshold for tissue damage depending on the laser power and the exposure time described by Arrhenius rate equation. There is a degeneracy between the exposure time and the laser power, in terms of reaching this threshold.

The degree of thermal damage does not only depend on the maximum temperature reached within the target tissue but also on the time interval during which the tissue was

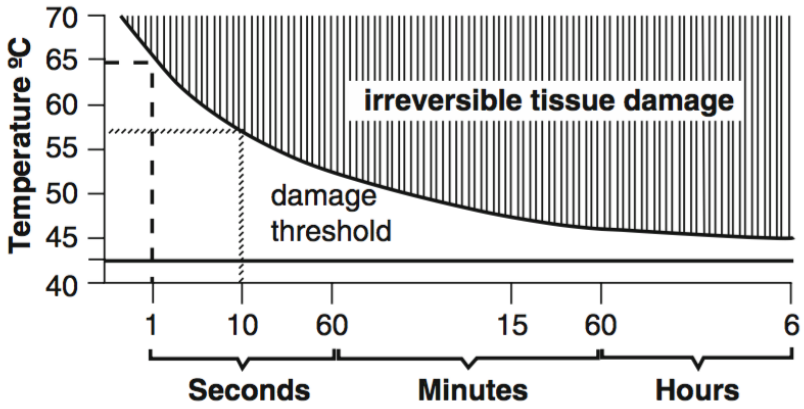

Figure 2.5 Time-temperature characteristic of tissue damage. The threshold for tissue damage at different temperatures depends on laser power and application time. A 1-s pulse reaches the thresh- old at 65°C, whereas a 10-s pulse reaches the threshold at 57°C [16].

exposed and on the heat conductivity of the tissue itself. If the temperature of the tissue is increased for 10°C in minutes, cell damage or death without structural alterations will be observed. For an increase of 20-30°C in shorter time intervals around 1 s, thermal coagulation of the tissue with cellular death and irreversible damage to the tissue due to the denaturation of proteins will be observed. If the tissue is heated above its boiling point a thermally-mediated tissue removal by explosive vaporization will be observed [21].

It is fair to assume that tissues are homogeneous and isotropic optical media and the light propagation in them is governed by the standard phenomena like reflection, absorption, transmission and diffusion [22]. Right dose for the target tissue in laser applications can be selected via predosimetry studies through which the parameters like wavelength, pulse width and shape, beam profile and power density can be determined. Important laser parameters like wavelength, power, mode (continuous/pulsed), pulse duration and frequency and exposure time usually depend on each other and therefore the adjustment of a single parameter can change the others [23].

Penetration depth depends directly on the applied wavelength. In order to have an even heating within the tissue, the applied wavelength should be well-adjusted, matching the tissue characteristics like degree of pigmentation, water content, tissue depth and thickness. For example, if the penetration depth is much smaller than the tissue thickness, most of the energy will be dissipated at the surface of the tissue, and if the

penetration depth is greater than the thickness, most of the energy may be transmitted to the underlying structures, causing unwanted damage [24].

Even for the wavelengths carefully chosen there will be differences in the absorptions at different depths. The preferred spot sizes and power densities, on the other hand, depend mostly on the relevant clinical application. For example, the use of a larger spot diameter can reduce the attenuation of the laser beam by the deeper layers of the tissue, which results in a uniform and deeper heating [24].

There are three parameters that describe the optical properties of the tissue: 1) The scattering coefficient, μ_s 2) the absorption coefficient, μ_a and 3) anisotropy factor, g. These parameters are determined by the tissue structure, geometry and cromophores, and together they affect the optical parameters (reflectance, transmittance, scattering, etc.) that describe the whole light propagation in the tissue [22, 23, 25–27]. It is remarkable that absorption coefficient, μ_a is more important than the scattering coefficient, μ_s at high frequencies, regarding the tissue damage [6, 28, 29].

Laser light is absorbed mainly by the water molecules, pigments, proteins and other macromolecules in the tissue and the absorption coefficient is a function of incident wavelength. Energy of the absorbed radiation is turned into heat and translational and vibrational kinetic energies in the tissue. Electronic and nuclear properties of the atom and molecules inside the medium are also important factors in absorption. For example, in a medium with discrete electric charges oscillations at the frequencies of the incident electric field occur. The natural frequencies at which atoms and molecules vibrate are at the infrared region, so if frequency of the incident electromagnetic field is comparable to those, resonances may occur, increasing the amplitude of vibrations. This will result in a higher number of collisions between atoms or molecules and more dissipation incident energy in terms of heat [30].

2.2 Soft tissue laser applications of photothermal interactions

Biological effects and therapeutic applications of lasers were first investigated in opthalmology and dermatology. In 1961, only one year after the introduction of Ruby lasers, Leon Goldman, the father of laser medicine, showed that they could be used to remove the wine stains and melanomas from skin [31–33]. Later that year, Campbell and Koester applied Ruby laser on a patient to destroy a retinal tumor via coagulation for the first time [34–37]. After that, research on photothermal applications of lasers had a rapid growth and many medical laser systems were developed. Today laser applications are performed in medical fields such as ophthalmology, dermatology, dentistry, oncology, and surgery.

The most widely used laser in soft tissue surgeries has been 980-nm diode laser due its good absorption for haemoglobin which provides good homeostasis [38–42]. 980-nm diode laser was investigated in oral surgeries and found to provide a good coagulation without pain, discomfort, infection or scarring [43, 44], however healing is delayed at the initial stage [45, 46].

Beer *et al.* reported the reduction of collateral thermal damage of 980-nm diode laser on liver tissue by setting the laser parameters in accordance with the absorption characteristics of the tissue, while maintaining an acceptable cutting ability. A smaller zone of carbonization and necrosis were found in micropulsed mode applications [47].

In another in vitro study, high-powered 940-nm diode laser was investigated for ablation of fatty tissue in non-contact mode. Irradiance from 250 to 400 W/cm^2 revealed both increased ablation capacities and the decreased collateral damages [48].

Nd:YAG lasers have also many applications in medical fields. Being a solid state laser, it emits light at a typical wavelength of 1064-nm in the near infrared region and operates both in continuous and pulsed modes. Nd:YAG laser can penetrate deep in the tissue due to its low absorption by tissue chromophores. On the other hand, due to its high absorption by oxyhemoglobin [49], it can be used in selective photothermolysis, a

targeted therapy in which the radiation is absorbed by a target area only, using a specific wavelength [50–53]. Therefore Nd:YAG lasers are being used in many dermatological applications like treatment of vascular and pigmented lesions [54–60], hair-removal, long-term hair reduction [61–64], dark tattoo removal [51, 65, 66] and wrinkle removal [67–69].

Outside dermatology, Nd:YAG lasers are being used successfully in intraoral surgeries [70–72] and when coupled to fiber optics they can also be used in laser induced interstitial thermotherapy (LITT). There are promising results reported, about the application of Nd:YAG lasers on prostate to treat benign prostatic hypertrophy [73, 74].

Several in vitro soft tissue applications of Tm:fiber laser have been studied. Fried *et al.* investigated the ablative effect of the continuous 1940-nm Tm:fiber laser in non-contact mode with a power of 40 W on canine prostate. Histological examinations showed a thin layer of carbonization followed by a vacuolized layer, which indicates a mechanical effect of an incomplete ablation of tissue and thermally coagulated layer ranging from 500 μm to 2000 μm. The results were compared with that of CO_2 and obtained coagulated layers were found to be larger than that of CO_2 laser, which indicates the 1940-nm Tm:fiber laser as a promising tool for its good homeostasis even for highly vascularized tissues [75].

Another in vitro study was carried out by Keller *et al.* on chicken breast, porcine skin and bovine liver, in which continuous wave 1940-nm Tm:fiber laser was used at power ranging from 11 W to 20 W in non-contact mode. The zone of thermal damage was measured to be ranging from 600 μm to 1 mm with thin carbonization layer and vacuolization around the thermal damage [76].

Sroka *et al.* also studied the clinical feasibility of Tm:fiber laser in a prospective study on eleven patients. It is achieved to reduce of hyper plastic inferior nasal turbinates significantly by coagulating the tissues in non-contact mode at 5 W, without bleeding and complications. A very good and fast superficial coagulation was observed [77].

Kang *et al.* investigated and compared the ablative effects of 532-nm and 2.01-μm laser on porcine kidney tissue in vitro and reported the former one as more efficient in

tissue ablation with a smaller coagulated zone [78].

In orthopedic surgeries, 2.1-μm Holmium laser was used as an orthroscopic surgical tool [79]. It was able to cut and ablate tissues easily with a minimum thermal necrosis [80] and provides an effective destruction of human adipose tissue [81]. The use of Thulium laser in prostate and superficial tumors in the lower and upper urinary tracts gave effective results. Better visualization of ablation and absence of collateral damage in the nearby tissue were the advantages of this method [82].

When comparing CO_2 diode and Thulium lasers, which are both efficient in superficial tumor ablation, Thulium laser applications resulted in a significantly lower threshold of ablation and less residual thermal energy [83]. It is shown that Thulium laser, which operates at 2.0-μm can be delivered through a silica fiber, unlike 10.6-μm CO_2 laser [84].

Its ability to operate near 1940-nm (water absorption peak) turns out to be an advantage in tissue cutting when compared to Holmium and KTP lasers [85]. In another study, the effects of 2.12-μm Holmium-YAG laser on rabbit skin regarding the damage and recovery were examined by measurement of the lesions and histology [86].

2.2.1 Temperature measurements and monitoring techniques during photothermal interactions

In order to propose an effective alternative to conventional surgical techniques, photothermal damage must be taken under control by a detailed dose study. Laser power, energy delivered to target tissue, spot size, power density, exposure time, mode of operation can be tested and resulting effect can be defined in terms of the amount of ablation, coagulation, and carbonization. Real-time temperature measurements can also be very helpful for describing the photothermal effect and also for controlling the laser parameters.

There are different temperature measurement and monitoring techniques that exist, which can be summarized as point thermometry, surface thermometry and volumetric

thermometry [21].

Point thermometry utilizes thermocouples and fiber optic sensors. Advantages of point thermometry are the simplicity and low-cost of its components, wide range temperature measurement it provides and its rapid response and accuracy. Main drawback of the method is that it is invasive. Additionally, metallic constitution of the equipment may result in absorption of laser radiation, hence an overestimation of the measured tissue temperature [87–89]. Measurements of the rates of temperature change using thermocouple in the following studies provided an indicator for the thermal damage induced in the tissue [90, 91].

Monitoring the surface temperature with thermal sensor (e.g. infrared cameras), is called surface monitoring [92, 93]. Non-invasiveness and large area measurements are the main advantages of this method. However, surface-only measurement and low accuracy are the drawbacks, in addition to the high prices of the equipment. In tissue welding, because the region of interest for temperature monitoring is the skin surface, non-invasive techniques can be advantageous. On the other hand, for the inner organs laser surgery, temperature measurement with non-invasive thermal sensors is not applicable. It is also shown that surface temperature can be also measured radiometically to give user an insight about the tissue status during laser irradiation. Silverhalide fiber optically focused onto a photonic thermal detector was developed for surface temperature measurement [94–96]. Photothermal interaction is a very fast and very localized process; thermal response of the tissue to the laser irradiation is on nanosecond levels [97]. Time response of the equipment is not that critical for the relatively slow heating processes like welding, however, for the processes that involve ablation/vaporization, equipment with a higher time response is needed for accuracy.

Volumetric thermometry, on the other hand, involves monitoring of multiple points in a large volume via, for example, MRI thermometry or ultrasound thermometry. MRI thermometry, being the most popular imaging method, allows high contrast and spatial resolution imaging. It is non-invasive, therefore can be used in monitoring the temperature of targeted locations and tissues nearby [98,99]. Despite being a precise method, it is more

expensive and complex than the point thermometry.

There are studies that reported real-time temperature measurement by magnetic resonance imaging systems or thermal cameras [38, 100–105]. But those techniques have their own limitations; they are not easy to implement or not practical for clinical usage. Moreover, there has been made modifications to facilitate the use of laser in neurosurgery, such as laser systems merged with imaging systems in order to target the region to be treated and achieve precise ablation [106, 107].

2.2.2 Lasers in neurosurgery

Lasers are an important developmental milestone in neurosurgery. A considerable number of continuous wave (cw) lasers with several wavelengths are used in medical applications to cut, shape, and remove soft tissue of the body. It has been also reported in several studies that the lasers at the wavelength with higher absorption by water that constitutes the main element of biological tissues are used in tissue ablation. In this part of the thesis these studies will be discussed.

The introduction of lasers into neurosurgery began with the use of focused and unfocused ruby laser beam to the cranium of mice, which results in immediate death in 1965 [108, 109]. In late 1965 Fox *et al.* repeated these experiments on guinea pigs, and found that the immediate death was due to apnea [110]. The effects of ruby laser was continued to be investigated with the direct application of laser beam to the cortex of cats, and histological effects of lasers were reported in detail. It is also reported that focused laser light caused greater damage to the brain tissue than defocused light, and radiation of cortex with intact dura result with smaller damage to the brain. Another important outcome of these studies was that the laser created a wedge-shaped lesion when applied directly to the cortical tissue [111–114]. In 1965 Rosomoff and Carroll reported two human cases of the application of ruby lasers but the prolongation of survival was not documented [115]. In late 1966, Brown *et al.* reported that neurons are highly sensitive to the deconstructive effect of laser light and thus grey matter is more susceptible

than white matter to the effects of laser light [116, 117]. By the way, CO_2 laser was invented by Patel in 1965 [118]. The introduction of continuous wave lasers and improved delivery systems made lasers more applicable to neurosurgery. Much of the initial work of investigating the neurosurgical effects of CO_2 laser were reported by Stellar *et al.* [119–121]. They reported that precise and more controllable hemostatic incisions could be made in cat brain and spinal cord. They also demonstrated the coagulative effect of defocused CO_2 laser. In 1965 they used CO_2 laser to totally vaporize a recurrent glioma to the patients with inoperable glioblastomas. After a few publications and failures, Stellar personally advised not to use lasers in neurosurgery. The most technical difficulty of the CO_2 laser that the neurosurgeons encounter during surgery, was invisibility of the laser light to human eye and it was treated as invisible knife. However, laser as a noncontact and minimally traumatic cutting tool, convinced some surgeons to pursue its use in neurosurgery. Heppner [122, 123], Ascher [124, 125], Takizawa *et al.* [126] and Ascher and Cerullo [127] reported large series of neurosurgical applications with CO_2 laser. From 1976 to 1979 Ascher Ascher [124,125] and Heppner [122,123] performed >250 laser operations on the central nervous system. Many of these procedures were performed without the aid of microscope [128–131]. Ascher and Heppner modified the carbondioxide laser in two ways in 1976. The first modification was the addition of helium laser as a pilot beam for invisible CO_2 laser light [122]. The second modification was coupling the laser to the operating microscope. But one of the handicaps of the CO_2 laser was that it cannot reach the deeper sites of tissues, therefore results in limited applications. Second handicap of this laser was it cannot be guided through optical fibers and requires articulated arms.

Infrared (IR) lasers ranging from 800-nm up to 10600-nm have been widely studied for decades. In the near-IR part of the spectrum (i.e. 800-1200-nm) photons are poorly absorbed by water compared to the greater wavelengths in IR [132]. 980-nm must be noted as an exception with a local peak in the absorption coefficient of water and successful surgical applications with this wavelength was reported [41, 42]. Despite the poor absorption by water, hemoglobine absorption can have a considerable contribution for this region and those lasers have the advantage of coagulating blood vessels [41, 42, 133].

For higher wavelengths water absorption becomes more dominant and scattering loses its effect [6, 14]. Water absorption curve makes a maximum at 3-μm wavelength and it continues to be high during the mid-IR part of the spectrum [83, 134]. The ablative effects of Er:YAG (2.94-μm) and CO_2 (10.6-μm) lasers have been reported in literature accordingly [135–137]. However, those of the lasers cannot be transmitted via silica optical fibers and this limits the applicability of those wavelengths for minimal invasive surgery [83].

Cw high power Tm:fiber lasers emitting radiation around 2-μm have great potential for neurosurgery by overlapping of this wavelength to one of the absorption peak of the water [138]. The absorption coefficient of water for a specific wavelength is a crucial parameter, causes different wavelengths to penetrate different distances into the tissues; that is the success of lasers of different wavelengths in tissue removal are different. More clearly, higher absorption coefficient of water means less penetration depth and results with less collateral tissue damage and precise tissue removal. Moreover Tm:fiber laser can be coupled into silica fibers effectively. Silica fibers are cheap and easy to use but they cannot carry laser energies of wavelengths greater than 2-μm [83]; therefore Tm:fiber laser becomes a very attractive choice in neurosurgical applications.

3. MATERIALS AND METHODS

3.1 Laser systems

3.1.1 980-nm Diode Laser System

980-nm diode Laser (opto power corporation model no: OPC-D010-980-FCPS, Opto Power, Tuscon, AZ, USA) was used in this study. Controller instrument is used to control the laser by computer. Maximum current for 980-nm diode laser is 35 A and maximum output for this laser is 14 W. The system provides output through a 1 meter fiber-optic cable. The laser light was transferred to 385-micron laser fiber via coupler tool. LabView software interface (V 6.1) was used to control the laser parameters (power, exposure time, number of cycles, and on-off duration pulses).

Laser power was checked with an optical powermeter (Newport 1918-C, CA, USA) before and after each application.

3.1.2 1070-nm YLF Fiber Laser System

1070-nm YLF fiber laser (IPG Laser GMBH, Model: Laser Driver) was also used in this study as a different laser source. Maximum output power for this laser is 20 W. It is possible to use this laser in both continuous and pulsed-modulated-modes. The irradiation is selected via power or current by the control section by manually for continuous mode applications. For pulsed-modulated-mode emission a controller unit and an interface is necessary to choose laser parameters.

Laser light was coupled to 400 μm fiber (0.39 NA) via focusing lenses, and xyz alignment apparatus. Laser power was checked with an optical powermeter (Newport 1918-C, CA, USA) before and after each application.

3.1.3 1940-nm Tm:Fiber Laser System

Tm:fiber laser (IPG Photonics TLR-5-1940) emits at 1940-nm. Maximum output power of the laser is 5 W. Laser output power, exposure time, mode of laser delivery (pulsed modulated or cw), number of cycles and on-off duration of pulses are controlled by the custom-built controller unit (Teknofil Inc. Istanbul, Turkey). User can easily set those parameters via LabView interface of the controller unit. The system provides output laser through a 1-meter fiber-optic cable.

Laser light was coupled to 400 μm fiber (0.39 NA) via focusing lenses, and xyz alignment apparatus. Laser power was checked with an optical powermeter (Newport 1918-C, CA, USA) before and after each application.

It is a persisting incongruity in literature to use pulsed mode to chopped laser light. Thus we prefer to use pulsed-modulated-mode to prevent misunderstanding.

3.2 Preparation of brain samples for *ex vivo* studies

A total of 100 fresh lamb brains weighing 60-70 grams were used for the experiments. The lambs were 6-8 months. The brains were cooled to 4°C immediately after the animal was slaughtered and experiments were performed within 24 hours. Before the experiments temperature of the samples was increased to the room temperature (22°C). The temperature was checked with the thermoprobe. Laser applications were done on each 4-5 mm thick coronal section taken from brain samples closed to the midline. The other two dimensions of the samples were $3.5 \pm 0.2 \times 6.00 \pm 0.4$ cm. The laser dependent lesions were rather small with respect to dimensions of the samples in order to avoid boundary effects. Brain samples were covered with saline in order to prevent the tissue to dehydrate. Laser shots were performed and data were collected with respect to the brain structures (i.e. cortical and subcortical). Different laser power and exposure time combination had been studied and each laser dose had been performed 10 times.

3.3 Preparation of animals for *in vivo* studies

The experiments were conducted under a protocol approved by the Institutional Animal Research and Care Ethic Committee at Boğaziçi University (BUHADYEK). Healthy Male Wistar rats, randomly selected, 3-4 months old, weighing 150-250 gr were supplied from Boğaziçi University Life Sciences and Technologies Research Center; Vivarium. Rats were housed in plastic cages and maintained on a 12-h-light/12-h-dark cycle in a temperature-controlled vivarium (22±2°C). Food and water were available ad libitum.

3.4 Methods for *ex vivo* studies

3.4.1 Laser Application Procedure

Laser was applied to the cortical and subcortical tissue vertically a few mm above (0.0-0.2 mm). Before each application, fiber tip was checked for irregularities and cleaved if it was needed. Firstly, a predosimetry study was done in order to determine the parameters for continuous and pulse-modulated-mode: coagulation and carbonization onset times were recorded by increasing power. If the laser applications result in carbonizations consistently; power was not continued to increase. As a result a safe ablation/coagulation region of continuous (c-m) and pulse-modulated-modes (p-m-m) was set for various power-laser durations and laser sources (Tables 3.1 and 3.2).

In continuous-mode and pulsed-modulated-mode, laser power and pulse widths were chosen in order to deliver the same amount of energy to the tissue. All laser applications were performed via thermoprobe designed by our group.

3.4.2 Thermoprobe

A 1.3-mm needle was mounted in a hand piece with 1.5-cm in diameter. 400-μm optical fiber and 20-μm K-type thermocouple were inserted and fixed via that needle

Table 3.1
Dosimetry levels applied to brain tissue for ablation efficiency and temperature rates analysis for *ex vivo* studies with 980-nm diode laser.

Zone	Laser mode	Laser power (W)	Average light intensity (W/cm^2)	Duration (s)	Laser energy delivered (J)
Cortical/Subcortical	c-m	1	796	3	3
Cortical/Subcortical	c-m	1.5	1194	2	3
Cortical/Subcortical	c-m	2	1592	1.5	3
Cortical/Subcortical	c-m	2.5	1990	1.2	3
Cortical/Subcortical	c-m	3	2387	1	3
Cortical/Subcortical	c-m	1	796	4	4
Cortical/Subcortical	c-m	1.5	1194	2.6	4
Cortical/Subcortical	c-m	2	1592	2	4

Table 3.2
Dosimetry levels applied to brain tissue for ablation efficiency and temperature rates analysis for *ex vivo* studies with 1940-nm Tm:fiber laser.

Zone	Laser mode	Laser power (mW)	Average light intensity (W/cm^2)	Duration (s)	Laser energy delivered (J)
Cortical/Subcortical	c-m	200	159	10	2
Cortical/Subcortical	p-m-m	200	159	20 (100 ms on 100 ms off)	2
Cortical/Subcortical	c-m	400	318	5	2
Cortical/Subcortical	p-m-m	400	318	10 (100 ms on 100 ms off)	2
Cortical/Subcortical	c-m	600	478	3.33	2
Cortical/Subcortical	p-m-m	600	478	6.67 (100 ms on 100 ms off)	2
Cortical/Subcortical	c-m	800	636	2.5	2
Cortical/Subcortical	p-m-m	800	636	5 (100 ms on 100 ms off)	2
Cortical/Subcortical	c-m	200	159	20	4
Cortical/Subcortical	p-m-m	200	159	40 (100 ms on 100 ms off)	4
Cortical/Subcortical	c-m	400	318	10	4
Cortical/Subcortical	p-m-m	400	318	20 (100 ms on 100 ms off)	4
Cortical/Subcortical	c-m	600	478	6.67	4
Cortical/Subcortical	p-m-m	600	478	13.34 (100 ms on 100 ms off)	4
Cortical/Subcortical	c-m	800	636	5	4
Cortical/Subcortical	p-m-m	800	636	10 (100 ms on 100 ms off)	4

(Figure 3.1). The distance between optical fiber and thermocouple tip is 0.5 mm. The tip of the thermocouple is always inserted into the tissue by 0.3 mm. The response time of the thermoprobe is 0.1 second and it can detect 0.1°C changes. Temperature changes were observed real-time and a LabView program was utilized for data acquisition. Before each application, thermoprobe was calibrated to different reference temperatures (room temperature, 0°C cold water and 100°C hot water measured by a conventional Hg-thermometer). In order to be sure that thermocouple is not directly irradiated by the laser light, the experiments were performed without sample at the beginning of the each application, the temperature were recorded and it is observed that temperature did not change. The experiments were also performed on water, but the changes in temperature were not significantly different because heat convection is dominant for liquids.

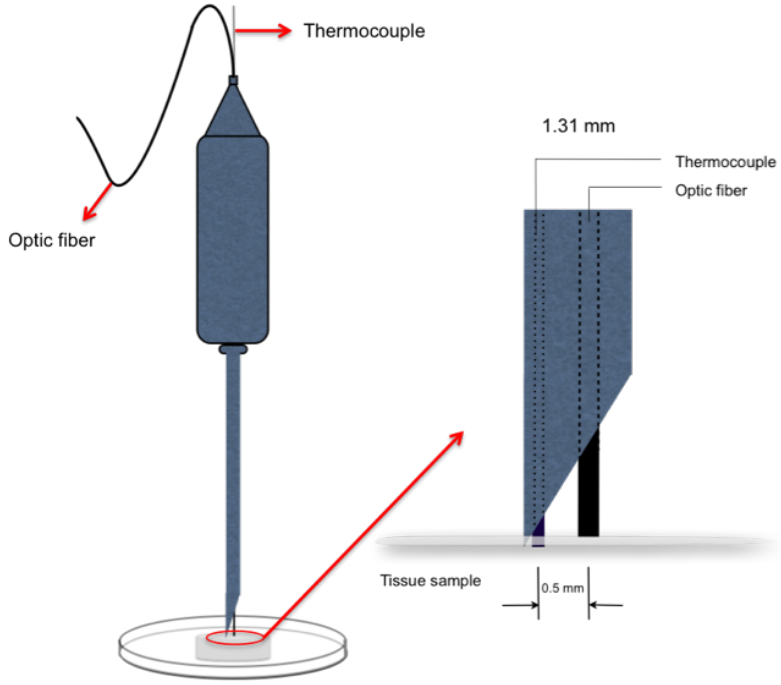

Figure 3.1 Schematic presentation of laser-thermoprobe system to measure the temperature of the nearby tissue during laser irradiation

3.4.3 Quantifying the Thermal Damage

Thermal effects of the laser were quantified in terms of ablation (thermally removed tissue) and coagulation (irreversible thermal damage) areas. The ablation and coagulation diameters were measured under light microscope (Eclipse 80i, Nikon Co., Tokyo, Japan)

(Figure 2). Measurements were performed using Imaging Software (NIS Elements-D, Nikon Co, Tokyo, Japan). It is aimed to find the appropriate laser parameters in order to perform highest ablation efficiency (AE) (Equation 3.1) with minimum collateral damage, which is calculated as the ratio of ablation zone diameter (AD) to the total thermally altered zone diameter (AD+CD).

$$\%\mathrm{AE} = \frac{\mathrm{AD}}{\mathrm{AD} + \mathrm{CD}} \times 100 \tag{3.1}$$

During laser application, temperature rise in the tissue was observed with thermoprobe as described in detail in previous section. The relationships between laser parameters (power, exposure time), temperature changes and ablation efficiencies were determined. Correlations between rates of temperature change over time (Equation 3.2) and ablation efficiencies were calculated.

$$\text{rate of temperature change} = \frac{\Delta \mathrm{T}}{\mathrm{t}} \tag{3.2}$$

3.4.4 Data Analysis

Analysis of variance (ANOVA) was performed to reveal the effects of parameters on the ablation and coagulation diameters. In order to determine statistical differences between the ablation and coagulation diameters, Tukey test was used as a post hoc test after ANOVA test and $p < 0.05$ was used as significance level. Ablation efficiencies and rates of temperature change were calculated. Ablation efficiencies above 50% were specified as successful laser ablation. The relationship between ablation efficiencies and rate of temperature change were revealed with Spearman's rank correlation coefficient calculations, if applicable.

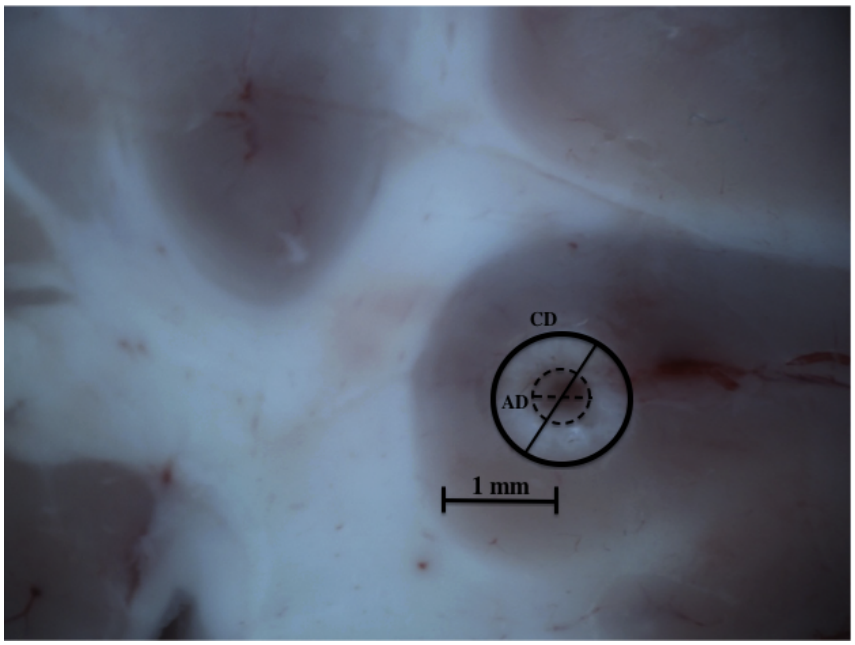

Figure 3.2 A brain tissue sample which exposed to 1940-nm Tm:fiber laser. CD indicates the diameter of the coagulated zone, AD indicates the diameter of the ablated zone.

3.5 Stereotaxic Laser Surgery Experiments *in vivo*

3.5.1 Stereotaxic Surgery

Rats were anesthetized with ketamine (10% ketamidor, RichterPharma, AG, Wels, Austria) by intraperitoneal injection (1.65 ml/kg). Hairs at the site of application of each subject were shaved and if needed, epilation cream were applied to remove remaining hair. Rats were placed in the stereotaxic instrument. Body temperature of the rats during the surgery was regulated using animal temperature controller (ATC1000, World Precision Instruments, FL, USA). The skin was retracted and holes were drilled in the skull. Dura was removed. Bilateral lesions were created at the following coordinates: +3.73 mm from bregma, ±3.0 mm lateral to midline, and -1.1 mm below the dura for primary motor cortex (cortical tissue), 0 mm from bregma, ±3.0 mm lateral to midline, and -6.0 mm below the dura for Caudate putamen (subcortical tissue) [139]. After lesions were created, fiber was waited for 2 minutes at the lesion area. The tip of the fiber was cut with a tungsten carbide knife whenever a defect is observed. After surgery, animals were sacrificed immediately by a retractor.

3.5.2 Laser Application Procedure

Laser was applied to the cortical and subcortical tissue vertically. Before each application, fiber tip was checked for irregularities and cleaved if it was needed. The parameters, which were studied, were determined from *ex vivo* studies (Table 3.3). All laser applications were performed via thermoprobe designed by our group.

Table 3.3
Dosimetry levels applied to brain tissue for ablation efficiency and temperature rates analysis for *in vivo* studies with 980-nm diode and 1940-nm Tm:fiber lasers.

Zone	Laser source	Laser mode	Laser power (W)	Average light intensity (W/cm^2)	Duration (s)	Laser energy delivered (J)
Cortical/Subcortical	980-nm diode	c-m	2	1592	1.5	3
Cortical/Subcortical	980-nm diode	c-m	2	1592	2	4
Cortical/Subcortical	1940-nm Tm:fiber	c-m	0.4	318	2.5	1
Cortical/Subcortical	1940-nm Tm:fiber	c-m	0.4	318	5	2
Cortical/Subcortical	1940-nm Tm:fiber	c-m	0.6	478	3.3	2
Cortical/Subcortical	1940-nm Tm:fiber	p-m-m	0.4	318	5	2
Cortical/Subcortical	1940-nm Tm:fiber	p-m-m	0.6	478	3.3	2

3.5.3 Temperature Measurements

During laser surgery the temperature increase in the tissue was observed with a t-type thermocouple. Thermocouple measured the temperature increase at a location 0.5 mm away from the laser irradiation site.

In surgical applications, thermocouple with a higher measurement rate was used instead of a thermoprobe.

3.5.4 Histological Procedures

After the sacrification of the animal, brain of the animal were extracted. Then the brain samples were fixed in 10% formalin solution (4 liters of phosphate buffered saline

(PBS) with 400 ml formaldehyde (37%-40%). Phosphate buffered saline solution was prepared by dissolving tablets of PBS in distilled water. Each tablet was dissolved in 100 ml of distilled water.) at least for 4 days (generally 7 days).

When the brains were fixed, 50 μm coronal sections were taken from rat brains with vibrotom (Leica VT1000 S Germany). Slices were waited in 0.1 molar phosphate buffer (PB) until CFV staining. Brain slices, which were taken from leisoned part of the brain, were moved to chrome-gelatinized slides. After this step, CFV staining procedure was applied. This procedure consists of the following steps:

1. 1 gram of CFV stain was dissolved in 100 ml of distilled water, then 0.25 ml Acetic Acid was added to this solution.
2. Slides were passed alcohol gradient given below
   (i) 95% alcohol (15 minutes)
   (ii) 70% alcohol (1 minutes)
   (iii) 50% alcohol (1 minutes)
3. Slides were embedded in distilled water twice, two minutes each
4. Slides were embedded in CFV stain for 7 minutes
5. Slides were embedded in distilled water for one minute
6. Slides were passed alcohol gradient given below
   (i) 50% alcohol (2 minutes)
   (ii) 70% alcohol + 1% Glacial Acetic Acid (2 minutes)
   (iii) 95% alcohol (2 minutes)
   (iv) 95% alcohol (1 minutes)
   (v) 100% alcohol (1 minutes)
7. Slides were dipped in Xylene twice, five minutes each

8. Slides were dried 24 hours

9. Slides were closed with cover slip. Entellan was used to stick.

3.5.5 Quantifying Thermal Damage

Thermal effects of the laser were quantified in terms of ablation (thermally removed tissue), severe and mild coagulation (irreversible thermal damage) and reversible (edema) thermal damage areas. The ablation and coagulation areas were measured under light microscope (Eclipse 80i, Nikon Co., Tokyo, Japan) and images were captured with two magnifications, 40X and 100X (Figures 3.3 and 3.4).

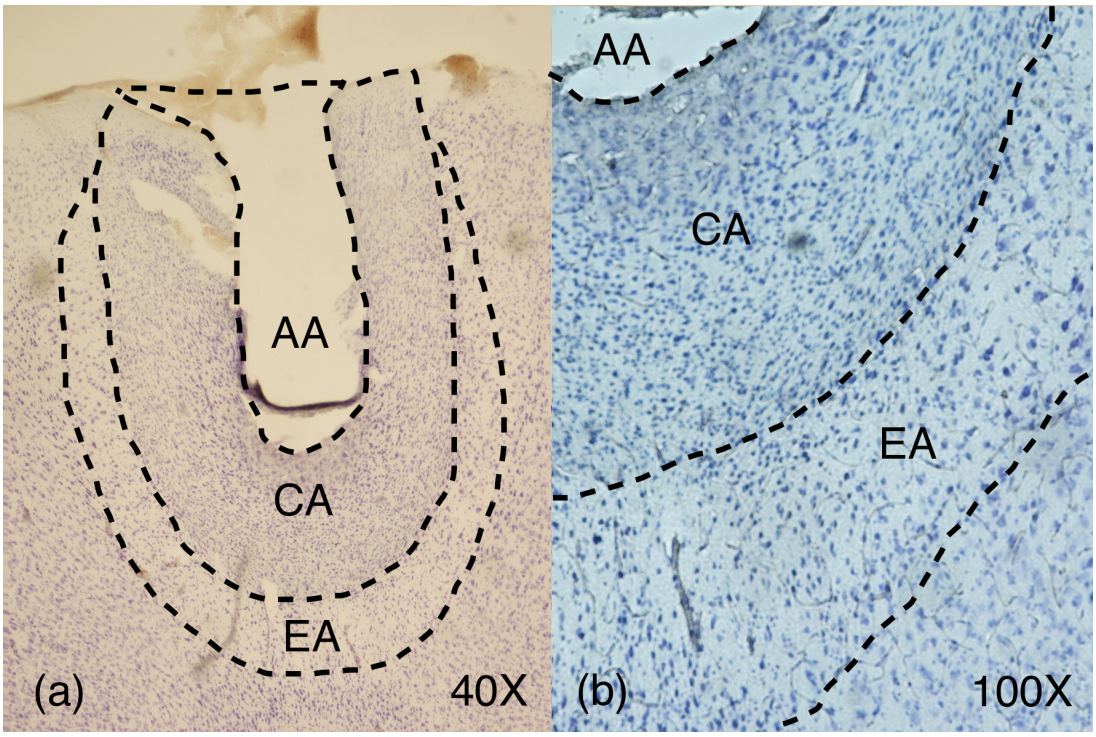

Figure 3.3 Laser induced micrographs of cortical tissue with a) 40X and b) 100X magnifications. Ablated (AA), coagulated (CA) and edematous (EA) areas were separated by dashed lines.

Measurements were performed using ImageJ Software (National Institute of Health, USA). It is aimed to find the appropriate laser parameters in order to get highest ablation efficiency with minimum collateral damage, which is calculated as the ratio of ablated area to the total thermally altered area. In this context, the ablated area (AA), the coagulated area (CA) and the edematous area (EA) generated through laser exposure were measured

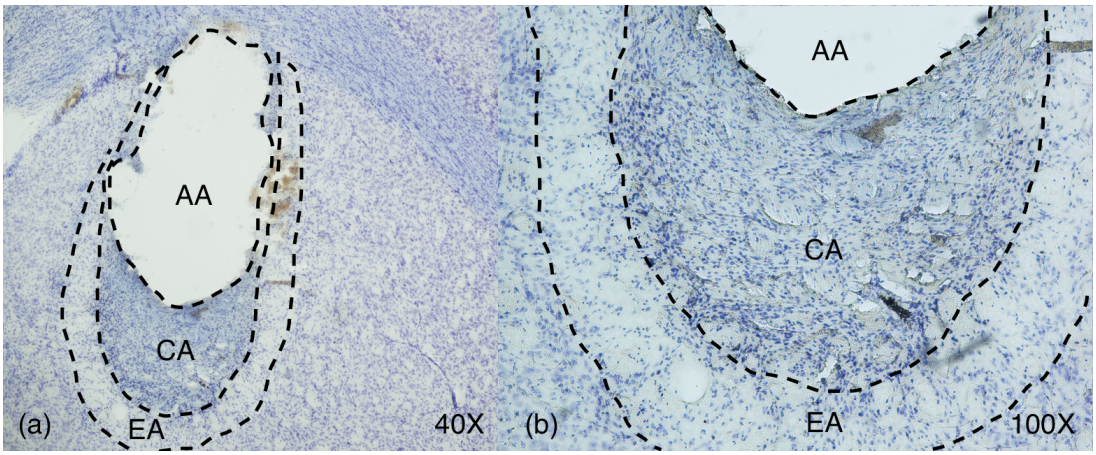

Figure 3.4 Laser induced micrographs of subcortical tissue with a) 40X and b) 100X magnifications. Ablated (AA), coagulated (CA) and edematous (EA) areas were separated by dashed lines.

and the percentage ablation efficiency (%AE) was calculated according to Equation 3.3.

$$\%\mathrm{AE} = \frac{\mathrm{AA}}{\mathrm{AA} + \mathrm{CA}} \times 100 \tag{3.3}$$

The temperature of the nearby tissue was observed during each laser surgery. For each observation, the maximum temperature rise with respect to the pre-laser temperature (ΔT), the time to reach that maximum, and the rate of temperature change were calculated.

Additionally edematous area was normalized (NEA) for each surgery (Equation 3.4) in order to have a reasonable comparison between the cases. That is, we aim to make a fair comparison for lesions having similar edematous but different ablated and coagulated areas.

$$\mathrm{NEA} = \frac{\mathrm{EA}}{\mathrm{AA} + \mathrm{CA} + \mathrm{EA}} \tag{3.4}$$

3.5.6 Data Analysis

Analysis of variance was performed to reveal the effects of parameters on the ablation and coagulation diameters. In order to determine statistical differences between the ablated, coagulated and edematous areas, Tukey test was used as a post hoc test after ANOVA test and $p < 0.05$ was used as significance level. Ablation efficiencies and rates of temperature change were calculated. Ablation efficiencies above 50% were specified as successful laser ablation. The relationship between ablation efficiencies and rate of temperature change were revealed with Spearman's rank and Pearson's correlation coefficient calculations, if applicable.

4. RESULTS and DISCUSSION

4.1 Laser Brain ablation with 980-nm Diode Laser; *ex vivo* experiments

The 980-nm diode laser which is preferred in many medical applications due to good absorption by haemoglobin providing good homeostasis during surgery was investigated by our laboratory for brain and intraoral surgery. A study of dose determination was performed to find the optimal parameters that provide less thermal damage to the surrounding healthy tissue.

The maximum output power of this laser is 14 W as mentioned before. In order to find which parameters are more suitable for brain ablation, first a predosimetric study was performed. In this predosimetric study, the laser was applied directly on the cortical and subcortical tissues, which were embedded into saline and the coagulation and carbonization onset times were recorded.

The results of predosimetric study performed by 980-nm diode laser had been shown in Figures 4.1 and 4.2. Figures 4.1 and 4.2 show the coagulation and carbonization onset time respectively, when 980-nm diode laser was applied to cortical and subcortical tissues. According to these results it is obvious that carbonization occurs immediately, when the power of the laser light is greater than 5 W. But this predosimetric study was an observation by naked eye. That is, the clock had been stopped when the coagulation or ablation was visible to human eye. That's why it has been decided not to apply light power greater than 3 W.

Studied groups with this laser source were given in Table 3.1. Applications of 3 J and 4 J of energy were performed via varying energy delivery in terms of output power and exposure time in order to determine the most appropriate laser doses for *in vivo* study. The thermal effects of this laser source on cortical and subcortical tissues were examined

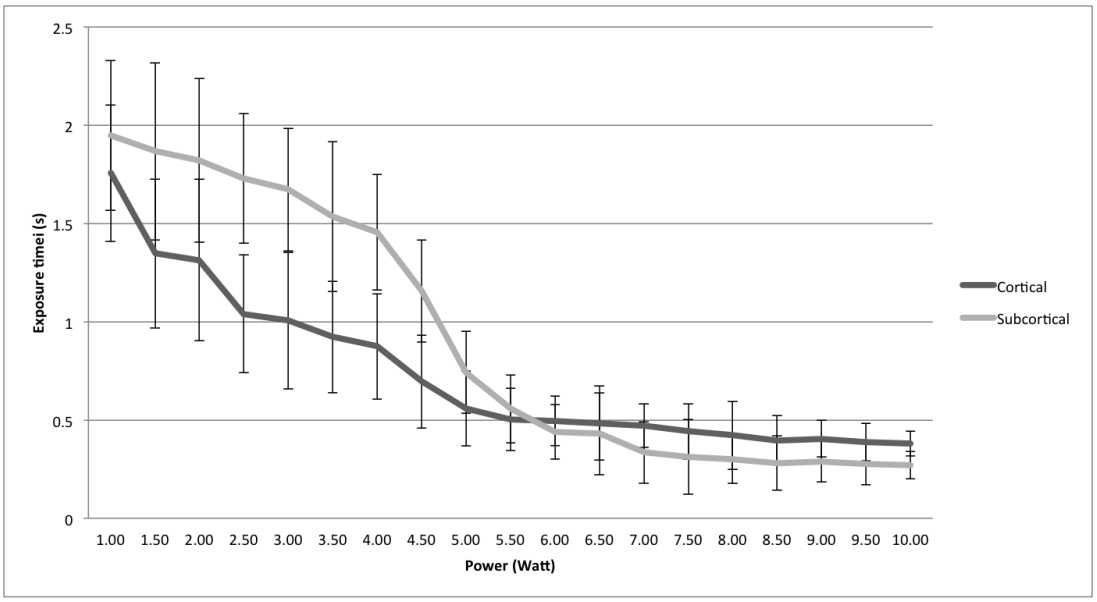

Figure 4.1 The coagulation onset time, when 980-nm diode laser was applied to cortical and subcortical tissue. The instances at which coagulation was observed, occurred earlier with increasing power. In cortical tissues, coagulation was observed earlier up to 5 W levels ($p<0.05$). After that value the behaviour of the tissues were observed to be same.

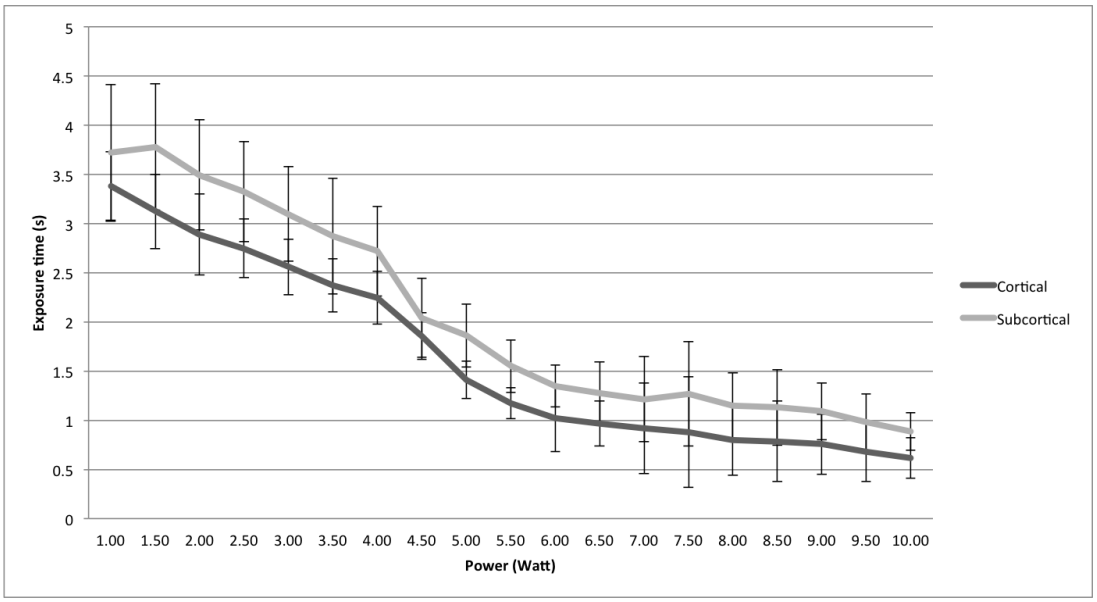

Figure 4.2 The carbonization onset time, when 980-nm diode laser was applied to cortical and subcortical tissue. The instances at which carbonization was observed, occurred earlier with increasing power. Even though there is not a statistically significant difference between the carbonization onset times for cortical and subcortical tissues, there is a trend of latency for the subcortical tissues.

microscopically. The ablation and coagulation diameters were measured and ablation efficiencies were calculated. Carbonization, which is an unwanted effect of photothermal laser application was not observed in any sample. Three-way ANOVA revealed that tissue type had affected ablation ($p<0.001$), coagulation ($p<0.001$) diameters and ablation

efficiencies ($p<0.001$), whereas varying energy delivery and the energy delivered to the tissue had effects on ablation diameters ($p<0.001$ and $p<0.001$) and ablation efficiencies ($p<0.001$ and $p<0.001$) but no effects on coagulation diameters ($p=0.600$ and $p=0.589$). Response of the cortical and subcortical tissues to the 980-nm diode laser, is discussed below in this perspective.

The thermal effects and ablation efficiencies of 980-nm diode laser with 3 J and 4 J energies on cortical and subcortical tissues were shown in Figures 4.3–4.6.

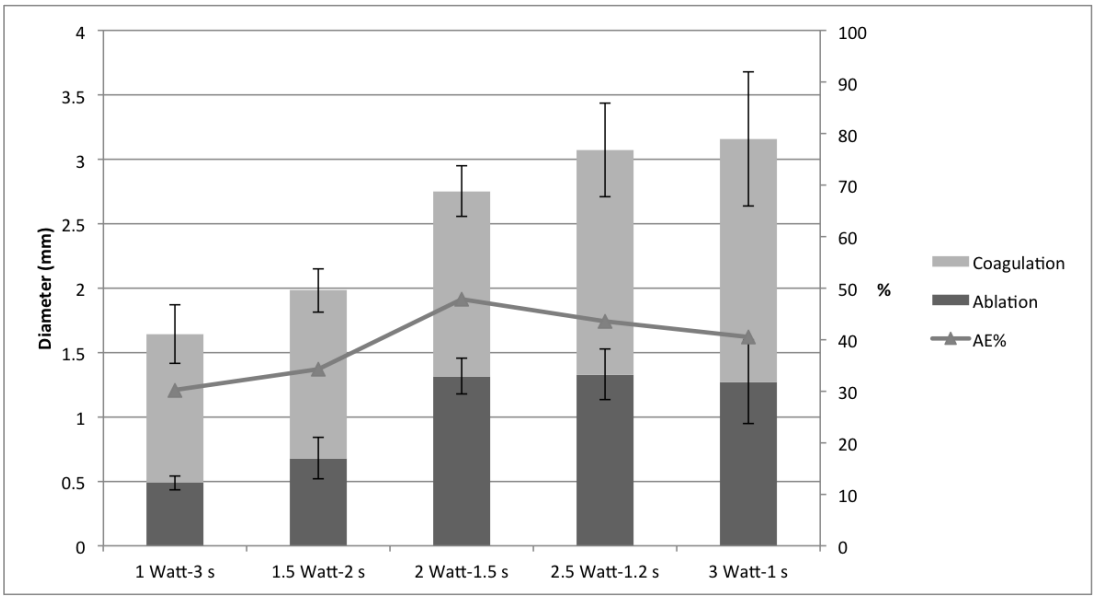

Figure 4.3 The thermal effects of 980-nm diode laser on cortical tissue at 3 Joules energy level (CD: Coagulation diameter, AD: Ablation diameter, AE: Ablation efficiency). Y1 axis and columns indicate the ablation and coagulation diameters, Y2 axis and line graph indicate the ablation efficiency values with respect to stated laser power. Ablation diameters and ablation efficiencies increased with increasing power up to 2 W and then reached a plateau ($p<0.001$ and $p<0.001$). On the other hand, coagulation diameters continued to increase with increasing power ($p<0.001$).

When 3 J of energy was applied on cortical tissues, ablated areas were increased with increasing power up to 2 W, but the coagulated areas remained almost same in that interval, which leads to an increase in ablation efficiencies up to that power. Beyond that point, histological analysis revealed no significant differences in terms of ablated areas. On the other hand with increasing power coagulated areas started to increase, which results in a slight decrease in efficiencies. When 4 J of energy was applied on cortical tissues, ablated areas increased with increasing power and coagulated areas remained almost same leading to an increase in efficiency. We observed a similar trend for subcortical tissues: ablated

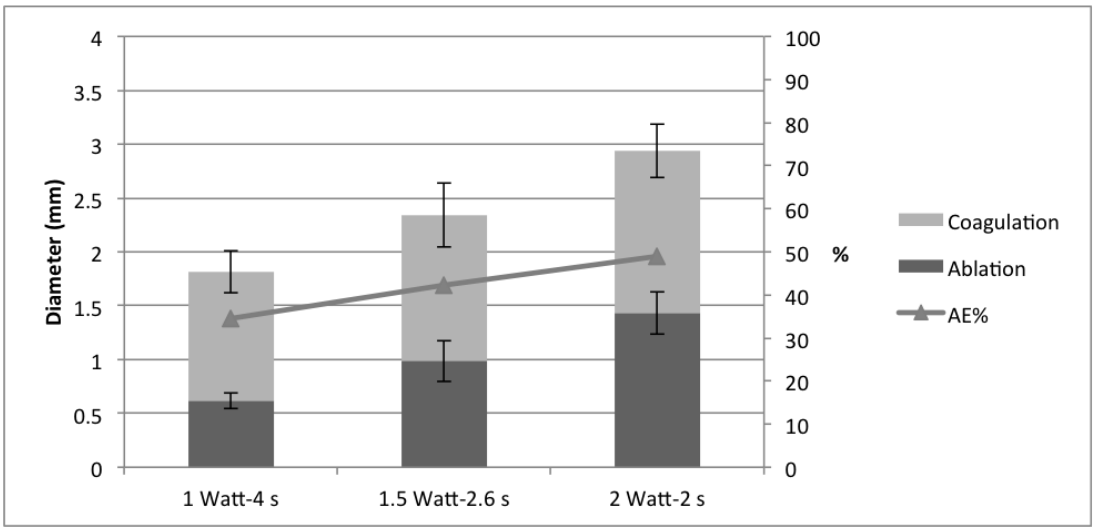

Figure 4.4 The thermal effects of 980-nm diode laser on cortical tissue at 4 Joules energy level (CD: Coagulation diameter, AD: Ablation diameter, AE: Ablation efficiency). Y1 axis and columns indicate the ablation and coagulation diameters, Y2 axis and line graph indicate the ablation efficiency values with respect to stated laser power. Ablation diameters increased with increasing power ($p<0.001$). There is an increasing trend in coagulation diameters ($p=0.067$). Ablation efficiencies also increased with increasing power ($p<0.001$).

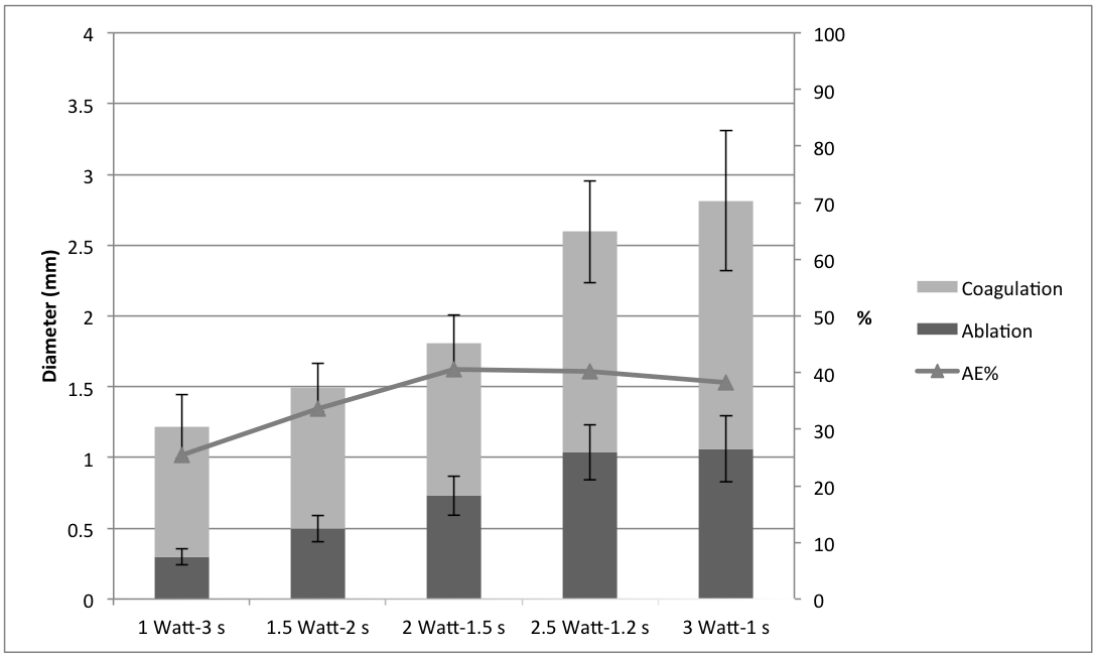

Figure 4.5 The thermal effects of 980-nm diode laser on subcortical tissue at 3 Joules energy level (CD: Coagulation diameter, AD: Ablation diameter, AE: Ablation efficiency). Y1 axis and columns indicate the ablation and coagulation diameters, Y2 axis and line graph indicate the ablation efficiency values with respect to stated laser power. Ablation and coagulation diameters increased with increasing power ($p<0.001$ and $p<0.001$) but the ablation efficiencies reached a plateau at 2 W ($p<0.001$).

areas were increased with increasing power up to 2.5 W this time and the coagulated areas remained almost same in that interval, which leads to an increase in ablation efficiencies up to that power. Beyond that point, ablated areas revealed no significant differences, but

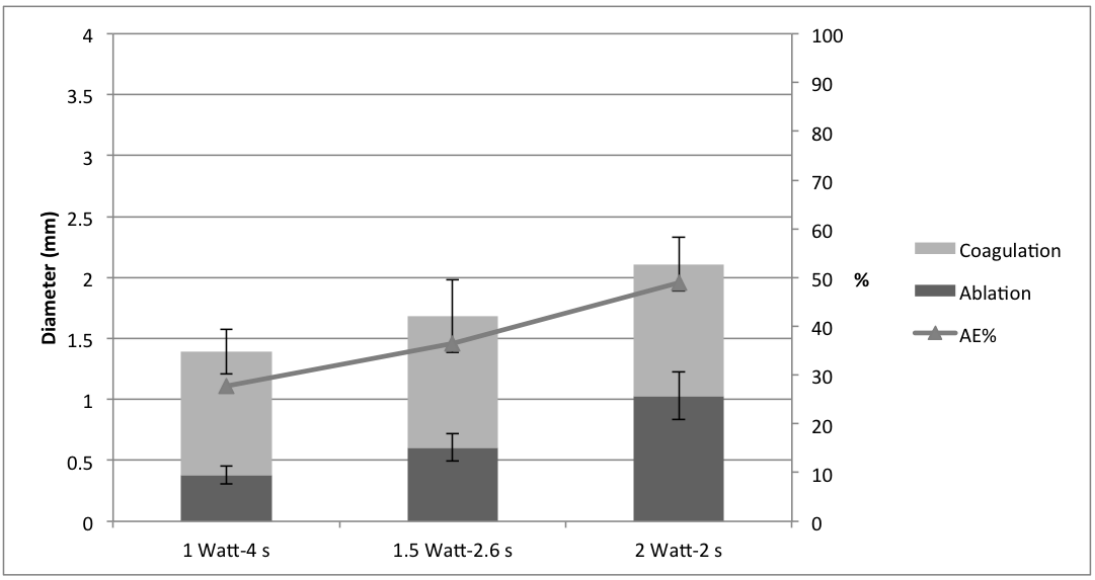

Figure 4.6 The thermal effects of 980-nm diode laser on subcortical tissue at 4 Joules energy level (CD: Coagulation diameter, AD: Ablation diameter, AE: Ablation efficiency). Y1 axis and columns indicate the ablation and coagulation diameters, Y2 axis and line graph indicate the ablation efficiency values with respect to stated laser power. Ablation diameters increased with increasing power ($p<0.001$) whereas coagulation diameters did not change ($p=0.809$). Ablation efficiencies also increased with increasing power ($p<0.001$).

the coagulated areas started to increase, which results in a slight decrease in efficiencies. When 4 J of energy was applied on subcortical tissues, ablated areas increased with increasing power and coagulated areas remained same leading to an increase in efficiency. It was also observed that lesions created in cortical tissues were bigger than the lesion created in subcortical tissues in general.

In summary, according to histological examinations the highest ablation efficiencies were obtained for 2 W-1.5 s and 2 s applications regardless of the tissue type. Secondly, subcortical and cortical tissue responses to the 980-nm diode laser were found to be similar in trend but statistically different from each other.

During laser applications temperature of the nearby tissue was measured with the thermoprobe. Results were given in Figures 4.7–4.10 and rate of temperature changes were calculated and plotted in Figures 4.11–4.14.

The thermoprobe recorded the temperature values 0.5-mm away from the laser fiber tip. The time response of the thermocouple used in the present study was 0.1 s.

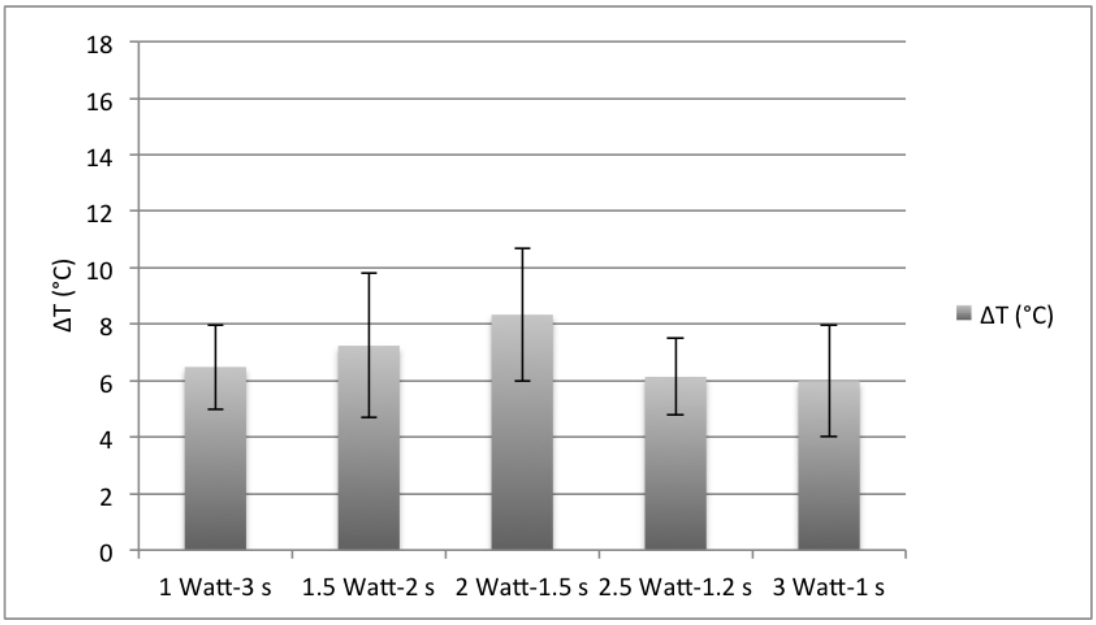

Figure 4.7 Temperature change for 3 J, 980-nm diode laser *ex vivo* study groups for cortical tissues. Even though there is a increasing trend in temperature change up to 2 W application, there are no statistically significant differences (p=0.136).

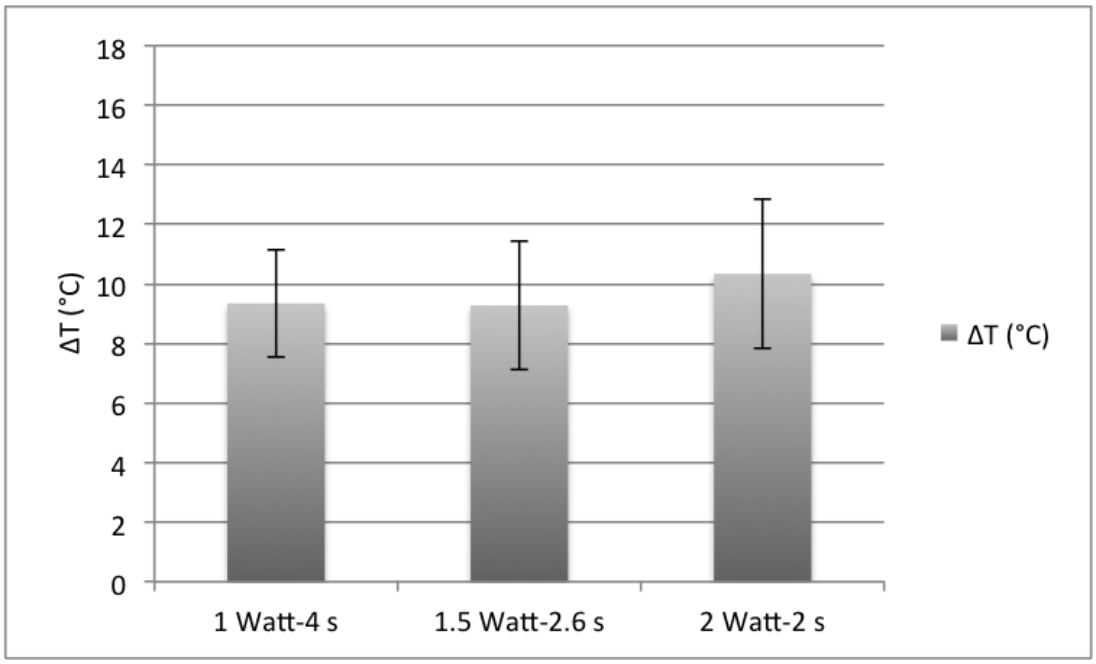

Figure 4.8 Temperature change for 4 J, 980-nm diode laser *ex vivo* study groups for cortical tissues. There is no significant difference in changes of temperature (p=0.560).

Fortunately, the nearby temperature measurement of the thermoprobe served as a good indicator of the photothermal effect; a strong correlation between the rate of temperature change and ablation efficiencies were found.

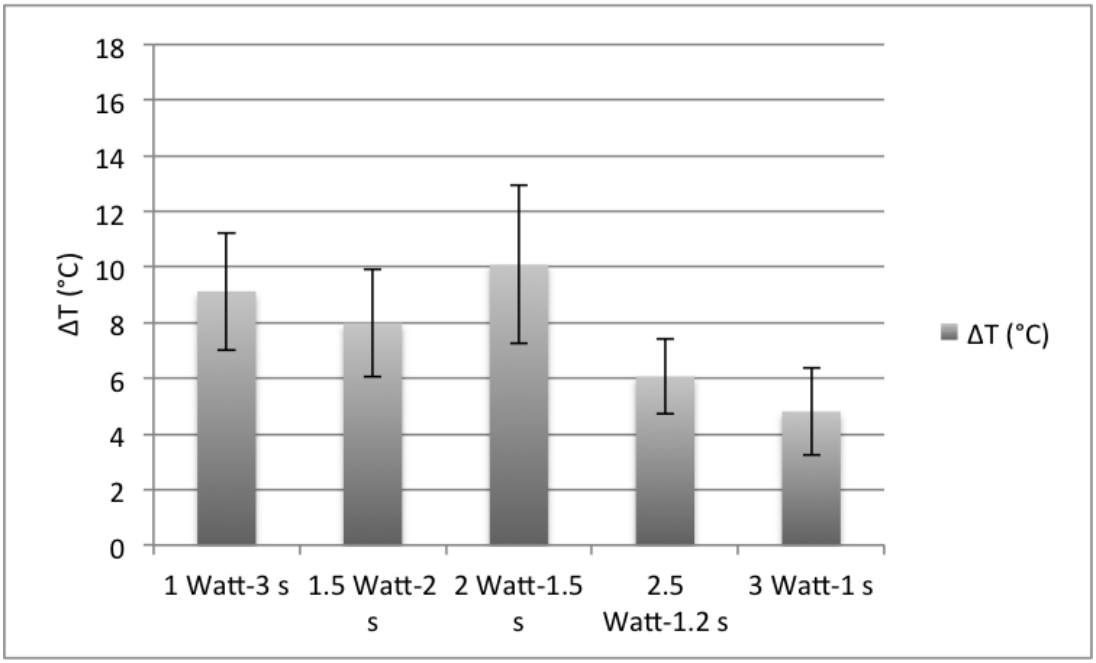

Figure 4.9 Temperature change for 3 J, 980-nm diode laser *ex vivo* study groups for subcortical tissues. There is an irregular but significant decrease in temperature change ($p<0.001$) with increasing power. The biggest temperature change was observed at 2 W-1.5 s application.

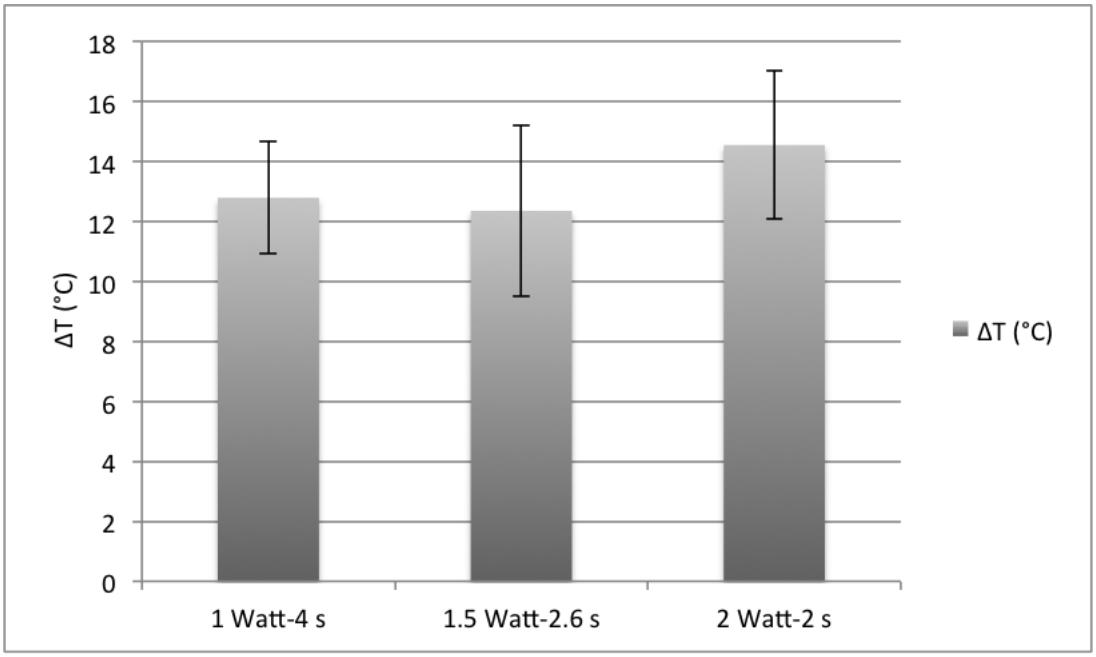

Figure 4.10 Temperature change for 4 J, 980-nm diode laser *ex vivo* study groups for subcortical tissues. There is no significant difference in changes of temperature ($p=0.188$).

The relationship between the ablation efficiencies and rate of temperature change with respect to varying energy delivery for cortical and subcortical tissues was shown in Figure 4.15. Data were presented as the change in ablation efficiency versus rate of temperature change over time. It was found that higher the rate of temperature change

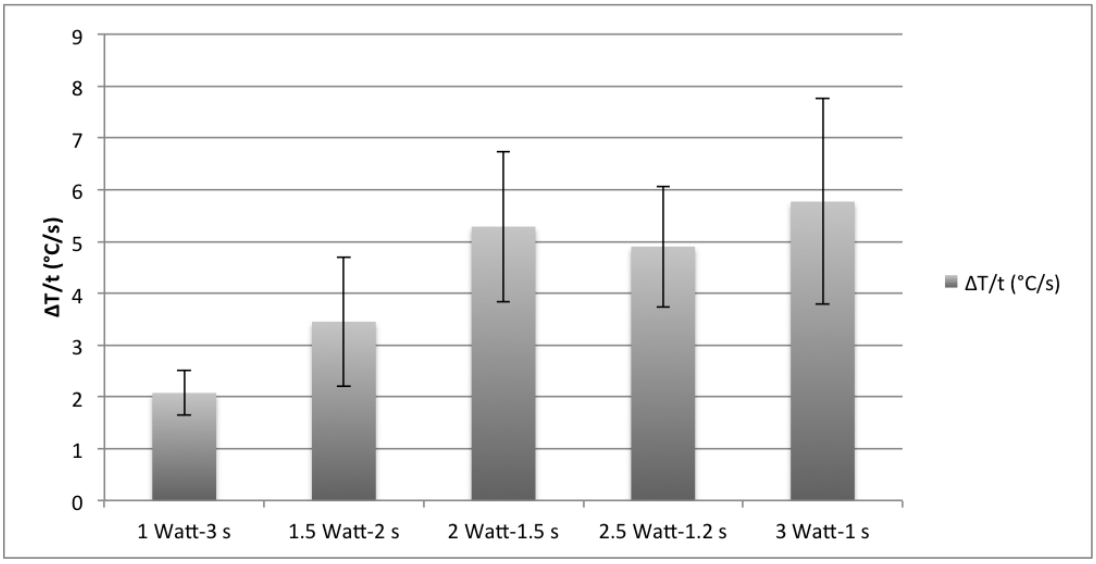

Figure 4.11 Rate of temperature change for 3 J, 980-nm diode laser *ex vivo* study groups for cortical tissues. Rates increased up to 2 W and then reached a plateau ($p<0.001$).

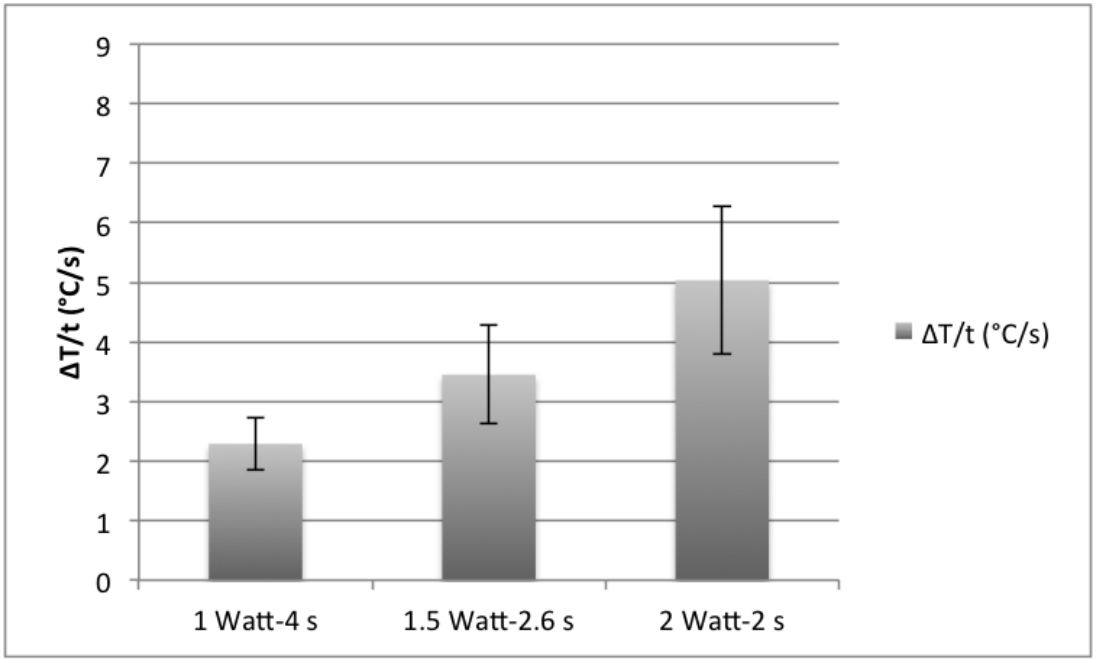

Figure 4.12 Rate of temperature change for 4 J, 980-nm diode laser *ex vivo* study groups for cortical tissues. Rates increased with increasing power ($p<0.001$), where the maximum rate of temperature change was observed at 2 W-2 s.

over time yielded higher ablation efficiency. 50% ablation efficiency was depicted with a horizontal line, above that level was defined as a success for ablation. By analyzing those graphs it can be obviously seen that the number of samples with higher ablation efficiencies for cortical tissue is much more than subcortical tissue. This analysis can help us to estimate the ablation efficiency of the applied laser procedure with respect to the

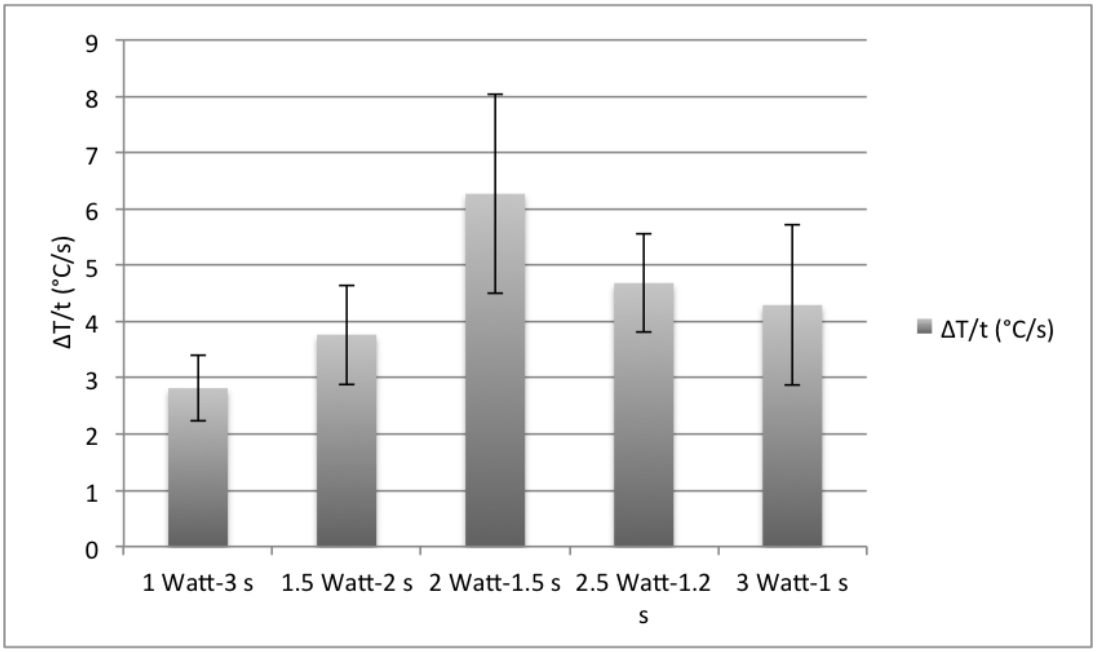

Figure 4.13 Rate of temperature change for 3 J, 980-nm diode laser *ex vivo* study groups for subcortical tissues. Rates first increased and then decreased with increasing power, peaking at 2 W-1.5 s application ($p<0.001$).

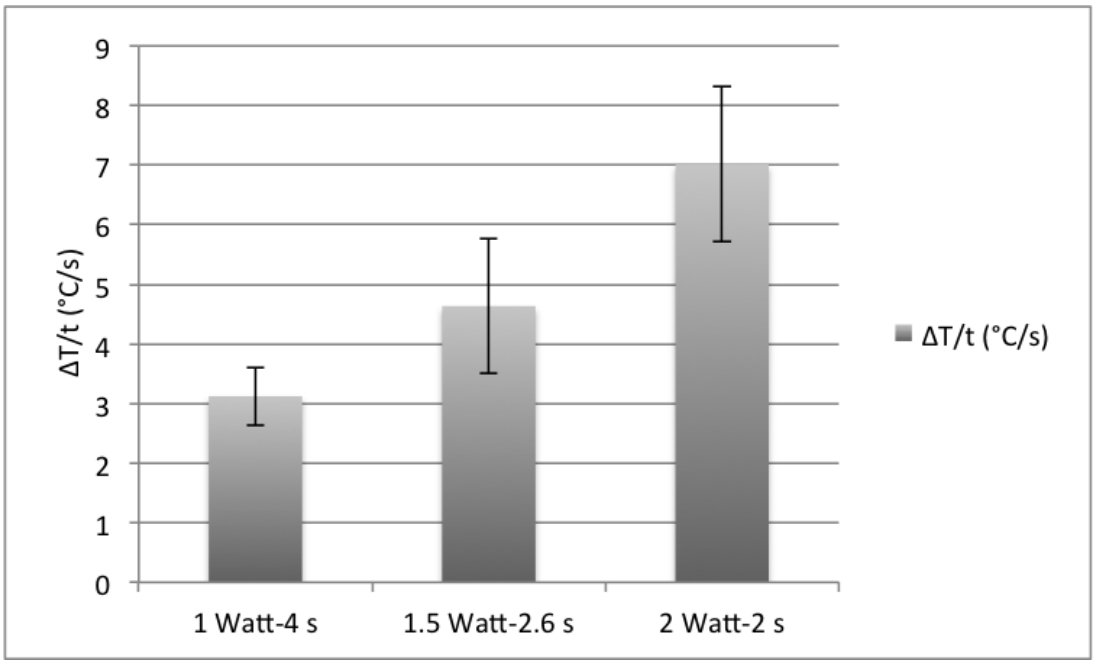

Figure 4.14 Rate of temperature change for 4 J, 980-nm diode laser *ex vivo* study groups for subcortical tissues. Rates increased with increasing power ($p<0.001$), where the maximum rate of temperature change was observed at 2 W-2 s.

tissue type. Spearman's rank correlation coefficients revealed a strong correlation between ablation efficiencies and rate of temperature change over time with ρ=0.81 and 0.84 for cortical and subcortical tissues respectively.

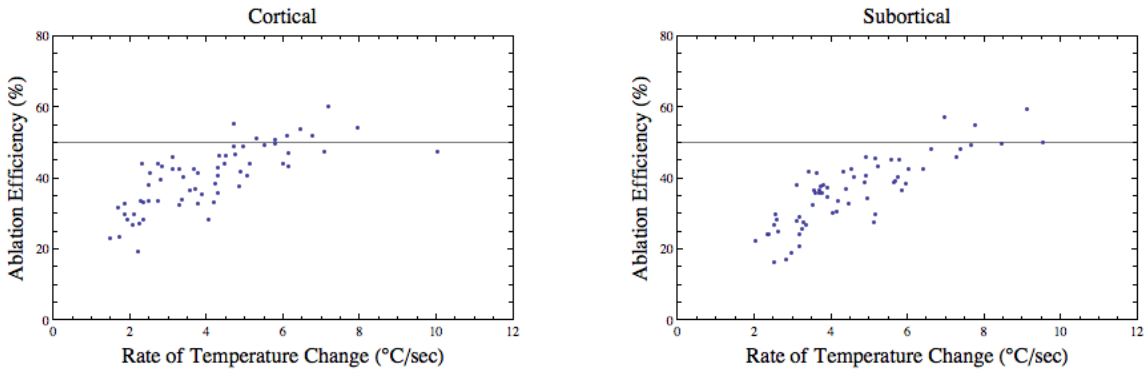

Figure 4.15 The ablation efficiencies as a function of rates of temperature change of the samples of cortical (left) and subcortical tissue (right). The right hand side of the vertical lines indicates the samples with carbonization, and the upper region of the horizontal lines indicates the samples, in which higher ablation efficiencies were succeeded

4.2 Laser Brain ablation with 1070-nm fiber laser; *ex vivo* experiments

Objective of this study was to examine the ablation capability of 1070-nm Ytterbium Fiber Laser (YLF) *ex vivo* and the determine the most proper laser dose in order to ablate cortical and subcortical tissue. A predosimetric study was performed before the *ex vivo* dosimetry study. The same methodology was followed as in 980-nm diode laser. The results of the predosimetric study performed by 1070-nm fiber laser had been shown in Figures 4.16 and 4.17. Figures 4.16 and 4.17 show the coagulation and carbonization onset time respectively, when 1070-nm fiber laser was applied to cortical and subcortical tissue. When we perform *ex vivo* study with 1070-nm fiber laser according to the result of the predosimetric studies, it was seen that this laser is not capable to vaporize the tissue. Hence, it is decided not to continue to investigate the effects of this laser on *in vivo* studies. The coagulation capabilities of 1070-nm fiber laser were shown in Figure 4.18.

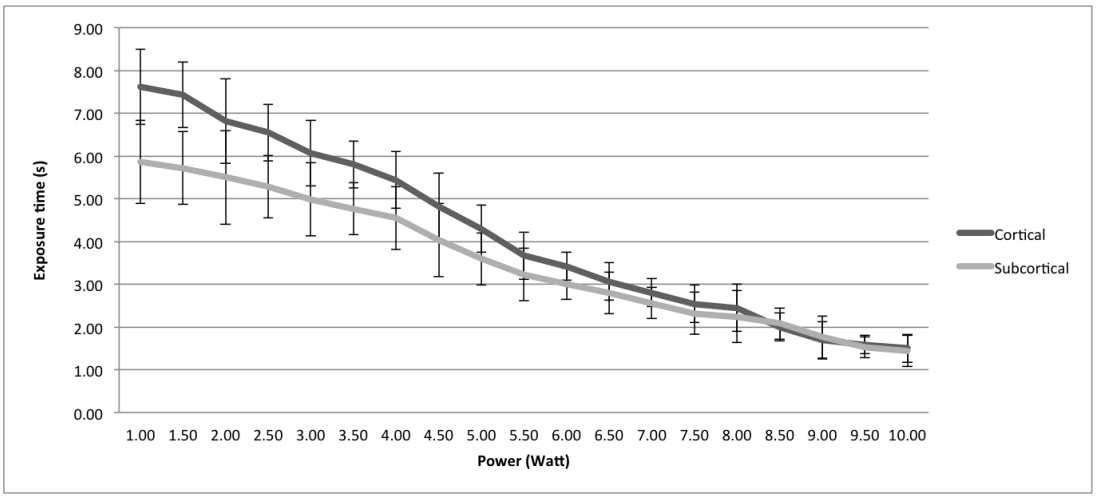

Figure 4.16 The coagulation onset time, when 1070-nm fiber laser was applied to cortical and subcortical tissue. The instances at which coagulation was observed, occurred earlier with increasing power. In subcortical tissues, coagulation was observed earlier up to 4 W levels ($p<0.05$). After that value the behaviour of the tissues were observed to be same.

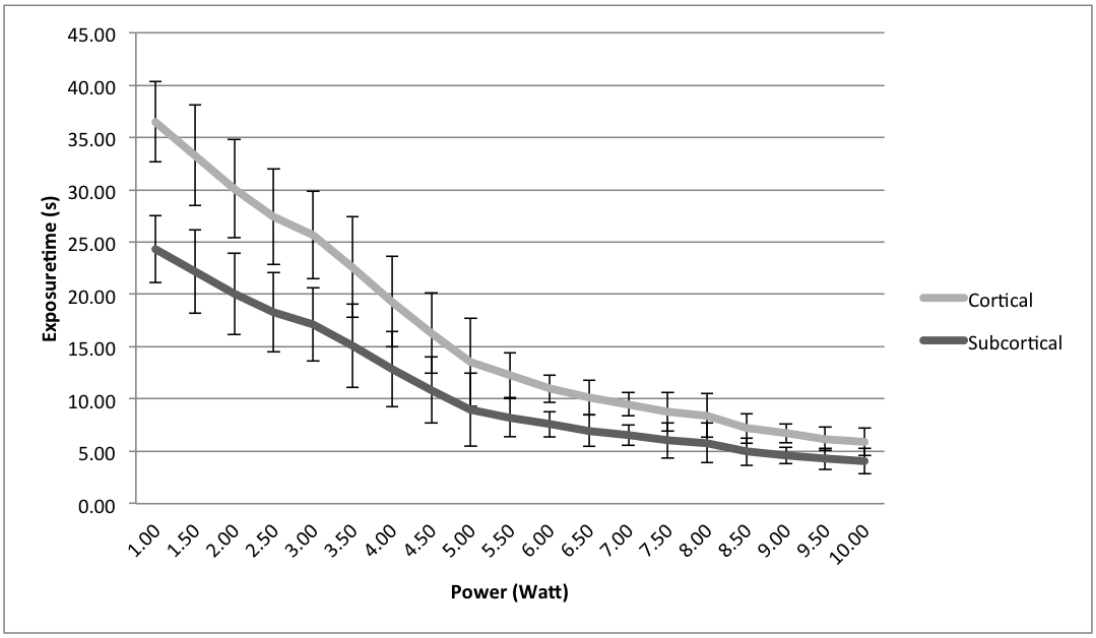

Figure 4.17 The carbonization onset time, when 1070-nm fiber laser was applied to cortical and subcortical tissue. The instances at which carbonization was observed, occurred earlier with increasing power. There is a statistically significant latency for the subcortical tissues.

4.3 Laser Brain ablation with 1940-nm Tm:Fiber laser; *ex vivo* experiments

Thulium doped around 2 μm wavelength lasers with silica based fiber have an important role in various minimally invasive surgeries. 1940-nm Tm:fiber lasers have great advantage in treating soft-tissues due to the high absorption coefficient of water

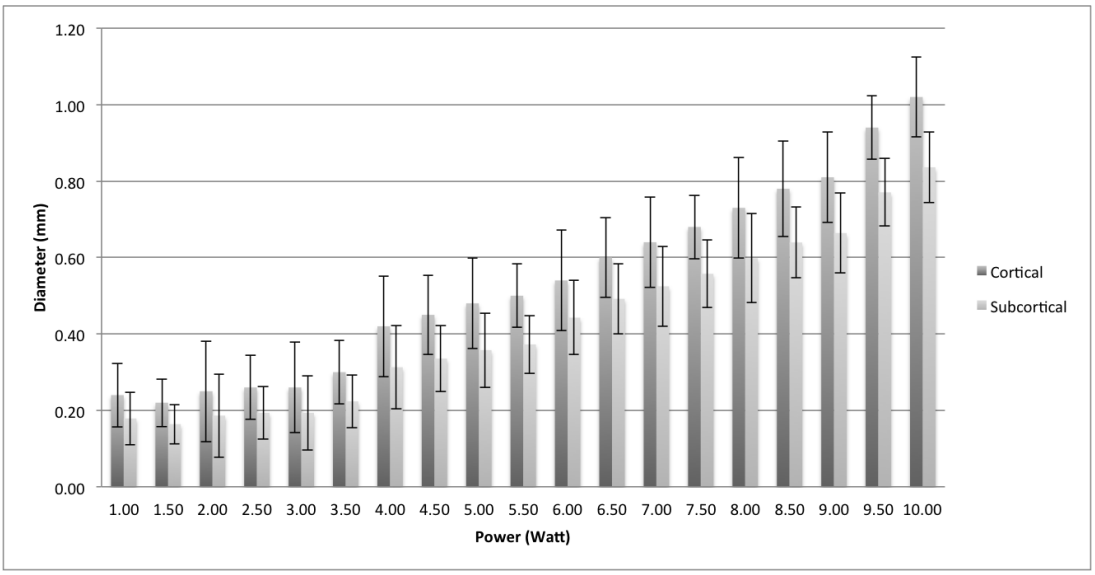

Figure 4.18 The coagulation diameters of cortical and subcortical tissue with respect to power 1070-nm fiber laser. The coagulation diameters increased with increasing power, where diameters in cortical tissues were bigger than the ones in subcortical tissues ($p<0.05$).

at that wavelength [140]. A study of dose determination was performed to find the optimal parameters that provide less thermal damage to the surrounding healthy tissue. The maximum output of this laser is 5 W as mentioned before. In order to find which parameters are more suitable for brain ablation, a predosimetric study was performed with same method as in 980-nm diode laser.

The predosimetric study performed by 1940-nm Tm:Fiber laser had been shown in Figures 4.19 and 4.20. Figures 4.19 and 4.20 show the coagulation and carbonization onset time respectively, when 1940-nm Tm:Fiber laser was applied to cortical and subcortical tissue. According to these results it is obvious that carbonization occurs immediately, when the power of the laser light is greater than the 800 milliwatts.

Dose determination study was performed, after the predosimetric study. Histological examinations were performed. The same methodology was used as in 980-nm diode laser experiments. The ablation and coagulation diameters were measured under light microscope and the ablation efficiencies were calculated. Four-way analysis of variance revealed that ablation and coagulation diameters were differentiated with all four parameters: laser power ($p<0.001$), tissue type ($p<0.001$), laser mode ($p<0.001$) and energy density ($p<0.001$). Changing the laser power, energy density, tissue type, and mode of

laser delivery can lead to dramatical changes within the ablation and coagulation diameters. The response of the cortical and subcortical tissue to the Tm:fiber laser is discussed below in this perspective.

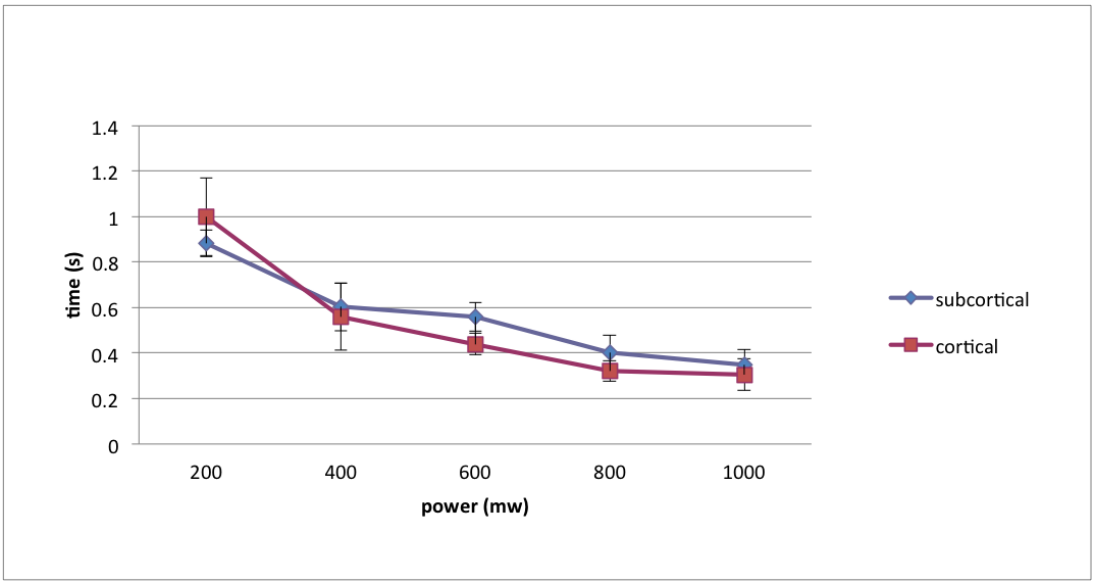

Figure 4.19 The coagulation onset time, when 1940-nm Tm:fiber laser was applied to cortical and subcortical tissue. The instances at which coagulation was observed, occurred earlier with increasing power, regardless of tissue type.

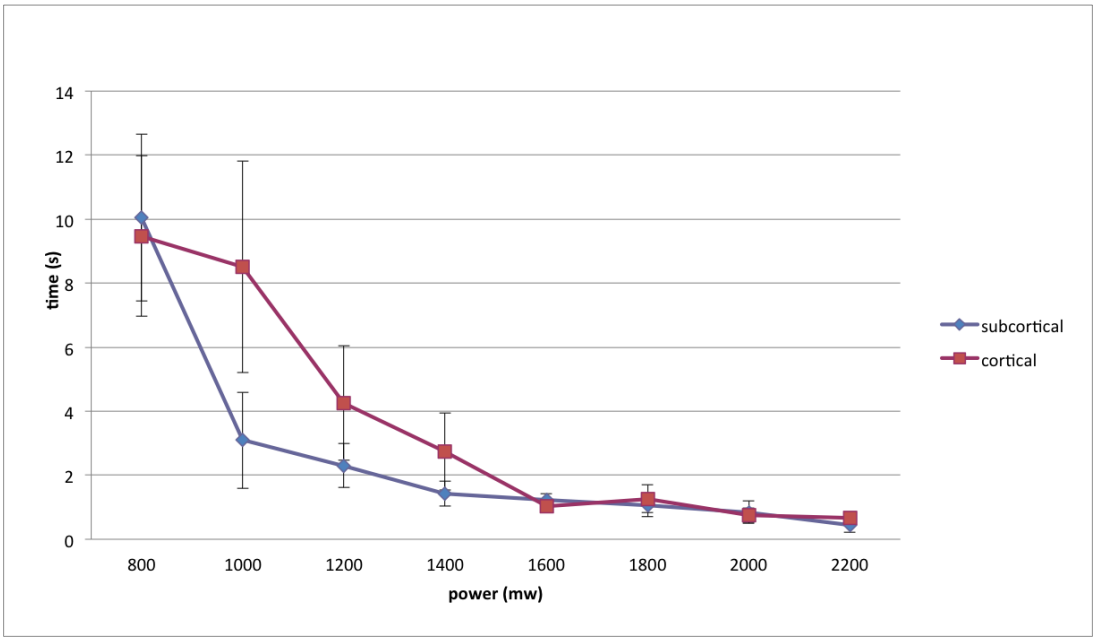

Figure 4.20 The carbonization onset time, when 1940-nm Tm:fiber laser was applied to cortical and subcortical tissue. The instances at which carbonization was observed, occurred earlier with increasing power. High power applications resulted in similar carbonization instances for both tissue types, but earlier instances were observed for subcortical tissues at lower powers ($p<0.001$).

Mean ablation and coagulation diameters for cortical tissues with 2 J and 4 J energy delivered were shown in Figure 4.21 and Figure 4.22, respectively. Ablation efficiencies

were also shown within the same figure. Diameters of total thermal damage and ablations were increased with increasing power for all types of applications except lower doses (200 and 400-mW) of p-m-m. Significant differences were also found with respect to the mode (c-m or p-m-m) for the same power and energy applied: c-m applications yielded more photothermal effect and more ablation (except lower doses). Then the ablation efficiencies were calculated in order to develop a better description for the laser application. It was defined as the ratio of ablation to the total thermal damage. It was found that ablation efficiencies were also significantly higher for the c-m laser applications.

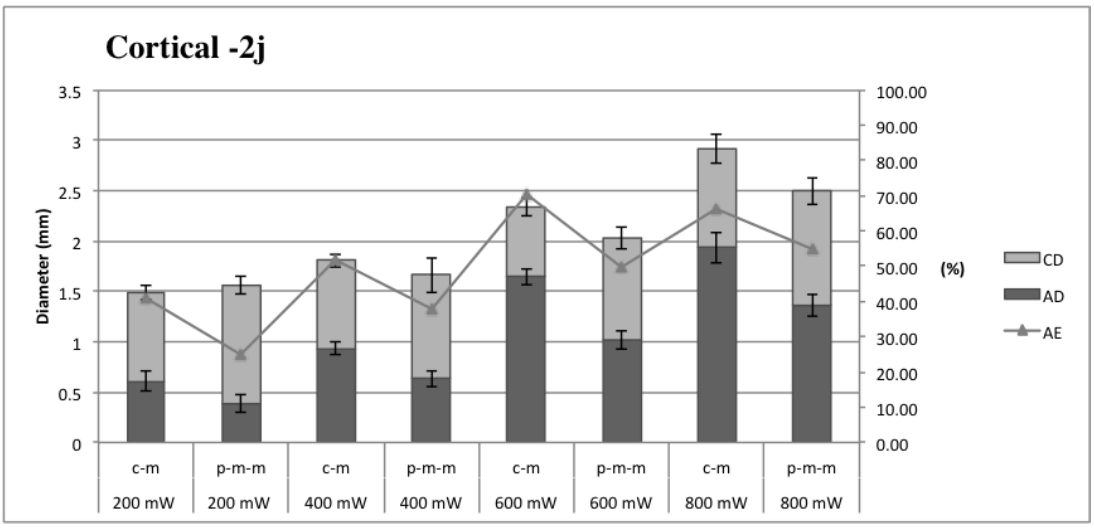

Figure 4.21 The thermal effects of 1940-nm Tm:fiber laser on cortical tissue at 2 joules energy level (CD: Coagulation diameter, AD: Ablation diameter, AE: Ablation efficiency). Y1 axis and columns indicate the ablation and coagulation diameters, Y2 axis and line graph indicate the ablation efficiency values with respect to stated laser power and mode. To switch the mode of operation from continuous to pulsed-modulated-mode decreased the ablation diameters and ablation efficiencies ($p<0.001$). Ablation diameters increased with increasing powers ($p<0.001$). The highest ablation efficiencies were achieved for 600 mW and 800 mW, but at 800 mW applications, carbonization was observed around the ablated area.

The thermal response of the subcortical tissue to the Tm:fiber laser was found similar to the cortical tissue (Figure 4.23 and Figure 4.24). However all the diameter values of subcortical tissue were significantly less then the corresponding ones of the cortical tissue ($p<0.001$). The result of the changing the mode of laser delivery from continuous to pulsed-modulated-mode was also similar for subcortical tissue experiments at both 2 and 4 joules experiments. Ablation and coagulation diameters were increased as the power levels increased. The most dramatic increase in ablation diameters were observed at 600 mW laser experiments ($p<0.001$ when compared to both 200 mW and 400 mW experiments) regardless of laser delivery mode.

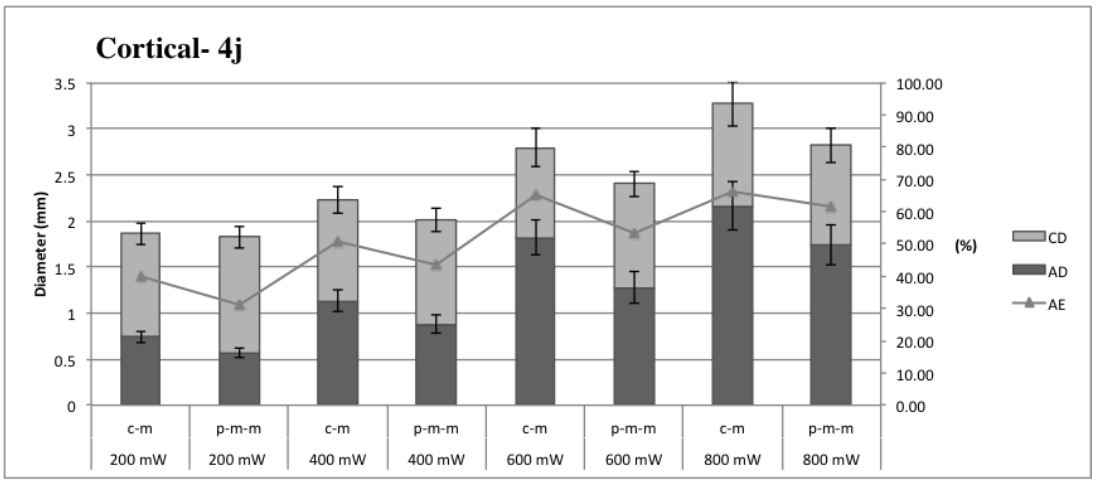

Figure 4.22 The thermal effects of 1940-nm Tm:fiber laser on cortical tissue at 4 joules energy level (CD: Coagulation diameter, AD: Ablation diameter, AE: Ablation efficiency). Y1 axis and columns indicate the ablation and coagulation diameters, Y2 axis and line graph indicate the ablation efficiency values with respect to stated laser power and mode. To switch the mode of operation from continuous to pulsed-modulated-mode decreased the ablation diameters and ablation efficiencies ($p<0.001$). Ablation diameters increased with increasing powers ($p<0.001$). The highest ablation efficiencies were achieved for 600 mW and 800 mW, but at 800 mW applications, carbonization was observed around the ablated area.

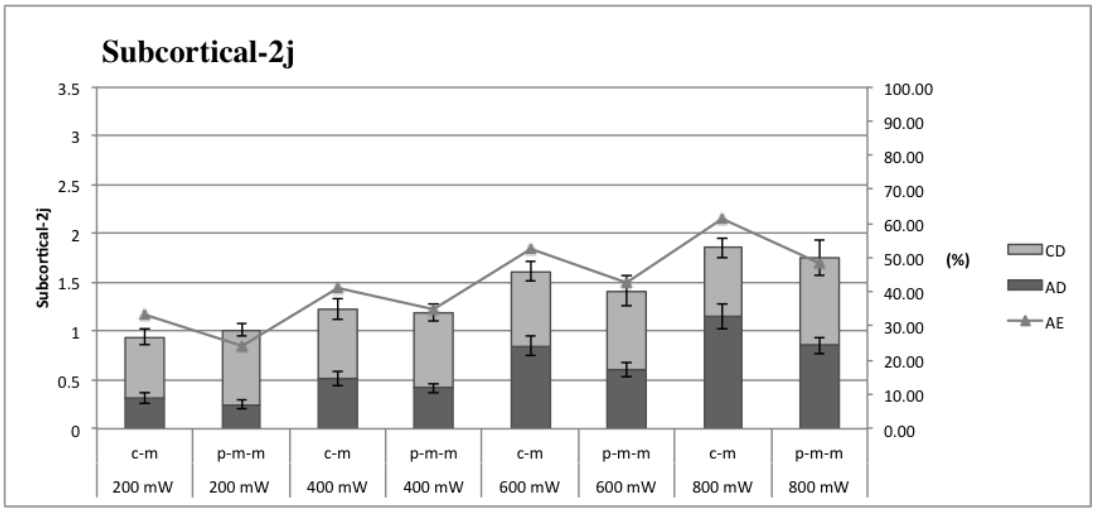

Figure 4.23 The thermal effects of 1940-nm Tm:fiber laser on subcortical tissue at 2 joules energy level (CD: Coagulation diameter, AD: Ablation diameter, AE: Ablation efficiency). Y1 axis and columns indicate the ablation and coagulation diameters, Y2 axis and line graph indicate the ablation efficiency values with respect to stated laser power and mode. To switch the mode of operation from continuous to pulsed-modulated-mode decreased the ablation diameters and ablation efficiencies ($p<0.001$). Ablation diameters increased with increasing powers ($p<0.001$). The highest ablation efficiencies were achieved for 600 mW and 800 mW, but at 800 mW applications, carbonization was observed around the ablated area.

In summary regardless of the tissue type, for lower laser power (200 and 400 mW) applications changing the laser delivery mode did not result significant differences in total thermal damage but resulted differences in terms of ablation with greater efficiency for the c-m. Secondly, subcortical and cortical tissue responses to the Tm:fiber laser found

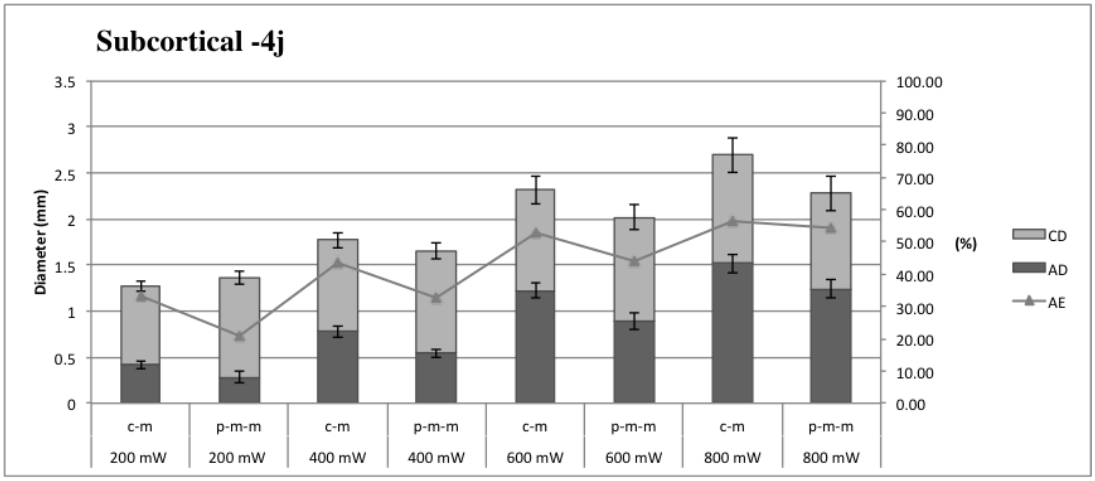

Figure 4.24 The thermal effects of 1940-nm Tm:fiber laser on subcortical tissue at 4 joules energy level (CD: Coagulation diameter, AD: Ablation diameter, AE: Ablation efficiency). Y1 axis and columns indicate the ablation and coagulation diameters, Y2 axis and line graph indicate the ablation efficiency values with respect to stated laser power and mode. To switch the mode of operation from continuous to pulsed-modulated-mode decreased the ablation diameters and ablation efficiencies ($p<0.001$). Ablation diameters increased with increasing powers ($p<0.001$). The highest ablation efficiencies were achieved for 600 mW and 800 mW, but at 800 mW applications, carbonization was observed around the ablated area.

to be statistically different for all experiments ($p<0.001$). Increasing power values of the Tm:fiber laser resulted with higher ablation and coagulation diameters regardless of delivery mode. It is observed that ablation efficiencies were higher for higher power levels. Even though the transferred total energy was doubled the thermally altered zones did not doubled, a slight increase in the thermally altered area was seen. Besides a threshold for the laser power (800 mW) was found; laser power greater than 800 mW lead to carbonization in all experiments performed for both tissue types.

During laser applications, temperature of the near-by tissue was measured with the thermoprobe. Results were given in Figures 4.25–4.28 and rate of temperature changes were calculated and plotted in Figures 4.29–4.32.

The thermoprobe recorded the temperature values 0.5-mm away from the laser fiber tip. The observed temperature values were small compared to the theoretical values. In order to observe tissue vaporization or ablation with continuous wave laser, tissue temperature must be increased by 100°C and over [19,141–143]. But photothermal interaction is a very fast (thermal response of the tissue to the laser irradiation on the nanosecond levels [97]) and very localized process; thus, it is almost impossible to measure the exact

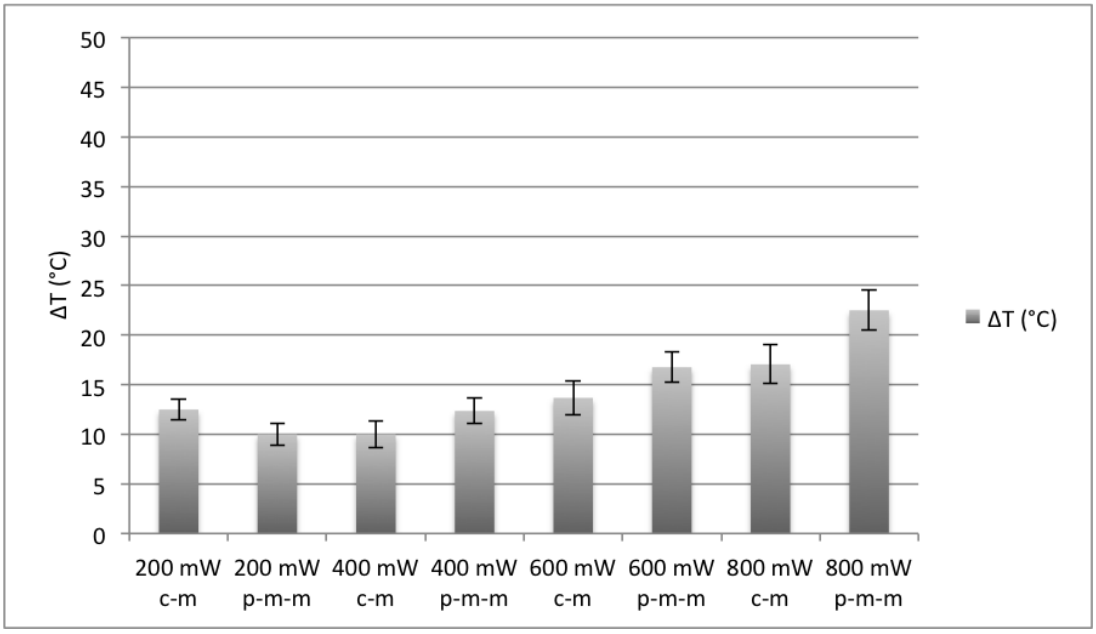

Figure 4.25 Temperature change for 2 J, 1940-nm diode laser *ex vivo* study groups for cortical tissues. Switching from continuous to pulsed-modulated-mode resulted in a higher temperature increase except for the 200 mW ($p<0.05$). Higher temperature increases were observed with increasing power, except for the change from 200 mW to 400 mW in continuous mode ($p<0.05$). Highest temperatures were observed at 800 mW applications.

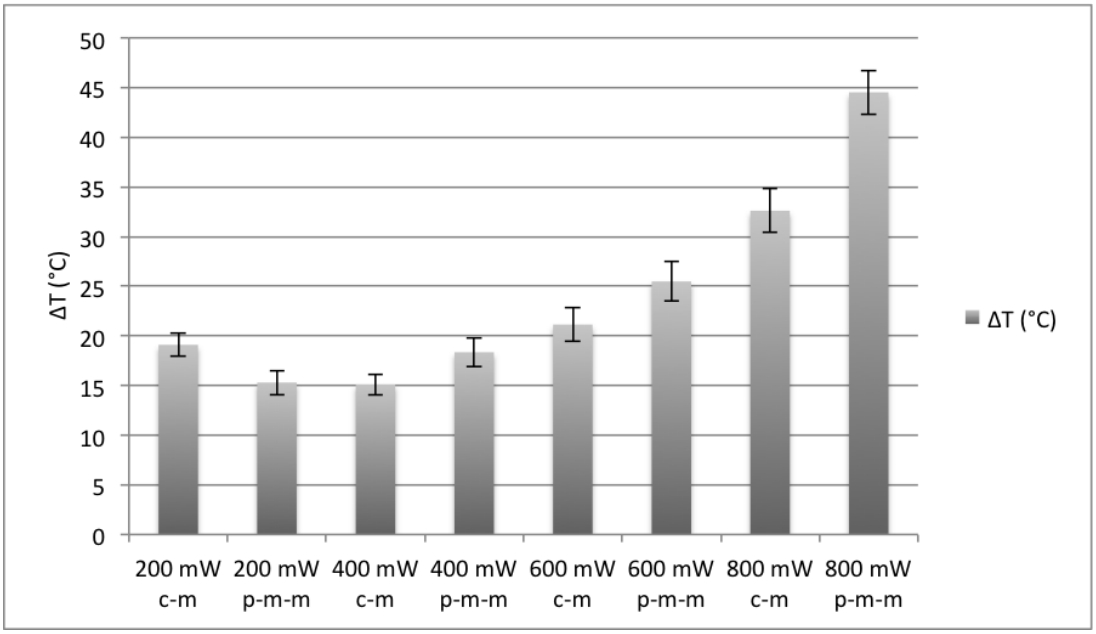

Figure 4.26 Temperature change for 4 J, 1940-nm diode laser *ex vivo* study groups for cortical tissues. Switching from continuous to pulsed-modulated-mode resulted in a higher temperature increase except for the 200 mW ($p<0.001$). Higher temperature increases were observed with increasing power, except for the change from 200 mW to 400 mW in continuous mode ($p<0.001$). Highest temperatures were observed at 800 mW applications.

temperature rise in real-time with thermocouples because of the high thermal conductivity of the tissue. The time response of the thermocouple used in the present study was 0.1

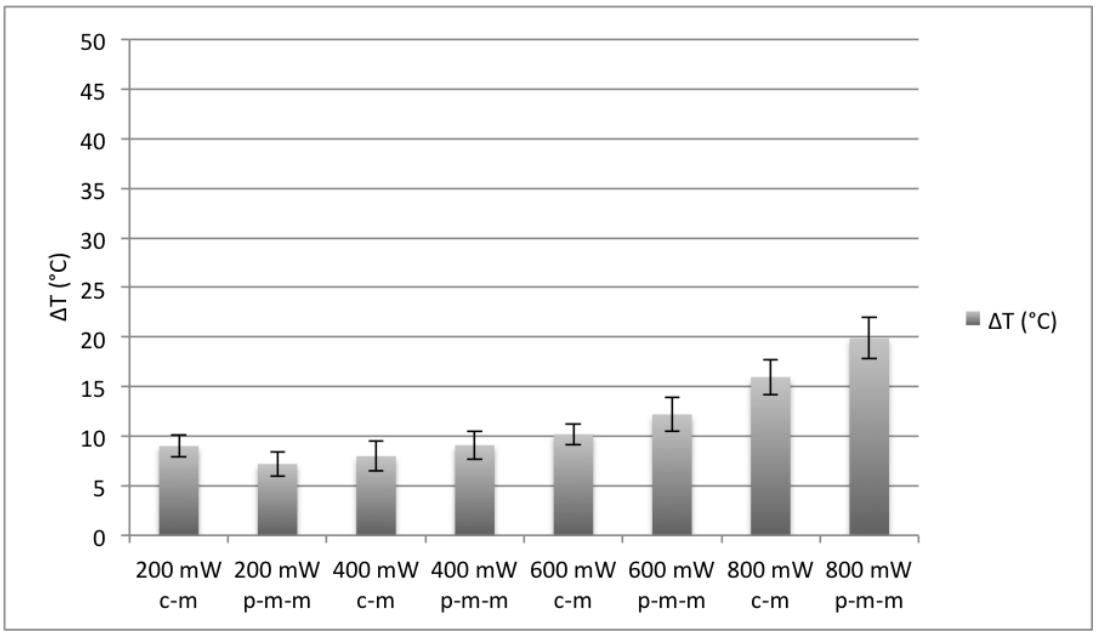

Figure 4.27 Temperature change for 2 J, 1940-nm diode laser *ex vivo* study groups for subcortical tissues. Switching from continuous to pulsed-modulated-mode resulted in a higher temperature increase except for the 200 mW ($p<0.05$). Higher temperature increases were observed with increasing power, except for the change from 200 mW to 400 mW in continuous mode ($p<0.05$). Highest temperatures were observed at 800 mW applications.

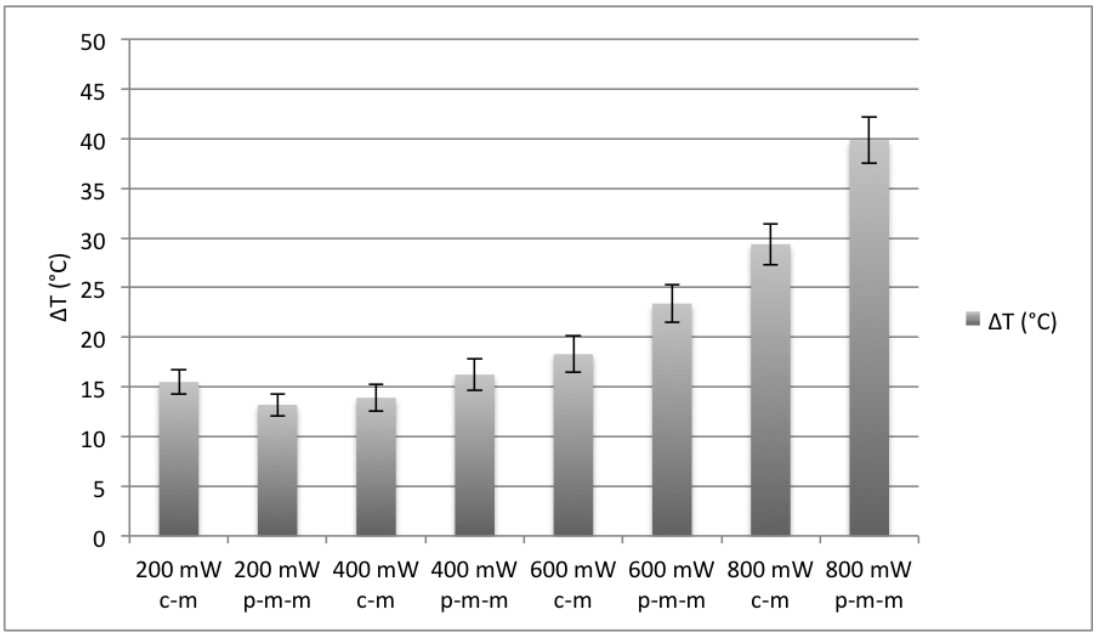

Figure 4.28 Temperature change for 4 J, 1940-nm diode laser *ex vivo* study groups for subcortical tissues. Switching from continuous to pulsed-modulated-mode resulted in a higher temperature increase except for the 200 mW ($p<0.001$). Higher temperature increases were observed with increasing power, except for the change from 200 mW to 400 mW in continuous mode ($p<0.001$). Highest temperatures were observed at 800 mW applications.

seconds. Fortunately, the near-by temperature measurement of the thermoprobe served as a good indicator of the photothermal effect; a strong correlation between the rate of

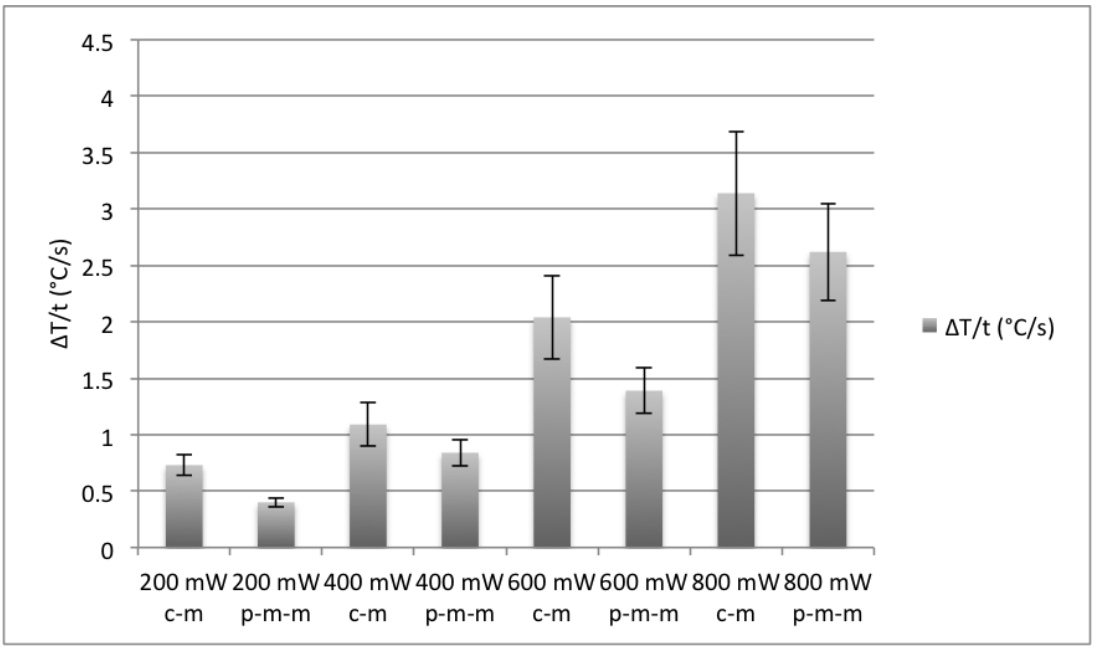

Figure 4.29 Rate of temperature change for 2 J, 1940-nm diode laser *ex vivo* study groups for cortical tissues. Switching from continuous to pulsed-modulated-mode resulted in a higher temperature rate ($p<0.001$). Rate of temperature change increased with increasing power ($p<0.001$). Highest rates were observed at 800 mW applications.

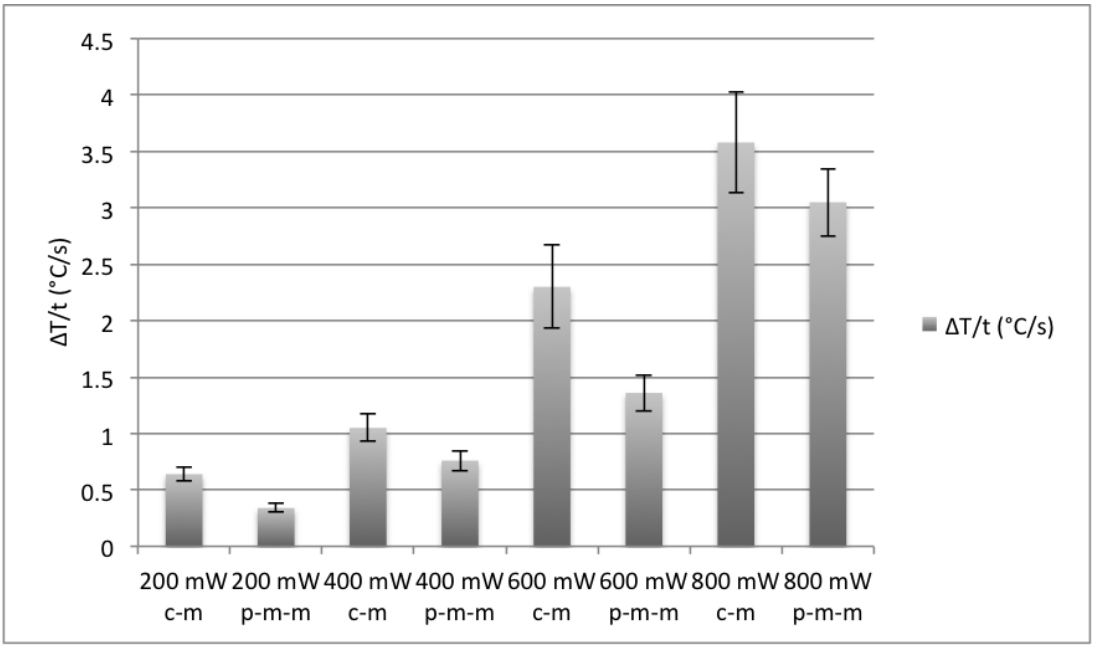

Figure 4.30 Rate of temperature change for 4 J, 1940-nm diode laser *ex vivo* study groups for cortical tissues. Switching from continuous to pulsed-modulated-mode resulted in a higher temperature rate ($p<0.001$). Rate of temperature change increased with increasing power ($p<0.001$). Highest rates were observed at 800 mW applications.

the temperature change and ablation efficiencies were found.

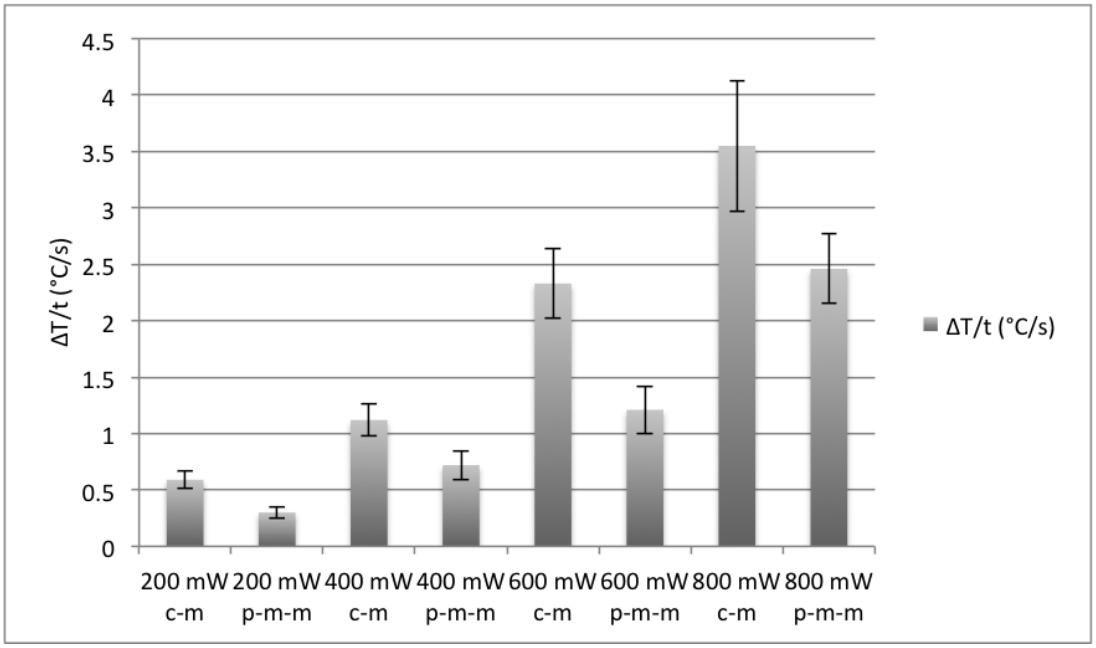

Figure 4.31 Rate of temperature change for 2 J, 1940-nm diode laser *ex vivo* study groups for subcortical tissues. Switching from continuous to pulsed-modulated-mode resulted in a higher temperature rate ($p<0.001$). Rate of temperature change increased with increasing power ($p<0.001$). Highest rates were observed at 800 mW applications.

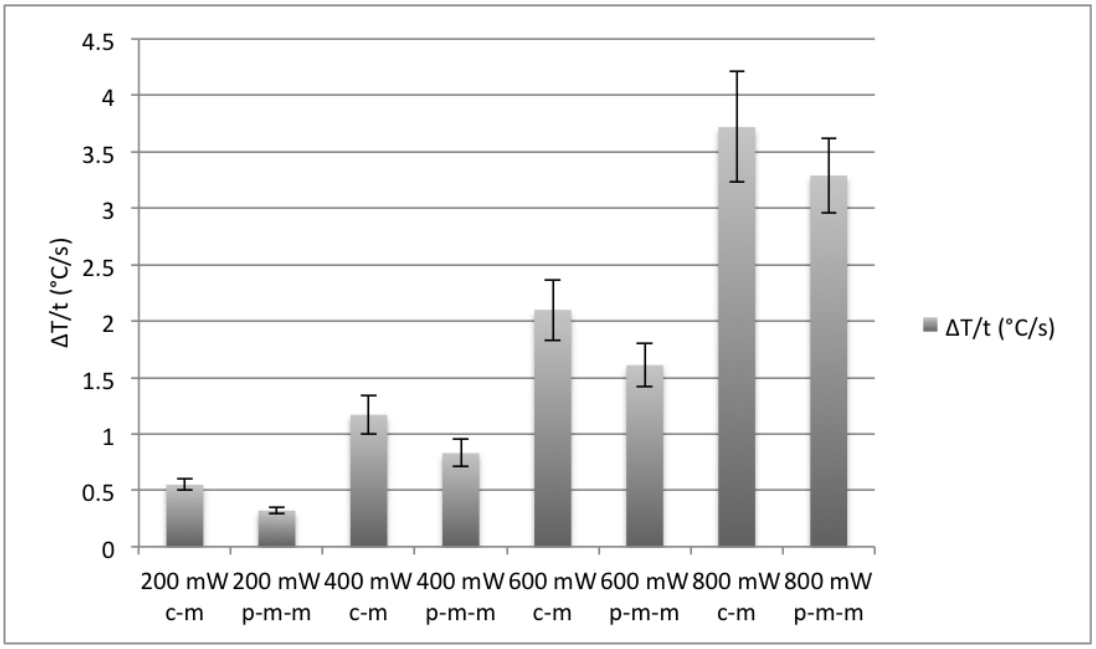

Figure 4.32 Rate of temperature change for 4 J, 1940-nm diode laser *ex vivo* study groups for subcortical tissues. Switching from continuous to pulsed-modulated-mode resulted in a higher temperature rate ($p<0.001$). Rate of temperature change increased with increasing power ($p<0.001$). Highest rates were observed at 800 mW applications.

The relationship between the ablation efficiencies and rate of temperature change with respect to the mode of laser delivery for cortical and subcortical tissues was shown

in the Figure 4.33. Data were presented as the change in ablation efficiency versus rate of temperature change over time. It was found that higher the rate of temperature change over time yielded higher ablation efficiency up to a certain threshold value. That threshold was shown with a vertical line on the graph and it represents the carbonization onset. 50% ablation efficiency was also depicted with a horizontal line, above that level was defined as a success for ablation. By analyzing those graphs, it can be obviously seen that the number of samples with higher ablation efficiencies for cortical tissue is much more than subcortical tissue and changing the laser delivery mode from c-m to p-m-m decreases the number of samples with higher ablation efficiencies. This analysis can help us to estimate the ablation efficiency of the applied laser procedure with respect to the tissue type and mode of laser delivery. The tissue differences can easily be tracked from the graphs given. For cortical tissue 50% (or greater) ablation efficiencies were achieved when the rate of temperature changes over time was between 1.2 and 2.8; but that region was found to be higher for the subcortical tissue, even though the calculated ablation efficiencies were low. The rate of temperature changes over time for p-m-m applications were found smaller, which resulted with lower ablation efficiencies. Spearman's rank correlation coefficient ρ revealed a strong correlation between ablation efficiencies and rate of temperature change over time, ρ=0.903, ρ=0.940, ρ= 0.944, ρ= 0.973 for cortical continuous-mode, pulsed-modulated-mode and subcortical continuous-mode and pulsed-modulated-mode applications respectively. If the data of the samples in which carbonization was observed are excluded from the analysis, which is more convenient to do so, the values of ρ's are increasing as expected (ρ=0.986, ρ=0.960, ρ=0.954, ρ=0.974 for cortical continuous-mode, pulsed-modulated-mode and subcortical continuous-mode and pulsed-modulated-mode applications respectively).

4.3.1 Discussion

Continuous wave laser irradiation -in addition to tissue heating and thermal injury- can lead to removal of tissue by vaporizing or ejection of the tissue which is called ablation process. In order to achieve more precise tissue removal and less thermal injury to surrounding tissue the temperature of the tissue must be monitored during laser irradiation.

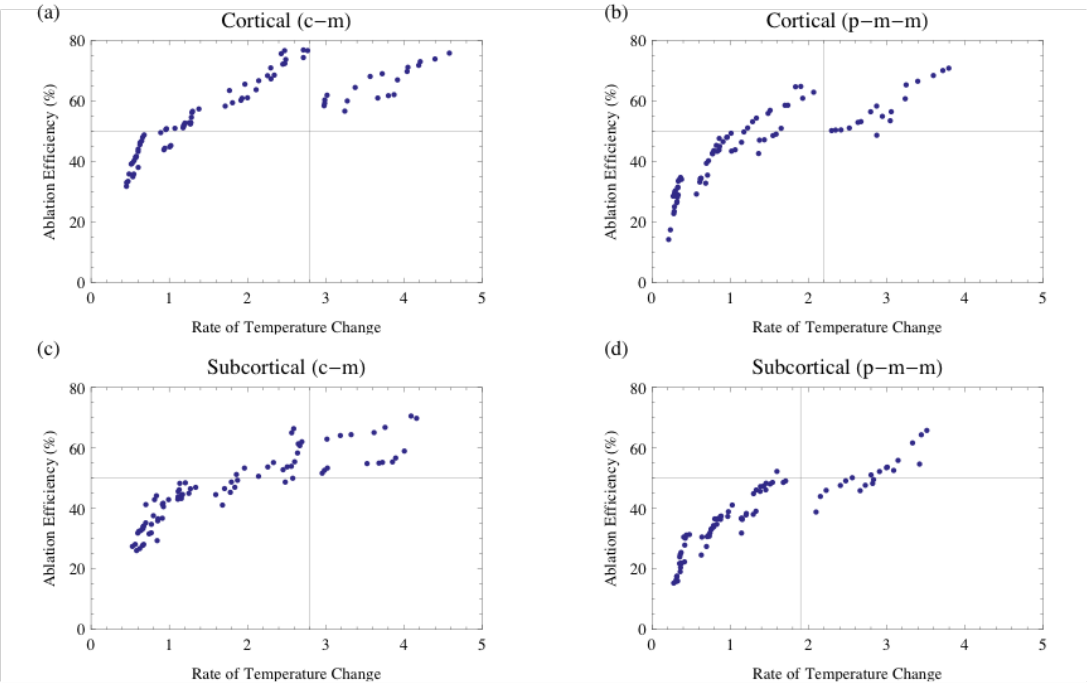

Figure 4.33 The ablation efficiencies as a function of rates of temperature change of the samples of cortical (a and b) and subcortical tissue (c and d). The mode of laser delivery was continuous (c-m) for (a) and (c) and pulsed-modulated (p-m-m) for (b) and (d). The right hand side of the vertical lines indicates the samples with carbonization, and the upper region of the horizontal lines indicates the samples, in which higher ablation efficiencies were succeeded.

Temperature changes in the tissue during laser irradiation can be a good indicator to understand and predict the tissue response to the laser irradiation. If the tissue is exposed to laser light for a long time that is heating times of the tissue is prolonged; cellular and tissue structural proteins will undergo structural changes and protein denaturation will occur which is called thermal coagulation. However, ablation process is dominated when the sudden increase in tissue temperature is achieved [6, 19].

In this study we investigated the ablative effects of three different infrared lasers and applicability of new designed thermoprobe which measures temperature of the nearby tissue during laser irradiation into laser dosimetry studies. 1070-nm ND:YLF laser was not able to ablate either cortical or subcortical tissue, which is correlated with literature [144–146]. 980-nm diode and 1940-nm Tm:fiber lasers were found to be successful for laser brain surgeries.

Although the subcortical and cortical tissues are brain samples, their optical prop-

erties are different [18, 147, 148]. During laser irradiation, this difference must be taken into account, because this dissimilarity affects the response of the tissue to laser irradiation. It has been shown that the response of the cortical and the subcortical tissue to both 980-nm diode and 1940-nm Tm: fiber lasers were different; the resultant ablation and coagulation diameters are greater for cortical tissue for all parameters ($p<0.001$). This reveals that the main absorber of the laser light in the tissue is water. The water contents and lipid contents are different for these two different tissue types. Because the myelin sheaths that are composed of lipids are higher in subcortical tissue, water absorption of this tissue is lower, which results in smaller coagulation and ablation diameters even though the observed temperature increase was higher.

It was observed that lesions created by 980-nm diode laser were bigger than those created by 1940-nm Tm:fiber laser, when the thermal effects of two lasers were compared. Additionally, increase in tissue temperature was greater for 1940-nm. This can be explained as follows: in 1940-nm applications, lower doses were applied for a longer time in comparison with 980-nm. Output power was on the order of mW's for 1940-nm applications, whereas it was on the order of Watts for 980-nm. This dosimetry strategy was necessary, since for 1940-nm, higher doses resulted in carbonization and for 980-nm, lower doses could not cause ablation. Greater increases in tissue temperature in 1940-nm applications may be due to longer exposure times in comparison with 980-nm applications and smaller lesions created may be explained by lower applied powers. As a result, optimum doses for *in vivo* studies were found to be 2 W for 980-nm diode laser and 400 mW and 600 mW for 1940-nm Tm:fiber laser, for which the ablation efficiencies were observed to be the highest.

In modulated-mode laser irradiations although the same energy was delivered to the tissue the resultant ablation efficiencies are found to be lower compared to continuous-mode laser irradiations. Because in modulated-mode applications tissue has a time to cool itself down, and conducts the heat to nearby tissue, thus heating of the tissue was dominated in these applications. So the resultant rate of temperature increase in the tissue was lower, which results in greater coagulation diameters and smaller ablation diameters, hence lower ablation efficiencies.

Results showed that relatively low power laser energy was efficient for ablating brain tissue in Tm:fiber laser applications. 200-800-mW of laser energy can be described as low power compared to the other IR lasers showed in literature (at least Watts of laser power was used.) [5]. 50% ablation efficiency values were reached by just applying hundreds miliwatts of laser energy. We used a Tm:fiber laser with 5 W of maximum output power but a smaller laser system can be implemented with this wavelength. Smaller size requires less space in the surgery room and also reduces the overall costs.

In all experiments sudden decrease in the tissue temperature by 0.5-1°C was observed, which indicates the beginning of the ablation process. We believed that this sudden decrease is most probably because of the water vapor of the removed tissue. Additionally, this indicates that when the tissue is irradiated by the laser, the superficial tissue layer is thermally coagulated immediately, temperature increase continues until the vaporization temperature is reached. Then the temperature of the tissue decreases immediately due to vaporization of the tissue. When this tissue layer is completely dehydrated and vaporized, the temperature begins to rise again. During these processes, heat will be transferred to the surrounding tissue layers by heat conduction that results in coagulation. In these layers of the tissue, coagulation will dominate because the ablation threshold temperature is not reached. If the irradiation continues enough to reach to carbonization temperature, this dried tissue will carbonized with color changing from white to black, which is observed in our studies when irradiating the tissue with 800 mW power output of the Tm:fiber laser.

In this study, it is aimed to investigate the thermal effects of the 980-nm diode and 1940-nm Tm:fiber lasers on the cortical and subcortical tissues in an *ex vivo* study with a new design laser-thermoprobe. This study can contribute to understand laser-tissue interaction mechanism and it also shows that rate of temperature change analysis could be a very useful and efficient method to understand and predict the tissue response to the investigated laser. It was also shown that the ablation and coagulation diameters could be controlled and predicted and carbonization can be avoided by temperature monitoring which will be a very useful method for scientists. It has been proven that the tissue temperature alone is not a sufficient variable for a comprehensive understanding of irradiated

tissue. Blood circulation would have a potential as a coolant under *in vivo* conditions. However the proposed laser-thermoprobe system measures the nearby tissue temperature and operator can use this information as a reference to estimate the probable thermal hazard corollary with the individual changes due to perfusion or any morphological inhomogeneity. These findings are particularly important for clinical use of the laser because higher ablation efficiencies directly related to the minimal thermal damage to surrounding healthy tissue.

4.4 Stereotaxic surgery with 980-nm diode and 1940-nm Tm:fiber laser

In the light of *ex vivo* studies the successful parameters for 980-nm diode and 1940-nm Tm:fiber lasers were studied in further *in vivo* experiments.

This study mainly focused on investigating the thermal effects of different laser sources with different power and mode settings on cortical and subcortical tissue and the relation between the thermal effects and the temperature change in the tissue.

4.4.1 980-nm diode laser

4.4.1.1 Thermal effects. With the help of the *ex vivo* studies, two different laser parameters were determined to be investigated throughout the *in vivo* studies for this laser source: 2 W-1.5 s and 2 W-2 s. Examples of CFV stained subcortical tissue samples can be seen in Figure 4.34.

With two-way ANOVA, it is investigated if the tissue type and exposure time affect the measured parameters listed above. The results revealed that the tissue type and the laser exposure time had a significant effect on ablated and coagulated areas ($p<0.001$ for both). Ablation efficiency was affected by the tissue type while the effects of laser exposure time were insignificant ($p=0.035$, $p=0.603$ respectively). On the other hand

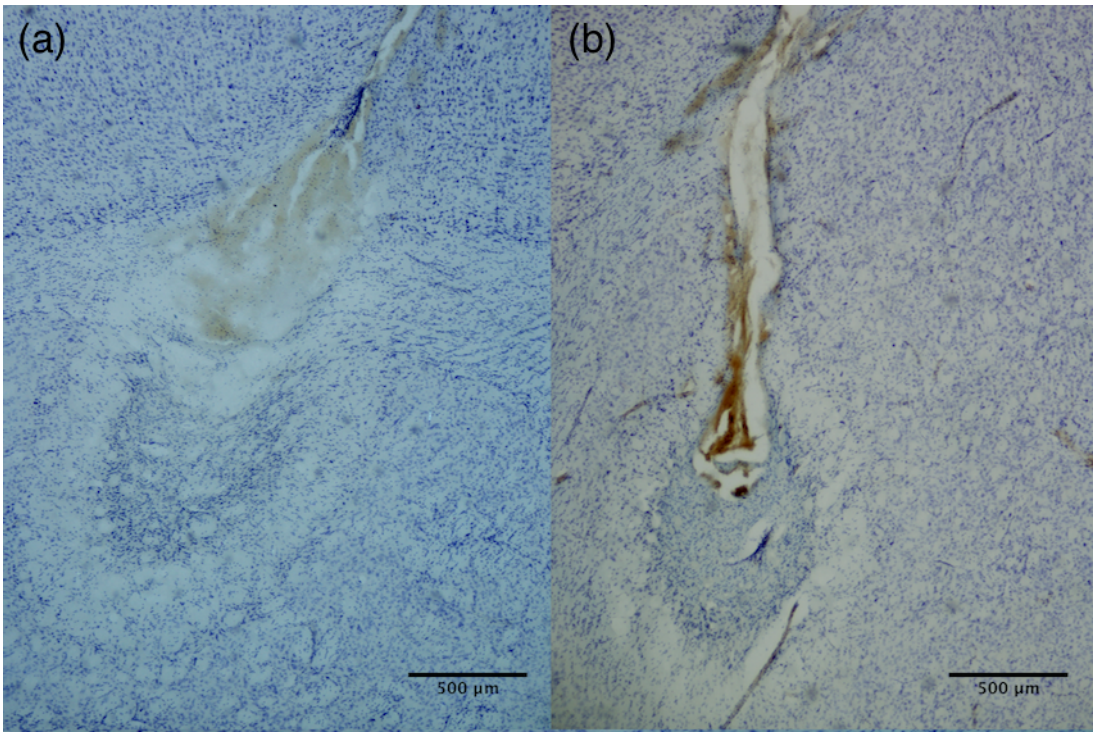

Figure 4.34 Light micrographs of CFV stained 50 μm sections of subcortical tissues induced by 2 W, 980-nm diode laser with exposure times of a) 1.5 s b) 2 s (Magnification=40X).

edamatous areas were found to be the same for each study group (p=0.427, p=0.251). The mean values and standard deviations of ablated area, coagulated area and edamatous area and ablation efficiencies were listed in Table 4.1 and plotted in Figure 4.35.

Table 4.1
Mean ablated areas (AA), coagulated areas (CA), edamatous areas (EA) and ablation efficiencies for the 980-nm diode laser applications with two different laser parameters in cortical and subcortical tissues.

Tissue	Exposure Time (s)	Energy Delivered (j)	AA (m^2)	CA (m^2)	EA (m^2)	Normalized Edema	AE (%)
Cortical	1.5	3	0.43 ± 0.14	0.70 ± 0.15	1.03 ± 0.45	0.46 ± 0.17	37.41 ± 4.91
	2	4	0.63 ± 0.17	1.01 ± 0.11	1.10 ± 0.39	0.40 ± 0.11	37.71 ± 5.31
Subcortical	1.5	3	0.28 ± 0.11	0.56 ± 0.2	0.84 ± 0.28	0.49 ± 0.5	32.83 ± 5.58
	2	4	0.39 ± 0.11	0.73 ± 0.13	1.08 ± 0.37	0.48 ± 0.13	34.40 ± 4.15

The biggest ablated and total affected areas were achieved at 2 s applications for both tissue types and the ablation efficiencies turned out to be higher for cortical tissues irrespective of the exposure times. For both types of tissue, even though the mean ablated area, coagulated area and edematous area for the 2 s applications were found bigger than the 1.5 s applications, the resultant ablation efficiencies are similar. The

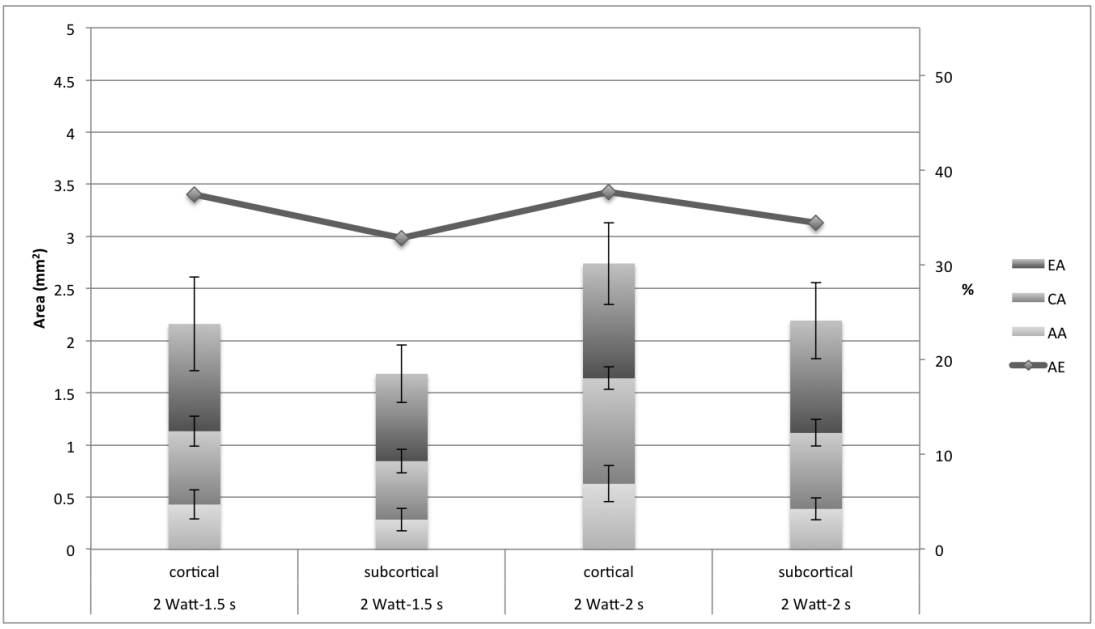

Figure 4.35 The thermal effects of 2 W, 980-nm diode laser applied on cortical and subcortical tissues for 1.5 s and 2 s (AA: Ablated area, CA: Coagulated area, EA: Edematous, AE: Ablation efficiency). Y1 axis and columns indicate the ablated, coagulated and edematous areas, Y2 axis and line graph indicate the ablation efficiency values with respect to stated laser power. For the cortical tissues, higher ablated areas, lower coagulated areas and higher ablation efficiencies were observed, compared to subcortical tissues ($p<0.001$, $p<0.00.1$ and $p<0.05$, respectively), whereas similar edematous areas around the coagulated zone were observed. Increasing laser exposure times increased ablated and coagulated areas, whereas the ablation efficiencies were found to be similar.

significance levels obtained via Tukey test, of ablated area, coagulated area, edematous area, normalized edematous area and ablation efficiency with varying exposure times were given in Table 4.2.

Table 4.2
The significance levels of ablated area, coagulated area, edematous area, normalized edematous area and ablation efficiency with varying exposure times for 980-nm diode laser applied on cortical and subcortical tissues.

Statistical Analysis \ Dependent Variable		p-values				
		AA	CA	EA	NEA	AE
ANOVA		<0.001	<0.001	0.500	0.536	0.174
post-hoc tests	Cortical 2 W-1.5 s - Cortical 2 W-2 s	0.031	<0.001			
	Cortical 2 W-1.5 s - Subcortical 2 W-1.5 s	0.159	0.126			
	Cortical 2 W-1.5 s - Subcortical 2 W-2 s	0.925	0.977			
	Cortical 2 W-2 s - Subcortical 2 W-1.5 s	<0.001	<0.001			
	Cortical 2 W-2 s - Subcortical 2 W-2 s	0.007	<0.001			
	Subcortical 2 W-1.5 s - Subcortical 2 W-2 s	0.426	0.054			

While we see no difference in ablation efficiency and normalized edema for 1.5 s and 2 s applications on subcortical tissue, when we consider cortical applications, 2 s application offer a good preference due to less formation of normalized edema. This conclusion is due to graphical representation (Figure 4.35) of the data, but we should mention that those quantities are not significantly different from each other statistically according to ANOVA (Table 4.2).

As stated above, for both tissue types the change in the exposure times did not alter the ablation efficiencies nor the edematous area, yet the decisions on which dose is going to be applied can be made according to the desired size of the lesions. It is possible to illustrate ablated and coagulated areas, exposure times and ablation efficiencies in a single plot. To do that, we plot ablated area against the coagulated area, mark exposure times with a color code and the ablation efficiencies manifest themselves as straight lines with varying slopes on that plot. As seen in Figures 4.36 and 4.37, even though ablation efficiencies remain in certain intervals, the size of the lesions increases with increased exposure time. Even though the majority of the results for both tissues remain in the 30-40% interval It is remarkable that some results have efficiencies above 40% for the cortical applications whereas we see some below 30% results for subcortical applications.

4.4.1.2 Temperature measurements. Temperature of the nearby tissue during lasing was measured at a distance of 1 mm above and 1 mm away from the fiber tip. For each application temperature of the tissue and the time to reach maximum temperature were measured. The changes in the temperature and the rates of the temperature change were calculated. Table 4.3 shows mean values and standard deviations of these variables for 980-nm diode laser study groups.

Changes in the temperature during lasing and the rates of the temperature change for both cortical and subcortical tissues were plotted in Figures 4.38 and 4.39 respectively.

Figure 4.38 shows that the maximum change in temperature was achieved when the laser was applied for 2 s, as expected. On the other hand, highest rate of temperature

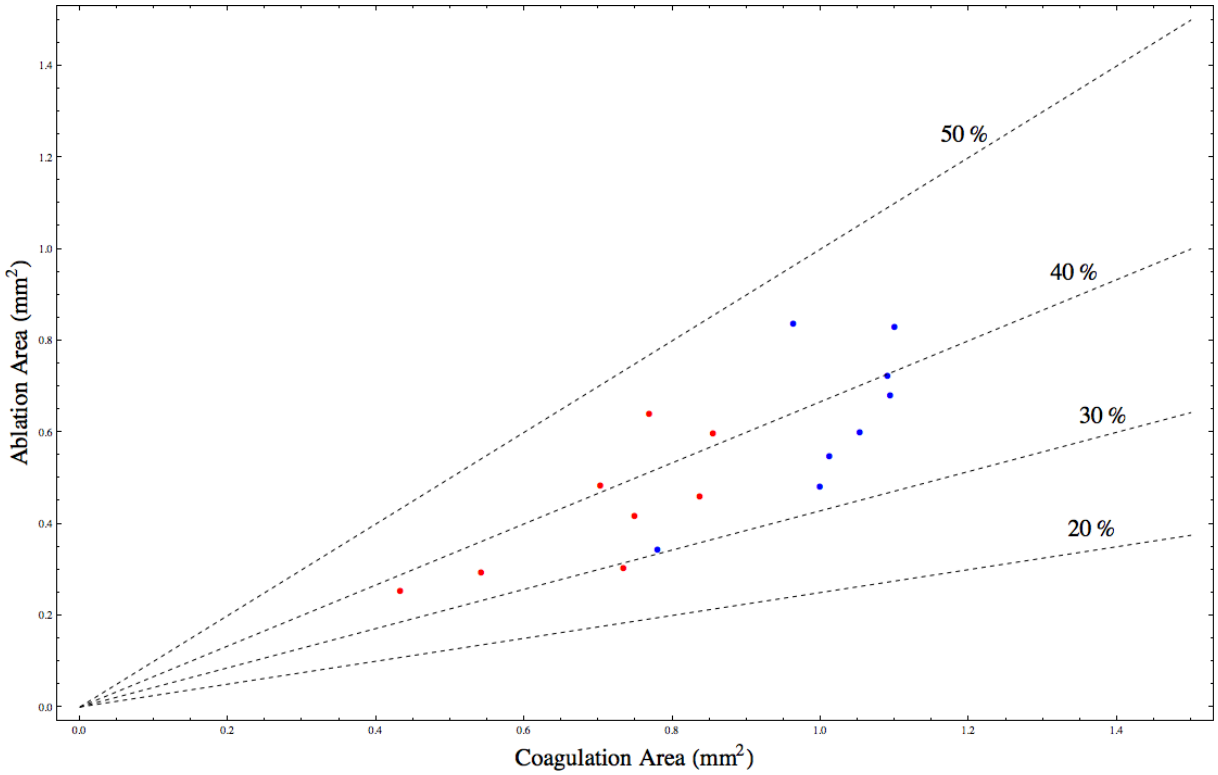

Figure 4.36 Ablated area versus coagulated area for 980-nm diode laser applied on cortical tissue. Red and blue dots represent 1.5 s and 2 s applications respectively. Ablation efficiencies are given as dashed straight lines.

Table 4.3
Mean values and standard deviations of the temperature change, the time to reach maximum temperature and the rate of temperature change for 980-nm diode laser study groups.

Tissue	Exposure Time (s)	Energy Delivered (J)	ΔT (°C)	Time (s)	ΔT/t (°C/s)
Cortical	1.5	3	37.81 ± 3.80	1.56 ± 0.05	24.30 ± 2.78
	2	4	45.12 ± 3.67	2.07 ± 0.05	21.84 ± 1.88
Subcortical	1.5	3	34.65 ± 3.08	1.57 ± 0.04	22.13 ± 2.40
	2	4	42.62 ± 4.21	2.08 ± 0.06	20.49 ± 2.20

change was achieved at 2 W-1.5 s applications (Figure 4.39). When the same amount of energy was delivered to the both types of tissue, the change in the temperature and the rate of temperature change observed to be higher for the cortical tissues.

Two-way ANOVA revealed that the changes in temperature and the rates of temperature change were differentiated by two parameters; tissue type ($p=0.040$ and $p=0.043$, respectively)and exposure time ($p<0.001$ and $p=0.019$, respectively). Table 4.4 shows the

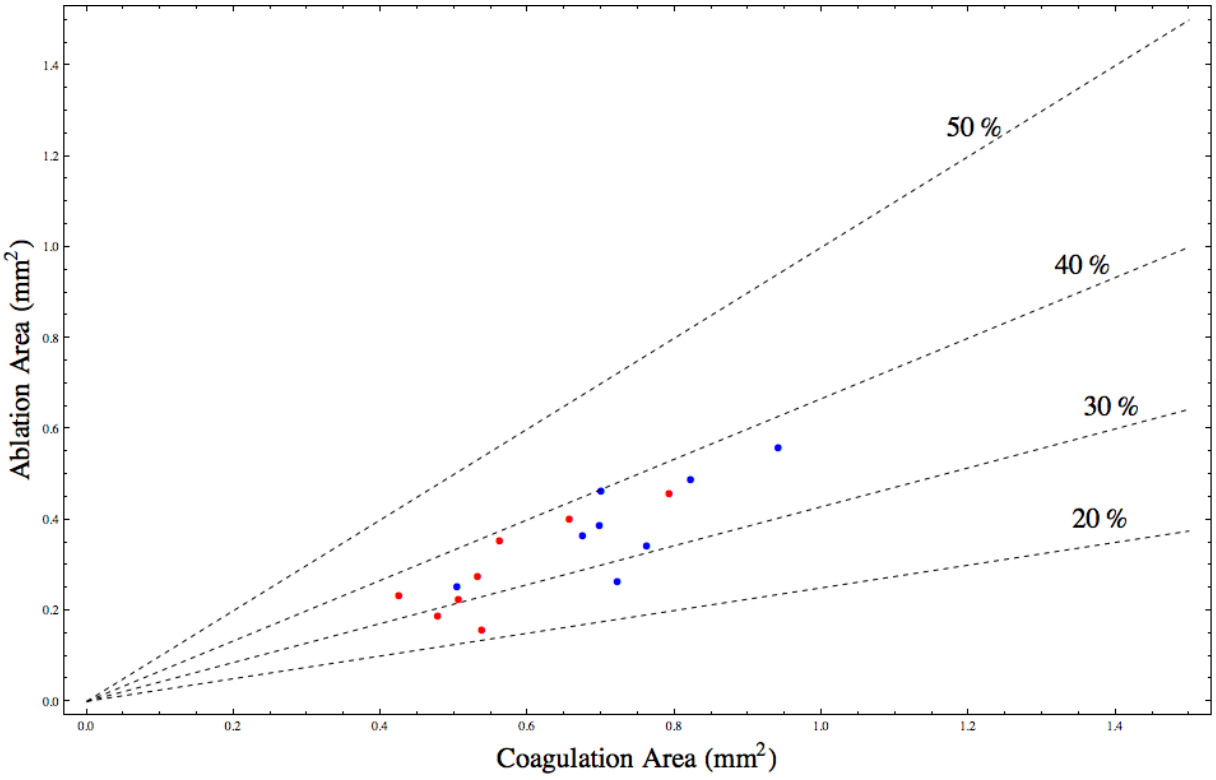

Figure 4.37 Ablated area versus coagulated area for 980-nm diode laser applied on subcortical tissue. Red and blue dots represent 1.5 s and 2 s applications respectively. Ablation efficiencies are given as dashed straight lines.

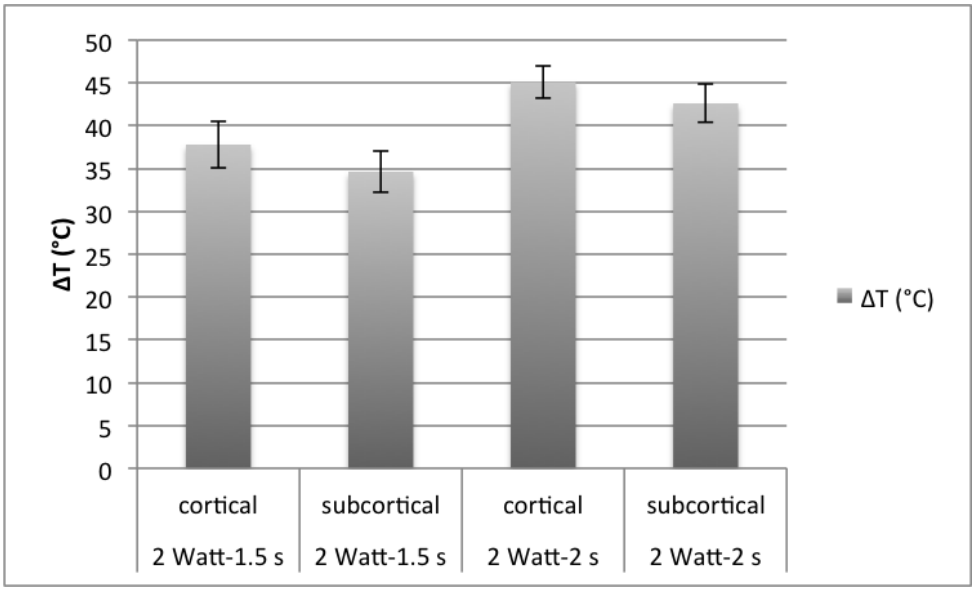

Figure 4.38 Temperature change for the 2 W, 980-nm diode laser study groups for cortical and subcortical tissues. Temperature increases in the cortical tissues were observed to be higher than the ones in subcortical tissues ($p<0.05$). Increasing exposure times resulted in higher temperature increase ($p<0.001$).

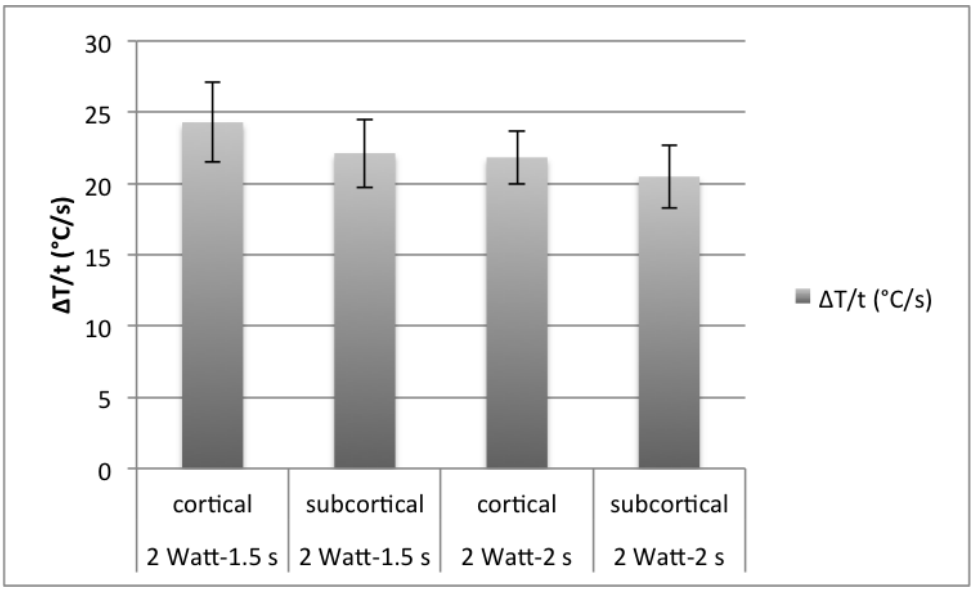

Figure 4.39 Rate of temperature change for the 2 W, 980-nm diode laser study groups for cortical and subcortical tissues. Rates of temperature change in the cortical tissues were observed to be higher than the ones in subcortical tissues ($p<0.05$). Increasing exposure times resulted in lower rates ($p<0.05$).

significance levels for the change in temperature and the rate of temperature change for both cortical and subcortical tissue when irradiated by 980-nm diode laser.

Table 4.4
The significance levels for the change in temperature and the rate of temperature change for both cortical and subcortical tissue when irradiated by 980-nm diode laser.

Statistical Analysis \ Dependent Variable		p-values	
		ΔT	ΔT/t
ANOVA		<0.001	0.025
post-hoc tests	Cortical 2 W-1.5 s - Cortical 2 W-2 s	0.003	0.176
	Cortical 2 W-1.5 s - Subcortical 2 W-1.5 s	0.341	0.271
	Cortical 2 W-1.5 s - Subcortical 2 W-2 s	0.067	0.015
	Cortical 2 W-2 s - Subcortical 2 W-1.5 s	<0.001	0.994
	Cortical 2 W-2 s - Subcortical 2 W-2 s	0.544	0.661
	Subcortical 2 W-1.5 s - Subcortical 2 W-2 s	0.001	0.507

Spearman's rank correlation coefficient revealed a strong correlation between the rate of temperature change and ablation efficiencies in *ex vivo* studies. For the results

of *in vivo* experiments it was also calculated to see if there is a similar correlation and additionally a correlation between rates of temperature change and total damage and edematous area. In addition to Spearman's rank correlation coefficients, Pearson's correlation coefficients were also calculated. Calculated Pearson's correlation coefficient, r and Spearman's rank correlation coefficient, ρ are given in Table 4.5. In Figure 4.40 those relations were presented.

Table 4.5
Pearson's correlation (r) and Spearman's rank correlation (ρ) coefficients for 980-nm diode laser.

Tissue Type	Exposure Time (s)	AE		Total Damage		Edema	
		r	ρ	r	ρ	r	ρ
Cortical	1.5	0.823	0.786	-0.715	-0.735	-0.768	-0.857
	2	0.779	0.833	-0.744	-0.690	-0.966	-0.952
Subcortical	1.5	0.895	0.905	-0.854	-0.833	-0.862	-0.857
	2	0.714	0.833	-0.894	-0.976	-0.964	-0.976

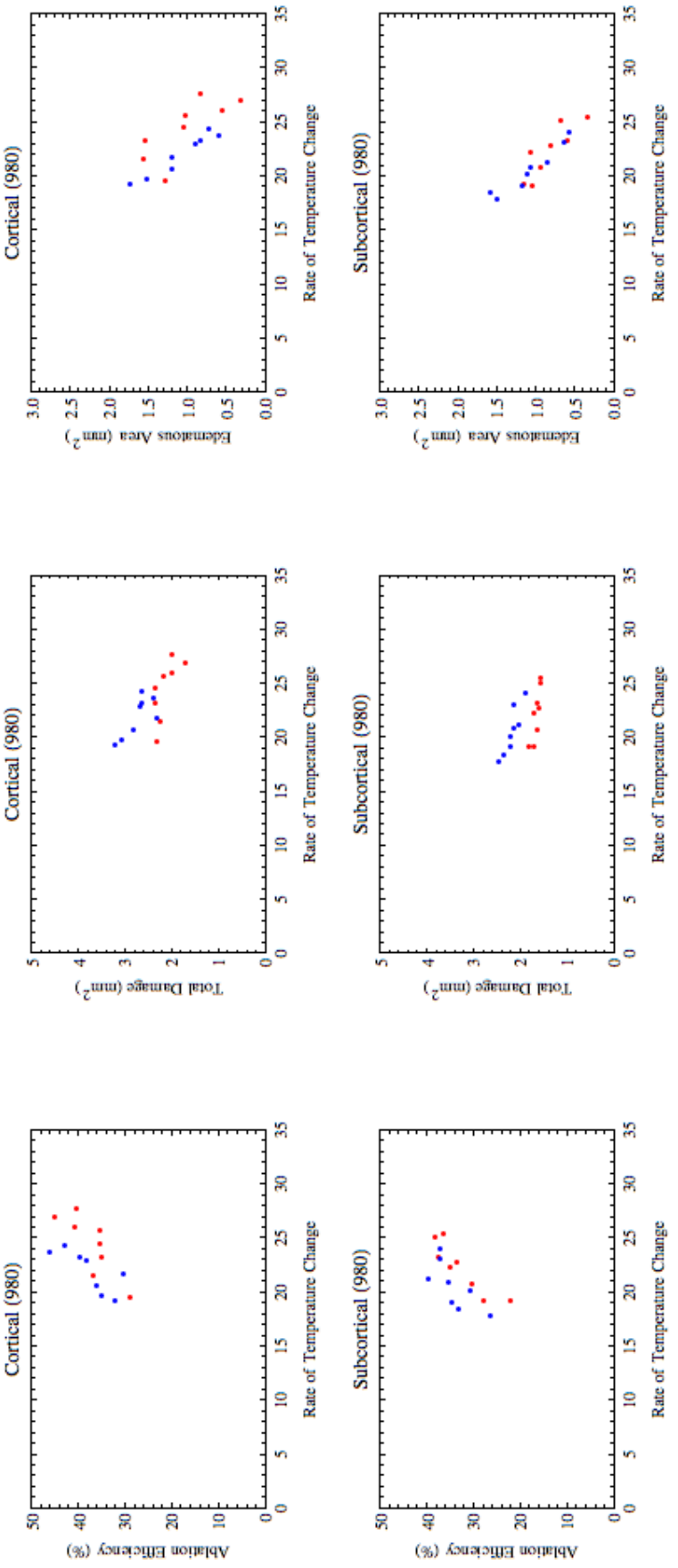

Figure 4.40 Ablation efficiency, total damage and edematous area versus rate of temperature change (from left to right) in 2 W 980-nm diode laser application for cortical (upper plots) and subcortical (lower plots) tissues. Red and blue dots represent 1.5 s and 2 s exposure times, respectively.

Irrespective of the tissue type, ablation efficiencies increased with increasing rate of temperature change, as it did for the *ex vivo* studies. We could also observe the edema for *in vivo* studies, which was not examined in *ex vivo*. A negative correlation between edemous tissue and rate of temperature change was also observed. A similar correlation exists between total damage and rate of temperature change.

In order to make a comprehensive analysis and to decide which parameter is more applicable compared to other one, edematous area around the lesion should be taken into account. The behaviours of the ablation efficiency and the edematous area with varying rate of temperature change were combined in a single three-dimensional plot for 2 W 980-nm diode laser. It is worth mentioning that these plots contain both exposure time data. In Figures 4.41 and 4.42, it is obvious that the ablation efficiency increases with the increasing rate of temperature change, where the edematous area decreases, for cortical and subcortical tissues, respectively. To make a reliable comparison, we calculated the normalized values for edema and presented them in Figures 4.43 and 4.44 for cortical and subcortical tissues, respectively. Normalization of edematous area did not change the behaviours explained above.

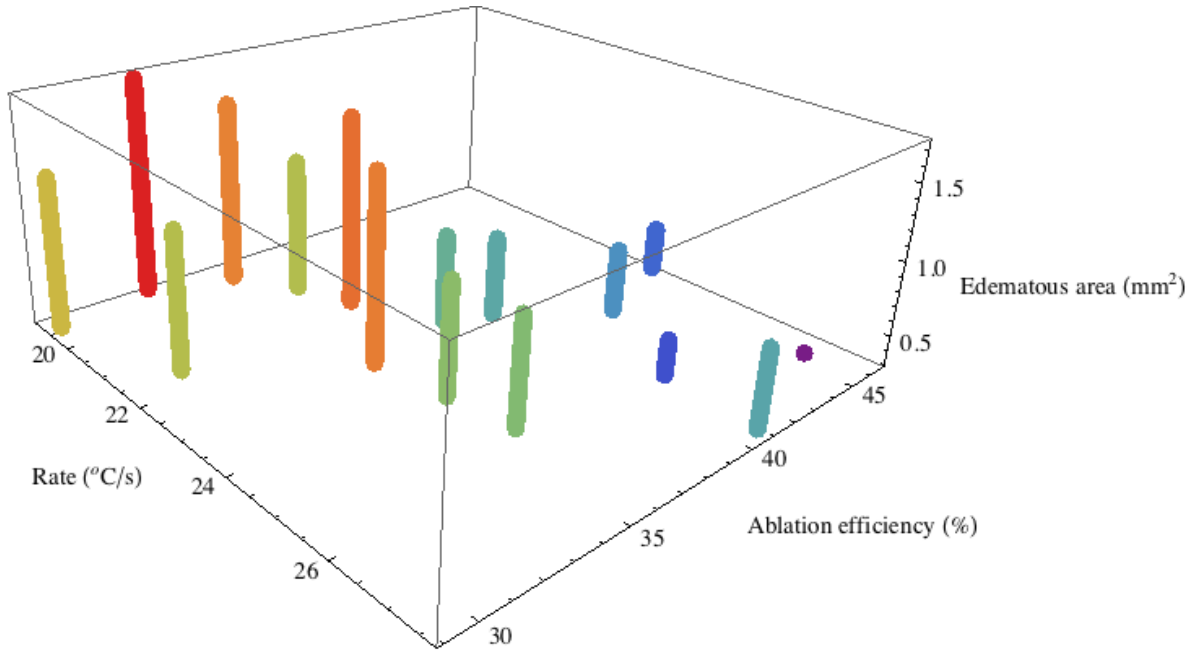

Figure 4.41 The ablation efficiency and the edematous area with varying rate of temperature change for 2 W 980-nm diode laser applied on cortical tissue. Color coding is proportional to the height of the bars.

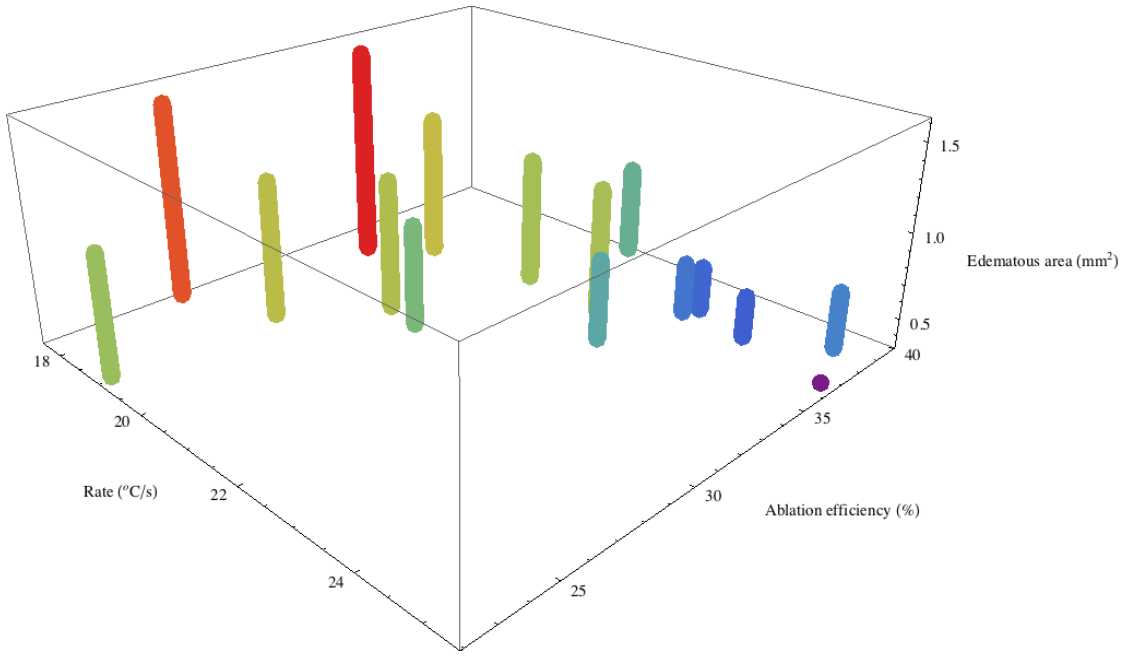

Figure 4.42 The ablation efficiency and the edematous area with varying rate of temperature change for 2 W 980-nm diode laser applied on subcortical tissue. Color coding is proportional to the height of the bars.

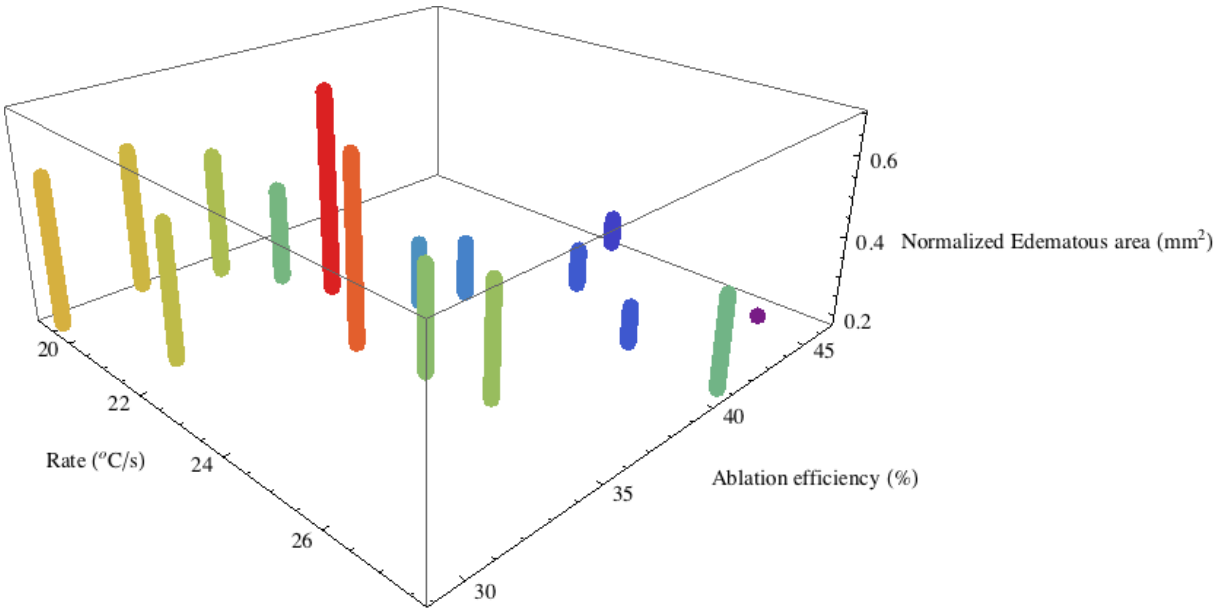

Figure 4.43 The ablation efficiency and the normalized edematous area with varying rate of temperature change for 2 W 980-nm diode laser applied on cortical tissue. Color coding is proportional to the height of the bars.

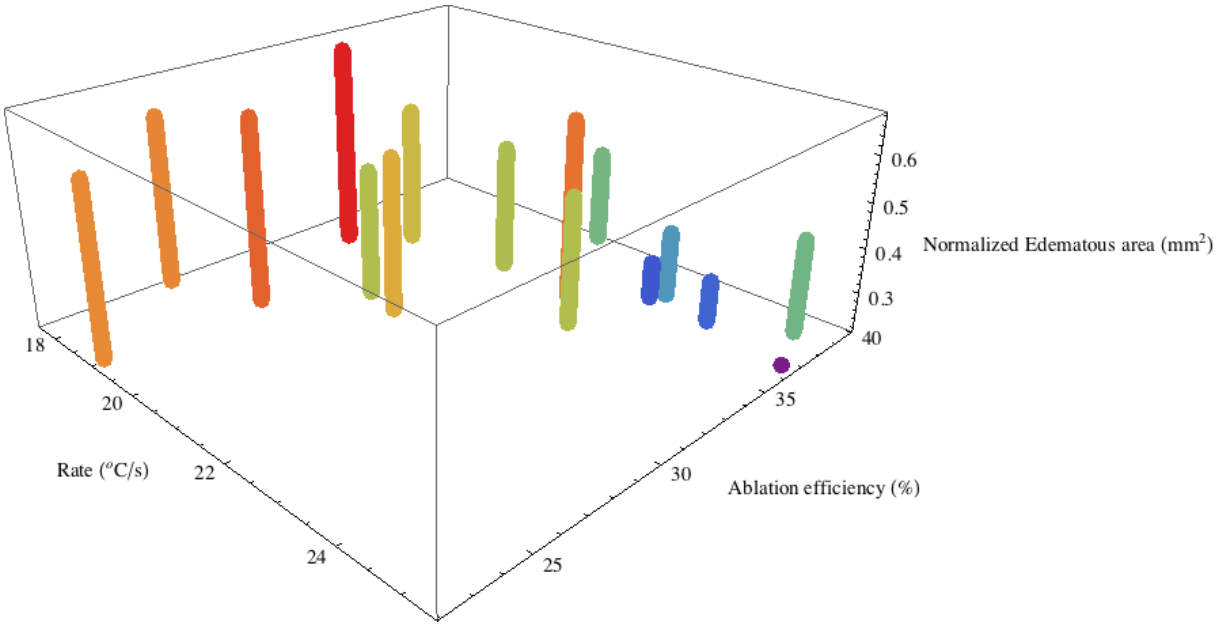

Figure 4.44 The ablation efficiency and the normalized edematous area with varying rate of temperature change for 2 W 980-nm diode laser applied on cortical tissue. Color coding is proportional to the height of the bars.

4.4.2 1940-nm Tm:fiber laser continuous mode

4.4.2.1 Thermal effects. With the help of the *ex vivo* studies, three different laser parameters were determined to be investigated throughout the *in vivo* studies for this laser source in continuos mode: 400 mW-2.5 s, 400 mW-5s and 600 mW-3.3s. Examples of CFV stained subcortical tissue samples can be seen in Figure 4.45.

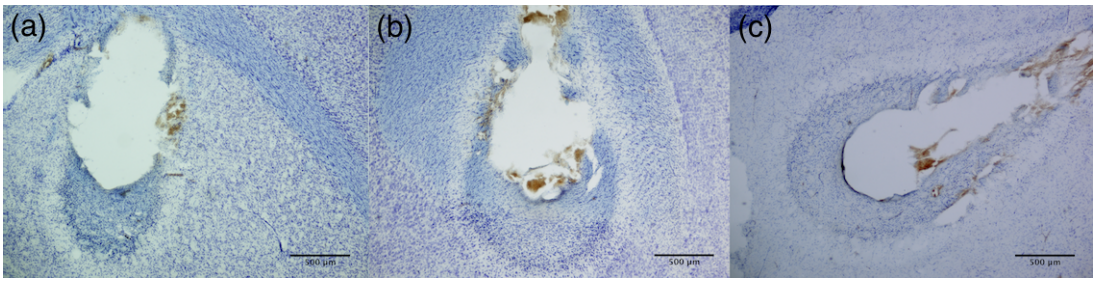

Figure 4.45 Light micrographs of CFV stained 50 μm sections of subcortical tissues induced by 1940-nm Tm:fiber laser in continuous mode with laser parameter combinations of a) 400 mW, 2.5 s b) 400 mW, 5 s c) 600 mW, 3.3 s (Magnification=40X).

Two different two-way ANOVA were performed. With the first one, it is investigated if the tissue type and exposure time affect the measured parameters studied with the 980-nm diode laser. The results revealed that the tissue type and the laser exposure time had a significant effect on ablated ($p<0.001$ for both) and coagulated areas ($p=0.002$ and $p<0.001$, respectively). Ablation efficiency was affected by the tissue type while the effects of laser exposure time were insignificant ($p<0.001$ and $p=0.161$ respectively). On the other hand edamatous areas were found to be the same for each study group ($p=0.063$ and $p=0.475$, respectively). But, when we normalize the edematous area, even though tissue type did not have a significant effect ($p=0.457$) the exposure time showed a statistically significant difference ($p=0.019$). Second two-way ANOVA was performed in order to find if the tissue type and the change in energy delivery via power and exposure time, affect the measurements. With the change “in energy delivery via power and exposure time", we mean that the same amount of energy is delivered to the tissue (2 J) with a lower power but in longer time or with a higher power but in shorter time. The results revealed that the tissue type had a significant effect on ablated ($p<0.001$) and coagulated ($p=0.031$) areas whereas change in energy delivery had not ($p=0.267$ and 0.108, respectively). Ablation efficiency was affected by both ($p=0.040$ and $p=0.011$, respectively). Edamatous areas were found to be the same for each study group ($p=0.060$ and $p=0.277$,

respectively). Normalizing the edematous area did not change the case (p=0.574 and p=0.523, respectively).

The mean values and standard deviations of ablated area, coagulated area, edamatous area, normalized edematous area and ablation efficiencies were listed in Table 4.6 and plotted in 4.46.

Table 4.6
Mean ablated areas (AA), coagulated areas (CA), edamatous areas (EA), normailzed edematous areas (NEA) and ablation efficiencies (AE) for the 1940-nm Tm:fiber laser in continuous mode applications with three different laser parameters in cortical and subcortical tissues.

Tissue	Laser Power (mW)	Exposure Time (s)	AA (m^2)	CA (m^2)	EA (m^2)	Normalized Edema	AE (%)
Cortical	400	2.5	0.25 ± 0.08	0.81 ± 0.13	0.82 ± 0.27	0.43 ± 0.11	23.35 ± 4.13
	400	5	0.68 ± 0.12	1.12 ± 0.23	0.64 ± 0.37	0.25 ± 0.11	38.16 ± 6.62
	600	3.3	0.93 ± 0.17	1.26 ± 0.34	0.69 ± 0.26	0.24 ± 0.05	42.97 ± 4.84
Subcortical	400	2.5	0.85 ± 0.20	0.83 ± 0.14	0.84 ± 0.29	0.30 ± 0.10	50.21±??
	400	5	1.20 ± 0.26	1.68 ± 0.36	1.24 ± 0.72	0.29 ± 0.15	41.76 ± 6.36
	600	3.3	1.12 ± 0.26	1.18 ± 0.24	0.79 ± 0.54	0.25 ± 0.16	48.44 ± 5.93

Sizes of the thermally altered areas in cortical tissues were found to be smaller compared to the areas in subcortical tissues. Ablation efficiencies were found to be lower in cortical tissues with respect to the subcortical tissues. Lowest ablation values were obtained for 400 mW-2.5 s for both tissues. The thermally altered area in the 400 mW-5 s application on subcortical tissue was observed to be significantly larger than the other applications. For the 400 mW-2.5 s application on cortical tissue, even though the energy delivered to the tissue was lowest, edematous area around the laser lesion was larger than the other groups. The significance levels obtained via Tukey test, of ablated area, coagulated area, edematous area, normalized edematous area and ablation efficiency with varying exposure times and energy delivery were given in Tables 4.7 and 4.8.

In Figure 4.47, it is more obvious that the ablated and coagulated areas created in 400 mW-2.5 s applications are smaller and efficiencies obtained in these applications is systematically lower. Ablation efficiencies for 400 mW-5 s are concentrated mostly in 30-40% intervals whereas efficiencies for 600 mW-3.3 s are in 40-50% intervals.

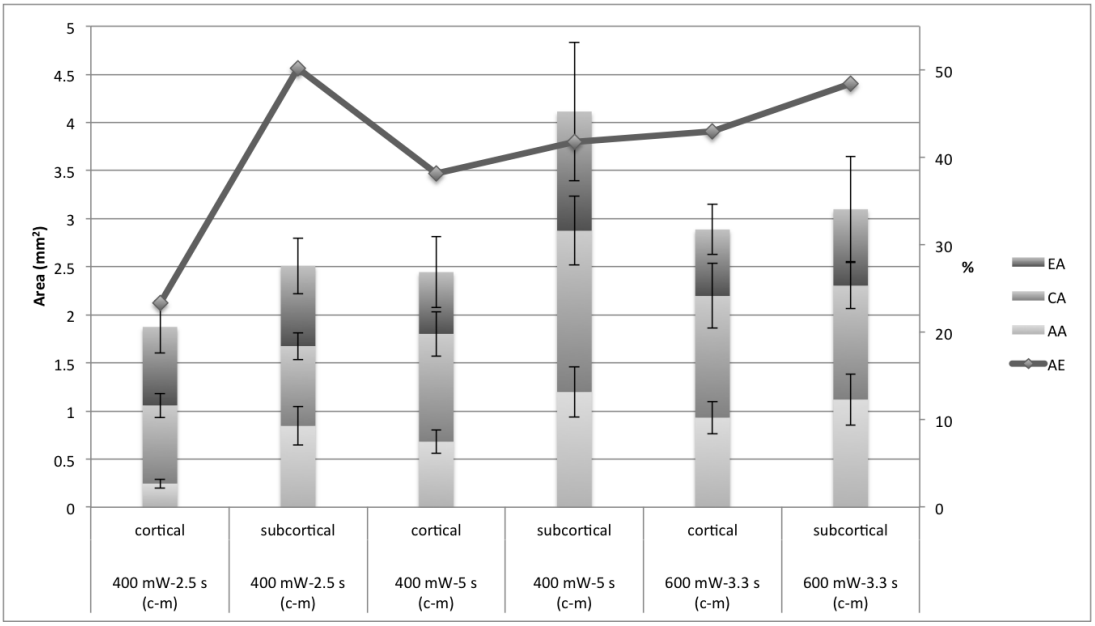

Figure 4.46 The thermal effects of 1940-nm Tm:fiber laser applied on cortical and subcortical tissues for different laser parameters at 4 joules energy level (AA: Ablated Area, CA: Coagulated Area EA: Edematous Area, AE: Ablation Efficiency). Y1 axis and columns indicate the ablated, coagulated and edematous areas, Y2 axis and line graph indicate the ablation efficiency values with respect to stated laser power. More ablation was observed for the subcortical tissues overall ($p<0.001$). Ablation efficiencies in subcortical tissues were higher with respect to cortical tissues ($p<0.001$). Even though, the highest coagulation and the edema were observed for subcortical tissues at 400 mW-5 s application, coagulated and edematous areas were similar for other groups.

Table 4.7
The significance levels of ablated area, coagulated area, edematous area, normalized edematous area and ablation efficiency with varying exposure times for 1940-nm Tm:fiber laser in continuous mode applied on cortical and subcortical tissues for.

Statistical Analysis \ Dependent Variable		p-values				
		AA	CA	EA	NEA	AE
ANOVA		<0.001	<0.001	0.078	0.041	<0.001
post-hoc tests	Cortical 400 mW-2.5 s - Cortical 400 mW-5 s	<0.001	0.061		0.034	<0.001
	Cortical 400 mW-2.5 s - Subcortical 400 mW-2.5 s	<0.001	0.999		0.356	<0.001
	Cortical 400 mW-2.5 s - Subcortical 400 mW-5 s	<0.001	<0.001		0.123	<0.001
	Cortical 400 mW-5 s - Subcortical 400 mW-2.5 s	0.270	0.082		0.614	0.003
	Cortical 400 mW-5 s - Subcortical 400 mW-5 s	<0.001	<0.001		0.929	0.660
	Subcortical 400 mW-2.5 s - Subcortical 400 mW-5 s	0.002	<0.001		0.924	0.053

In Figure 4.48, we see that 400 mW-2.5 s and 600 mW-3.3 s applications result in similar ablation efficiencies concentrated in 30-50% interval. Efficiencies for 400 mW-5 s are lower than those, concentrated in 20-40% interval. It is again obvious that ablated and coagulated areas in 400 mW-2.5 s applications are significantly lower than the other

Table 4.8
The significance levels of ablated area, coagulated area, edematous area, normalized edematous area and ablation efficiency with varying energy delivery for 1940-nm Tm:fiber laser in continuous mode applied on cortical and subcortical tissues for.

Statistical Analysis \ Dependent Variable		p-values				
		AA	CA	EA	NEA	AE
ANOVA		<0.001	0.004	0.096	0.844	0.016
post-hoc tests	Cortical 400 mW-5 s - Cortical 600 mW-3.3 s	0.113	0.770			0.390
	Cortical 400 mW-5 s - Subcortical 400 mW-5 s	<0.001	0.004			0.628
	Cortical 400 mW-5 s - Subcortical 600 mW-3.3 s	0.002	0.973			0.009
	Cortical 600 mW-3.3 s - Subcortical 400 mW-5 s	0.083	0.045			0.978
	Cortical 600 mW-3.3 s - Subcortical 600 mW-3.3 s	0.318	0.949			0.280
	Subcortical 400 mW-5 s - Subcortical 600 mW-3.3 s	0.880	0.013			0.139

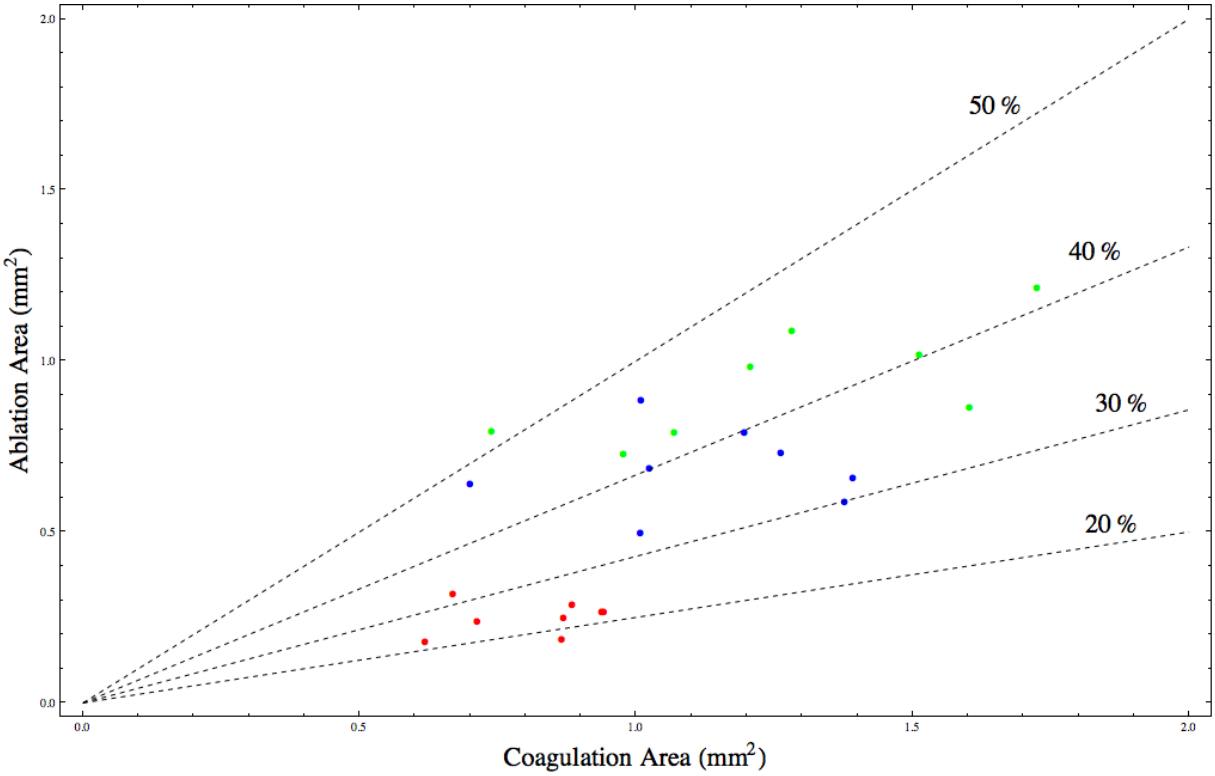

Figure 4.47 Ablated area versus coagulated area for 1940-nm Tm:fiber laser on continuous mode applied on cortical tissue. Red, blue and orange dots represent 400 mW-2.5 s, 400 mW-5 s and 600 mW-3.3 s applications respectively. Ablation efficiencies are given as dashed straight lines.

groups.

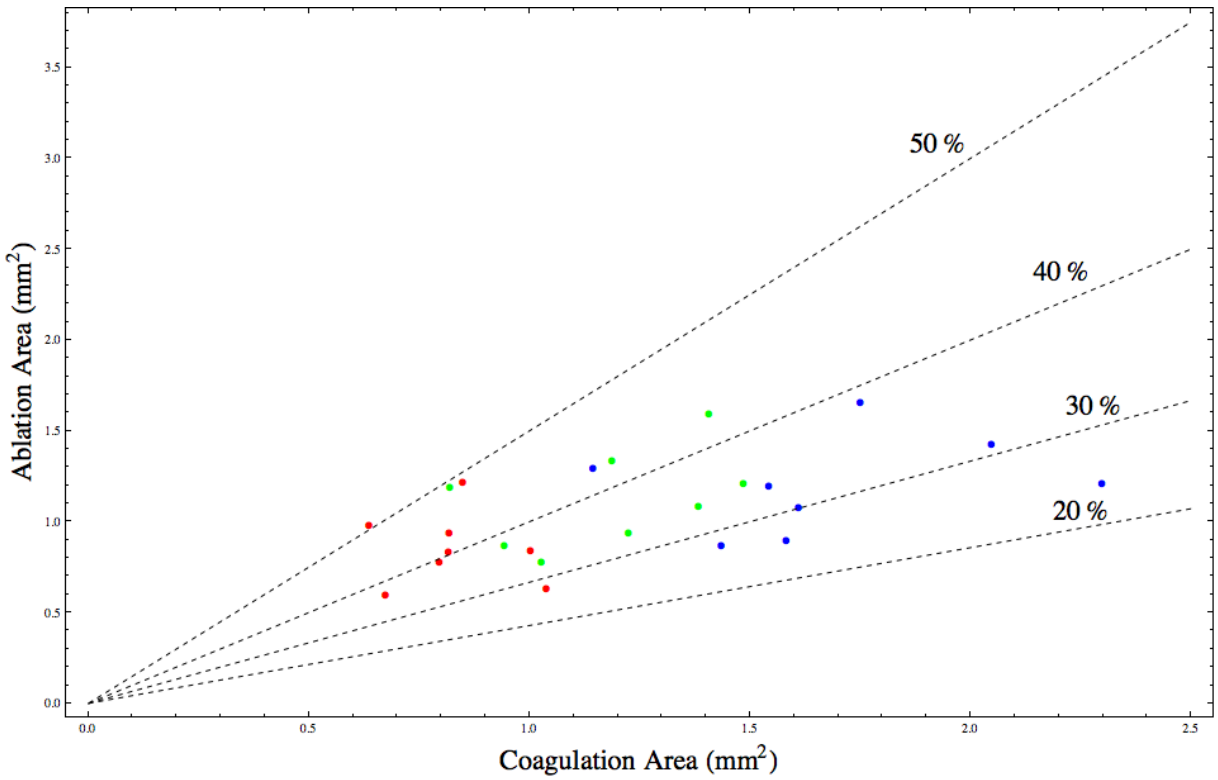

Figure 4.48 Ablated area versus coagulated area for 1940-nm Tm:fiber laser on continuous mode applied on subcortical tissue. Red, blue and orange dots represent 400 mW-2.5 s, 400 mW-5 s and 600 mW-3.3 s applications respectively. Ablation efficiencies are given as dashed straight lines.

4.4.2.2 Temperature measurements. Temperature of the nearby tissue during lasing was measured at a distance of 1 mm above and 1 mm away from the fiber tip. For each application temperature of the tissue and the time to reach maximum temperature were measured. The changes in the temperature and the rates of the temperature change were calculated. Table 4.9 shows mean values and standard deviations of these variables for 1940-nm Tm:fiber laser in continuous mode study groups.

Table 4.9
Mean values and standard deviations of the temperature change, the time to reach maximum temperature and the rate of temperature change for 1940-nm Tm:fiber laser in continuous mode study groups.

Tissue	Exposure Time (s)	Energy Delivered (J)	ΔT (C)	Time (s)	ΔT/t (C/s)
Cortical	2.5	1	38.47 ± 4.92	2.56 ± 0.03	15.00 ± 1.83
	5	2	54.85 ± 5.16	5.08 ± 0.07	10.81 ± 1.10
	3.3	2	57.18 ± 4.75	3.36 ± 0.05	17.00 ± 1.45
Subcortical	2.5	1	34.03 ± 4.79	2.54 ± 0.03	13.40 ± 1.89
	5	2	47.12 ± 5.40	5.06 ± 0.05	9.32 ± 1.13
	3.3	2	51.77 ± 4.85	3.36 ± 0.04	15.41 ± 1.50

Change in temperature during lasing and rates of the temperature change for both cortical and subcortical tissues were plotted in Figures 4.49 and 4.50, respectively.

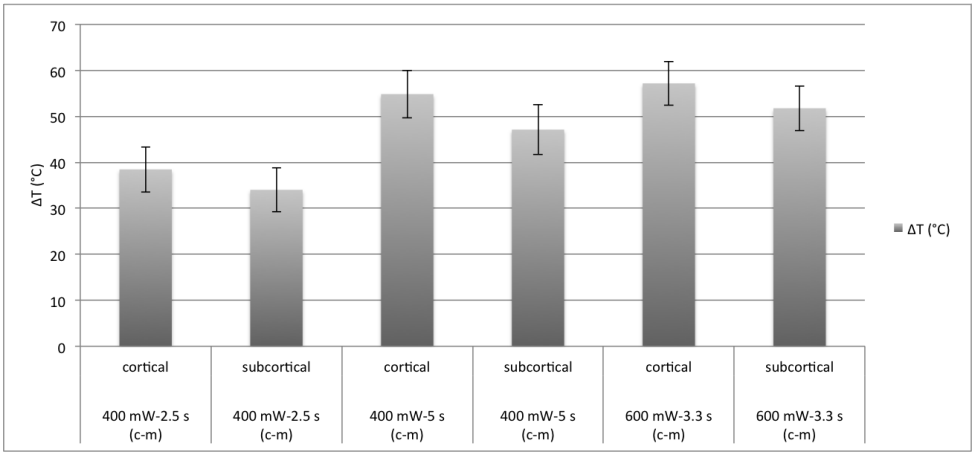

Figure 4.49 Temperature change for the 1940-nm Tm:fiber laser in continuous mode study groups for cortical and subcortical tissues. Temperature increase in cortical tissues observed to be higher with respect to subcortical tissues ($p<0.05$). Increasing exposure time resulted in a higher temperature increase ($p<0.001$), whereas increasing power did not affect the temperature increase in the tissue ($p=0.060$).

Figure 4.49 shows that the least change in temperature was achieved when the laser was applied for 2.5 s in 400 mW, as expected. The temperature changes during lasing,

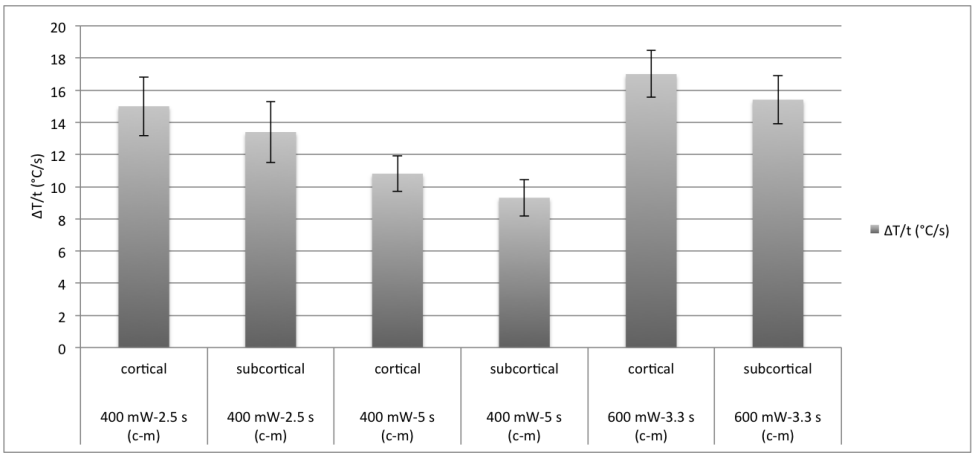

Figure 4.50 Rate of temperature change for the 1940-nm Tm:fiber laser in continuous mode study groups for cortical and subcortical tissues. Rate of temperature change in cortical tissues observed to be higher with respect to subcortical tissues ($p<0.05$). Increasing exposure time resulted in lower rates($p<0.001$), whereas increasing power resulted in higher rates ($p<0.001$).

when the amount of energy delivered to the tissue is same (400 mW-5 s and 600 mW-3.3s applications), were found to be similar. On the other hand, highest rate of temperature change was achieved at 600 mW-3.3 s and lowest was achieved at 400 mW-5 s (Figure 4.50). Both change in temperature and the rate of temperature change was observed to be higher at cortical tissues.

Two different two-way ANOVA were performed. With the first one, it is investigated if the tissue type and exposure time affect the change in temperature and the rate of temperature change. The results revealed that the tissue type and the laser exposure time had a significant effect on temperature change ($p=0.002$ and $p<0.001$, respectively) and the rate of change ($p=0.008$ and $p<0.001$, respectively). Second two-way ANOVA was performed in order to find if the tissue type and the change in energy delivery via power and exposure time, affect the measurements. The results revealed that the tissue type had a significant effect on temperature change ($p<0.001$) and rate ($p=0.002$) whereas change in energy delivery did not affect the temperature change ($p=0.060$) but the rate ($p<0.001$). Tables 4.10 and 4.11 show the significance levels of the change in temperature and the rate of temperature change for both cortical and subcortical tissues when irradiated by 1940-nm Tm:fiber laser with varying exposure times and energy delivery respectively.

Table 4.10
The significance levels of the change in temperature and the rate of temperature change with varying exposure times for 1940-nm Tm:fiber laser in continuous mode applied on cortical and subcortical tissue for 400 mW.

Statistical Analysis \ Dependent Variable		p-values	
		ΔT	ΔT/t
ANOVA		<0.001	<0.001
post-hoc tests	Cortical 400 mW-2.5 s - Cortical 400 mW-5 s	<0.001	<0.001
	Cortical 400 mW-2.5 s - Subcortical 400 mW-2.5 s	0.317	0.181
	Cortical 400 mW-2.5 s - Subcortical 400 mW-5 s	0.010	<0.001
	Cortical 400 mW-5 s - Subcortical 400 mW-2.5 s	<0.001	0.011
	Cortical 400 mW-5 s - Subcortical 400 mW-5 s	0.024	0.231
	Subcortical 400 mW-2.5 s - Subcortical 400 mW-5 s	<0.001	<0.001

Table 4.11
The significance levels of the change in temperature and the rate of temperature change with varying exposure times for 1940-nm Tm:fiber laser in continuous mode applied on cortical and subcortical tissue for 2 J.

Statistical Analysis \ Dependent Variable		p-values	
		ΔT	ΔT/t
ANOVA		<0.001	0.003
post-hoc tests	Cortical 400 mW-5 s - Cortical 600 mW-3.3 s	0.792	<0.001
	Cortical 400 mW-5 s - Subcortical 400 mW-5 s	0.023	0.126
	Cortical 400 mW-5 s - Subcortical 600 mW-3.3 s	0.619	<0.001
	Cortical 600 mW-3.3 s - Subcortical 400 mW-5 s	0.002	<0.001
	Cortical 600 mW-3.3 s - Subcortical 600 mW-3.3 s	0.164	0.094
	Subcortical 400 mW-5 s - Subcortical 600 mW-3.3 s	0.275	<0.001

For the results of *in vivo* experiments with 1940-nm Tm:fiber laser in continuous mode, the Spearman's rank correlation coefficients and Pearson's correlation coefficients were calculated to see if there is a correlation between rates of temperature change and ablation efficiencies and total damage and edematous area. Calculated Pearson's correlation coefficients, r and Spearman's rank correlation coefficient, ρ are given in Table 4.12.

In Figure 4.51 those relations were presented.

Table 4.12
Pearson's correlation (r) and Spearman's rank correlation (ρ) coefficients for 1940-nm Tm:fiber laser in continuous mode.

Tissue Type	Exposure Time (s)	Power (mW)	AE		Total Damage		Edema	
			r	ρ	r	ρ	r	ρ
Cortical	2.5	400	0.724	0.476	-0.872	-0.881	-0.738	-0.667
	5	400	0.908	0.928	-0.753	-0.810	-0.706	-0.690
	3.3	600	0.950	0.976	-0.807	-0.738	-0.884	-0.976
Subcortical	2.5	400	0.823	0.857	-0.584	-0.571	-0.675	-0.786
	5	400	0.890	0.905	-0.861	-0.881	-0.616	-0.690
	3.3	600	0.830	0.905	-0.802	-0.857	-0.662	-0.690

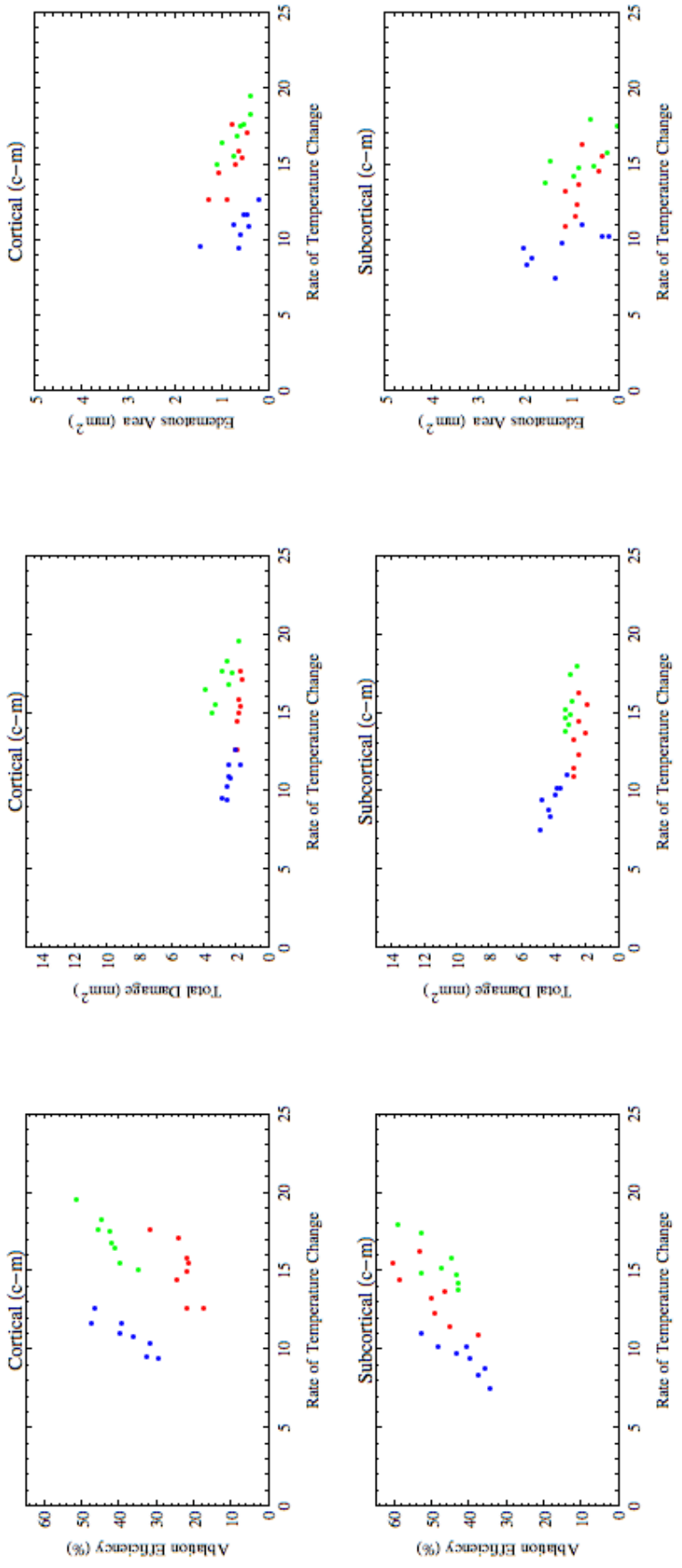

Figure 4.51 Ablation efficiency, total damage and edematous area versus rate of temperature change (from left to right) in 1940-nm Tm:fiber laser in continuous mode application for cortical (upper plots) and subcortical (lower plots) tissues. Red, blue and green dots represent 400 mW-2.5 s, 400 mW-5 s and 600 mW-3.3 s, respectively.

Irrespective of the tissue type, ablation efficiencies increased with increasing rate of temperature change, as it did for the *ex vivo* and 980-nm diode laser *in vivo* studies. A negative correlation between edemous tissue and rate of temperature change was also observed. A similar correlation exists between total damage and rate of temperature change.

In order to make a comprehensive analysis and to decide which parameter is more applicable compared to other one, edematous area around the lesion should be taken into account. The behaviours of the ablation efficiency and the edematous area with varying rate of temperature change were combined in a single three-dimensional plot for 1940-nm Tm:fiber laser. In Figures 4.52 and 4.53, it is obvious that the ablation efficiency increases with the increasing rate of temperature change, where the edematous area decreases, for cortical and subcortical tissues, respectively. To make a reliable comparison, we calculated the normalized values for edema and presented them in Figures 4.54 and 4.55 for cortical and subcortical tissues, respectively. Normalization of edematous area did not change the behaviours explained above for cortical tissue. For subcortical tissue, even though there is a similar trend, it is not that strong.

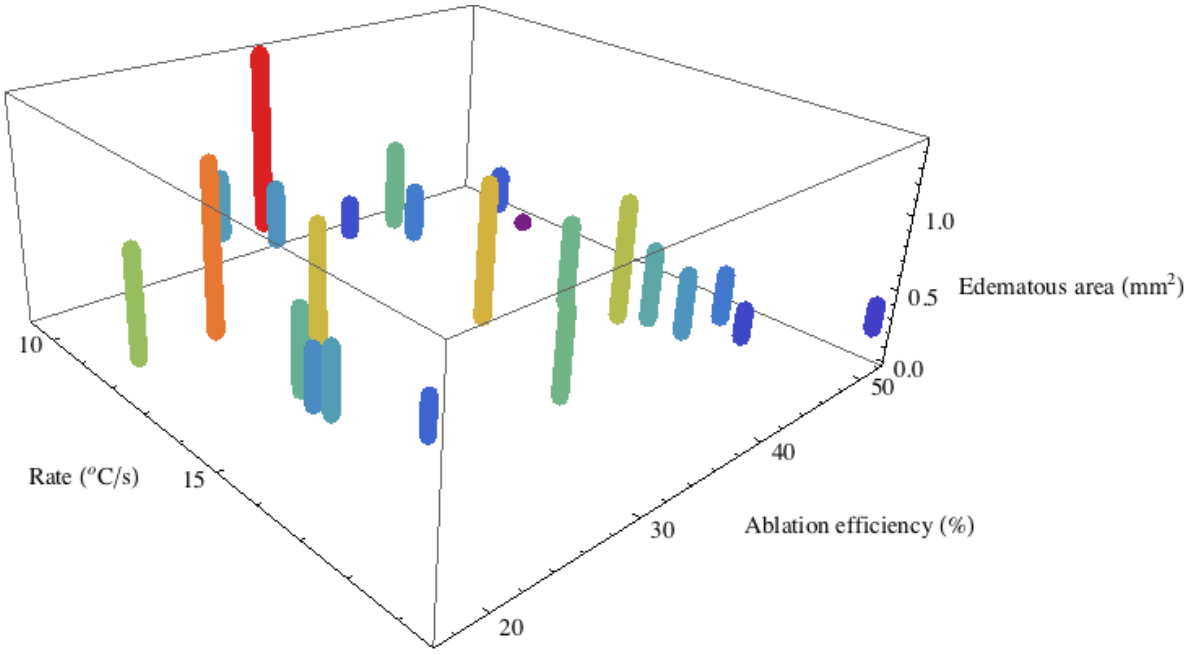

Figure 4.52 The ablation efficiency and the edematous area with varying rate of temperature change for 1940-nm Tm:fiber laser in continuous mode applied on cortical tissue. Color coding is proportional to the height of the bars.

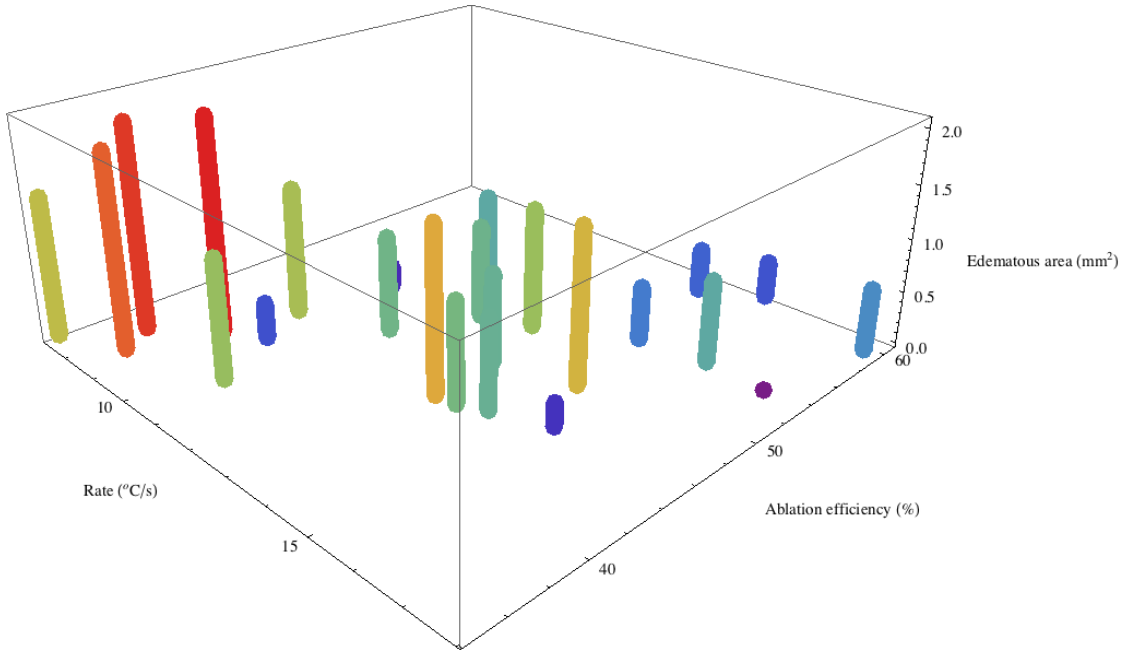

Figure 4.53 The ablation efficiency and the edematous area with varying rate of temperature change for 1940-nm Tm:fiber laser in continuous mode applied on subcortical tissue. Color coding is proportional to the height of the bars.

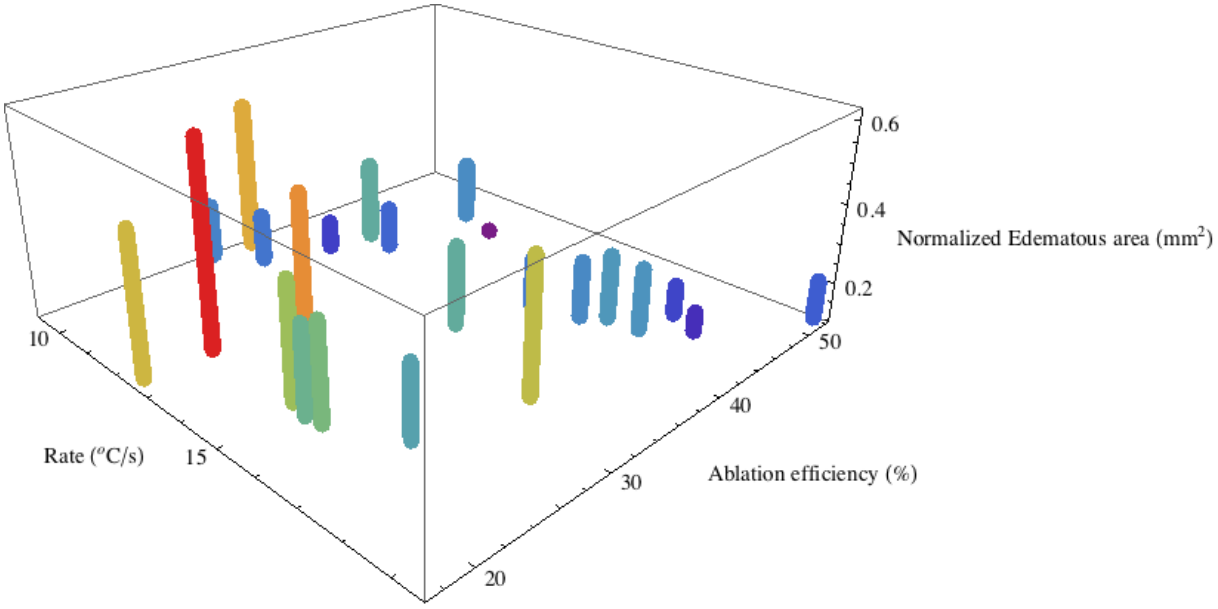

Figure 4.54 The ablation efficiency and the normalized edematous area with varying rate of temperature change for 1940-nm Tm:fiber laser in continuous mode applied on cortical tissue. Color coding is proportional to the height of the bars.

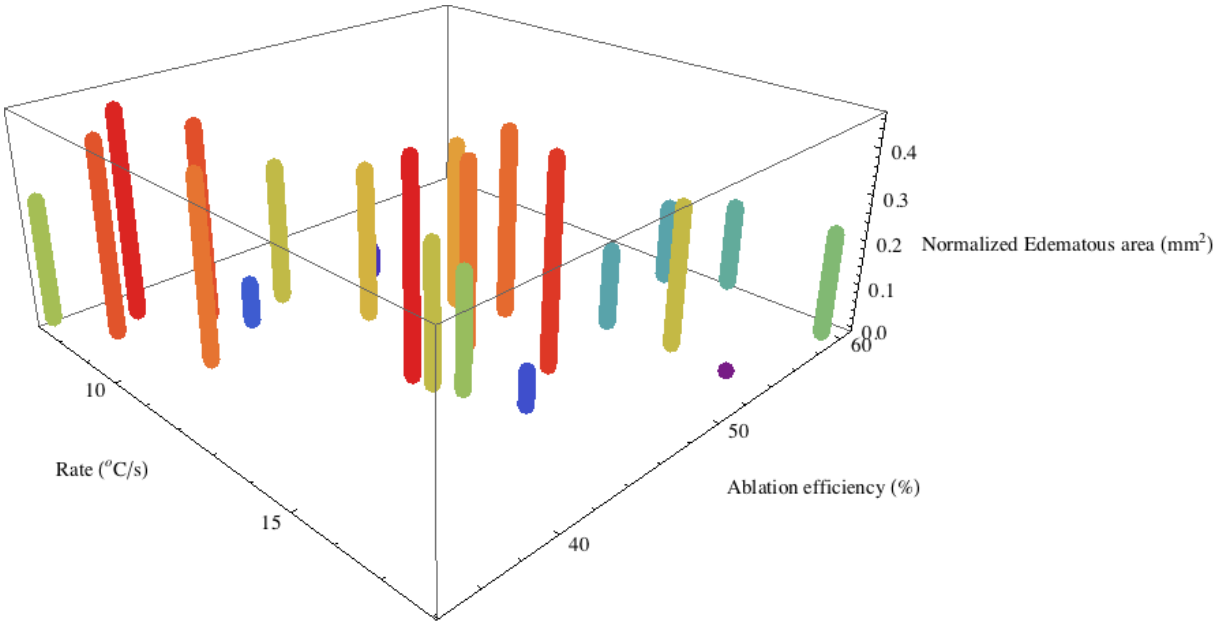

Figure 4.55 The ablation efficiency and the normalized edematous area with varying rate of temperature change for 1940-nm Tm:fiber laser in continuous mode applied on subcortical tissue. Color coding is proportional to the height of the bars.

4.4.3 1940-nm Tm:fiber laser pulsed-modulated-mode

4.4.3.1 Thermal effects. With the help of the *ex vivo* studies, two different laser parameters were determined to be investigated throughout the *in vivo* studies for 1940-nm Tm:fiber laser in pulsed-modulated-mode: 400 mW-5 s and 600 mW-3.3 s. Examples of CFV stained subcortical tissue samples can be seen in Figure 4.56.

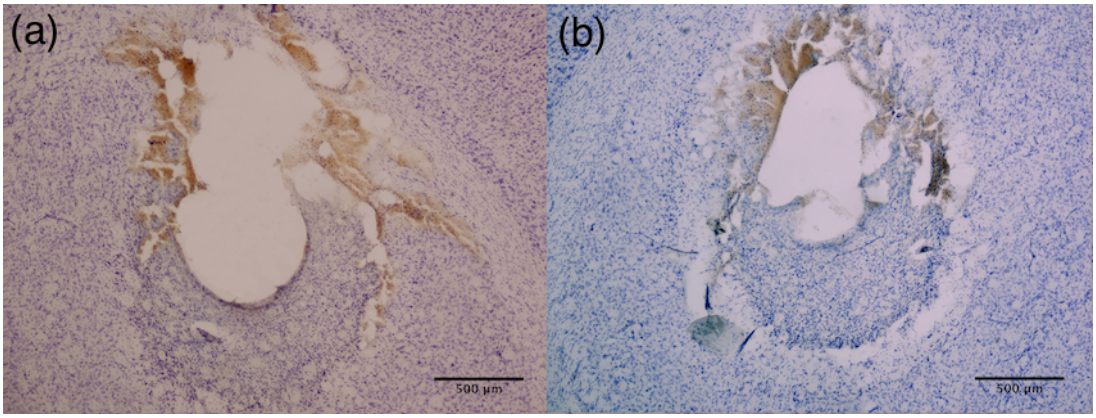

Figure 4.56 Light micrographs of CFV stained 50 μm sections of subcortical tissues induced by 1940-nm Tm:fiber laser in pulsed-modulated mode with laser parameter combinations of a) 400 mW, 5 s b) 600 mW, 3.3 s (Magnification=40X).

With two-way ANOVA, it is investigated if the tissue type and the change in energy delivery via power and exposure time affect the measured parameters. The results revealed that the tissue type and change in energy delivery had a significant effect on ablated ($p=0.004$ and $p=0.021$, respectively), coagulated ($p<0.001$ for both), edematous ($p=0.007$ and $p=0.002$, respectively), normalized edematous ($p<0.001$ and $p=0.013$, respectively) areas and ablation efficiency ($p=0.009$ and $p<0.001$, respectively). The mean values and standard deviations of ablated area, coagulated area and edamatous area and ablation efficiencies were listed in Table 4.13 and plotted in Figure 4.57.

Applications on cortical tissues resulted in smaller thermally altered areas with respect to subcortical tissues. But ablation efficiencies observed to be higher for cortical tissues, where the highest efficiency was obtained for 600 mW-3.3 s application on cortical tissue. We see a large edema for 400 mW-5 s on cortical tissue. Ablation areas in subcortical tissues are slightly higher than those in cortical tissues but the coagulated areas are almost doubled when the laser was applied on subcortical tissues, which explains

Table 4.13
Mean ablated areas (AA), coagulated areas (CA), edamatous areas (EA), normailzed edematous areas (NEA) and ablation efficiencies (AE) for the 1940-nm Tm:fiber laser in pulsed-modulated-mode applications with two different laser parameters in cortical and subcortical tissues.

Tissue	Power (mW)	Exposure Time (s)	AA (m^2)	CA (m^2)	EA (m^2)	Normalized Edema	AE (%)
Cortical	400	5	0.51 ± 0.16	0.87 ± 0.17	1.39 ± 0.49	0.49 ± 0.13	36.58 ± 8.53
	600	3.3	0.71 ± 0.24	0.71 ± 0.19	0.84 ± 0.42	0.36 ± 0.15	49.22 ± 10.75
Subcortical	400	5	0.76 ± 0.18	1.75 ± 0.17	0.93 ± 0.36	0.27 ± 0.09	30.01 ± 5.64
	600	3.3	0.90 ± 0.21	1.33 ± 0.15	1.46 ± 0.36	0.17 ± 0.11	40.13 ± 5.59

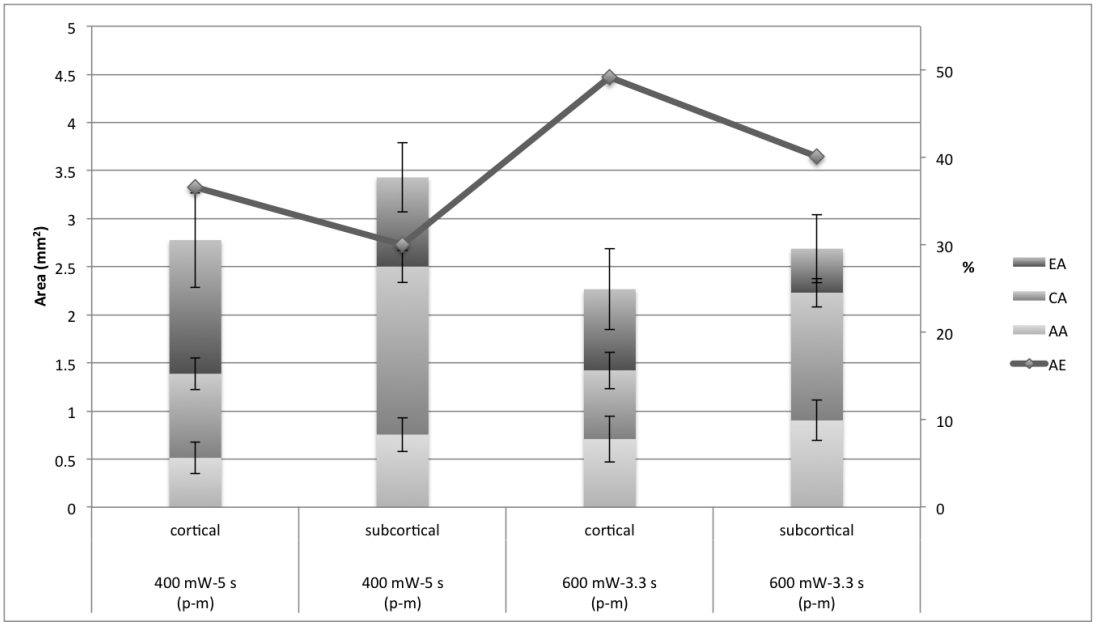

Figure 4.57 The thermal effects of 1940-nm Tm:fiber laser on cortical and subcortical tissues at 4 joules energy level (CD: Coagulation diameter, AD: Ablation diameter, AE: Ablation efficiency). Y1 axis and columns indicate the ablated, coagulated and edematous areas, Y2 axis and line graph indicate the ablation efficiency values with respect to stated laser power. Ablated and coagulated areas in cortical tissues were observed to be smaller compared to subcortical tissues ($p<0.05$ and $p<0.001$, respectively), whereas edematous areas and ablation efficiencies were observed to be bigger ($p<0.05$ for both). Increasing power resulted in an in increase in ablated areas ($p<0.05$), a decrease in coagulated and edematous areas ($p<0.001$ and $p<0.05$, respectively) and an increase in ablation efficiencies ($p<0.001$).

lower ablation efficiencies. The significance levels obtained via Tukey test, of ablated area, coagulated area, edematous area, normalized edematous area and ablation efficiency with varying exposure times were given in Table 4.14.

To illustrate ablated and coagulated areas, energy delivery method and ablation efficiencies in a single figure, we plot ablated area against the coagulated area, mark different energy deliveries with a color code and the ablation efficiencies manifest themselves

Table 4.14
The significance levels of ablated area, coagulated area, edematous area, normalized edematous area and ablation efficiency with varying energy delivery for 1940-nm Tm:fiber laser in pulsed-modulated-mode applied on cortical and subcortical tissues.

Statistical Analysis \ Dependent Variable		p-values				
		AA	CA	EA	NEA	AE
ANOVA		0.005	<0.001	0.001	<0.001	<0.001
post-hoc tests	Cortical 400 mW-5 s - Cortical 600 mW-3.3 s	0.225	0.253	0.058	0.181	0.017
	Cortical 400 mW-5 s - Subcortical 400 mW-5 s	0.093	<0.001	0.131	0.005	0.364
	Cortical 400 mW-5 s - Subcortical 600 mW-3.3 s	0.003	<0.001	0.001	<0.001	0.807
	Cortical 600 mW-3.3 s - Subcortical 400 mW-5 s	0.965	<0.001	0.978	0.411	<0.001
	Cortical 600 mW-3.3 s - Subcortical 600 mW-3.3 s	0.229	<0.001	0.258	0.016	0.124
	Subcortical 400 mW-5 s - Subcortical 600 mW-3.3 s	0.461	<0.001	0.127	0.371	0.073

as straight lines with varying slopes on that plot. In Figure 4.58, it can be seen that 600 mW applications result in higher ablated and lower coagulated areas compared to 400 mW applications, as stated before. As a consequence ablation efficiencies obtained in 600 mW applications (30-60%) are significantly higher than those obtained in 400 mW applications (20-50%). We also observed that in pulsed-modulated-mode applications on cortical tissues, results are more scattered compared to continuous mode applications.

In Figure 4.59, the differences in ablated and coagulated areas and therefore ablation efficiencies for varying power output are more apparent. Again we see higher efficiencies for fast delivery (600 mW-3.3 s) which lie between the interval of 30-50%. The efficiencies in slow delivery (400 mW-5 s) are about 20-40%.

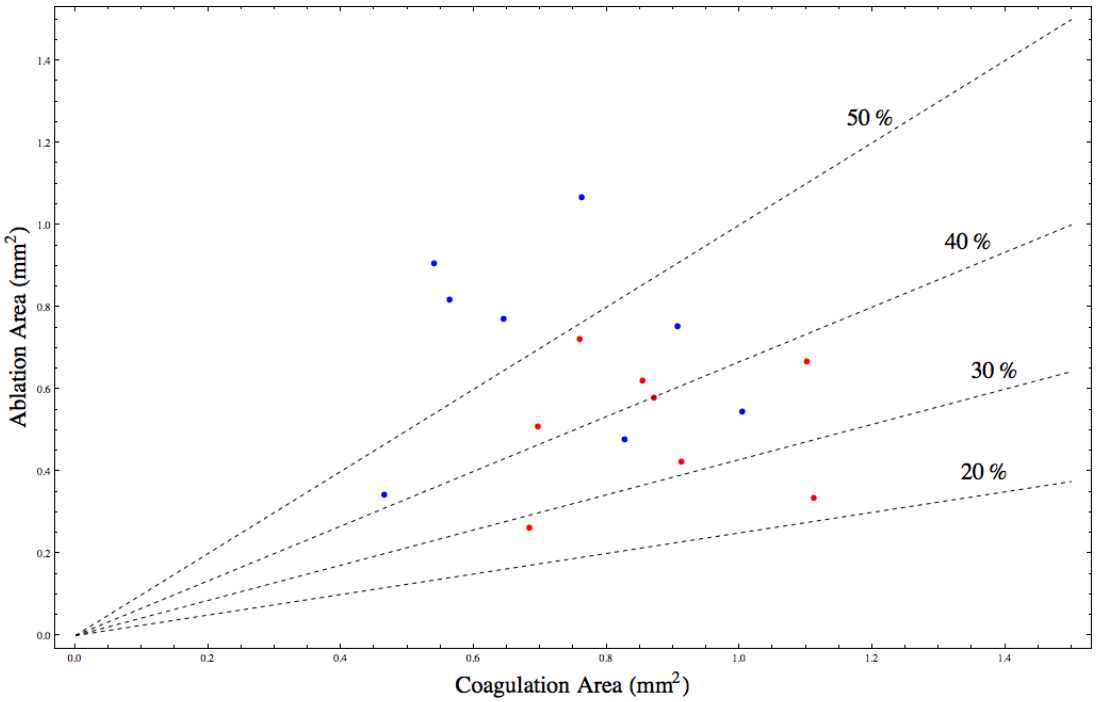

Figure 4.58 Ablated area versus coagulated area for 1940-nm Tm:fiber laser on pulsed-modulated-mode applied on cortical tissue. Red and blue dots represent 400 mW-5 s and 600 mW-3.3 s applications respectively. Ablation efficiencies are given as dashed straight lines.

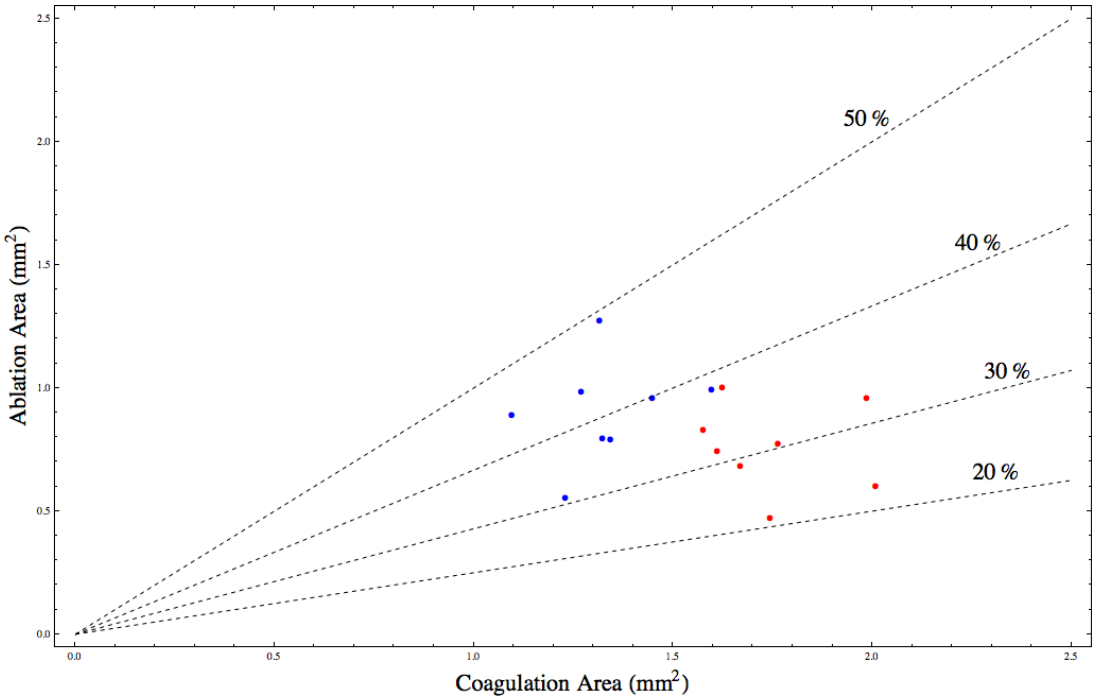

Figure 4.59 Ablated area versus coagulated area for 1940-nm Tm:fiber laser on pulsed-modulated-mode applied on subcortical tissue. Red and blue dots represent 400 mW-5 s and 600 mW-3.3 s applications respectively. Ablation efficiencies are given as dashed straight lines.

4.4.3.2 Temperature measurements. Temperature of the nearby tissue during lasing was measured at a distance of 1 mm above and 1 mm away from the fiber tip. Again, for each application temperature of the tissue and the time to reach maximum temperature were measured. The changes in the temperature and the rates of the temperature change were calculated. Table 4.15 shows mean values and standard deviations of these variables for 1940-nm Tm:fiber laser in pulsed-modulated-mode study groups.

Table 4.15
Mean values and standard deviations of the temperature change, the time to reach maximum temperature and the rate of temperature change for 1940-nm Tm:fiber laser in pulsed-modulated-mode study groups.

Tissue	Power (mW)	Exposure Time (s)	ΔT (C)	Time (s)	ΔT/t (C/s)
Cortical	400	5	24.49 ± 3.11	10.09 ± 0.13	2.42 ± 0.28
	600	3.3	27.37 ± 5.06	6.64 ± 0.07	4.12 ± 0.75
Subcortical	400	5	21.46 ± 3.03	10.09 ± 0.05	2.13 ± 0.30
	600	3.3	23.69 ± 2.73	6.66 ± 0.06	3.56 ± 0.41

Change in temperature during lasing and rates of the temperature change for the pulsed-modulated-mode applied on cortical and subcortical tissues were plotted in Figures 4.60 and 4.61, respectively.

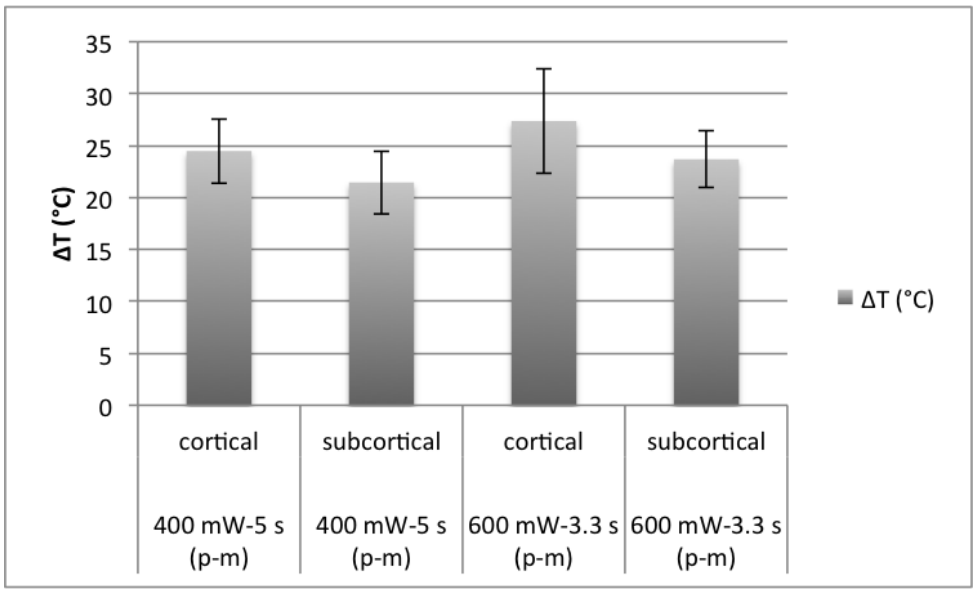

Figure 4.60 Temperature change for the 1940-nm Tm:fiber laser in pulsed-modulated-mode study groups for cortical and subcortical tissues. Temperature increase in cortical tissues observed to be higher with respect to subcortical tissues ($p<0.05$). Increasing power resulted in a higher temperature increase ($p=0.054$).

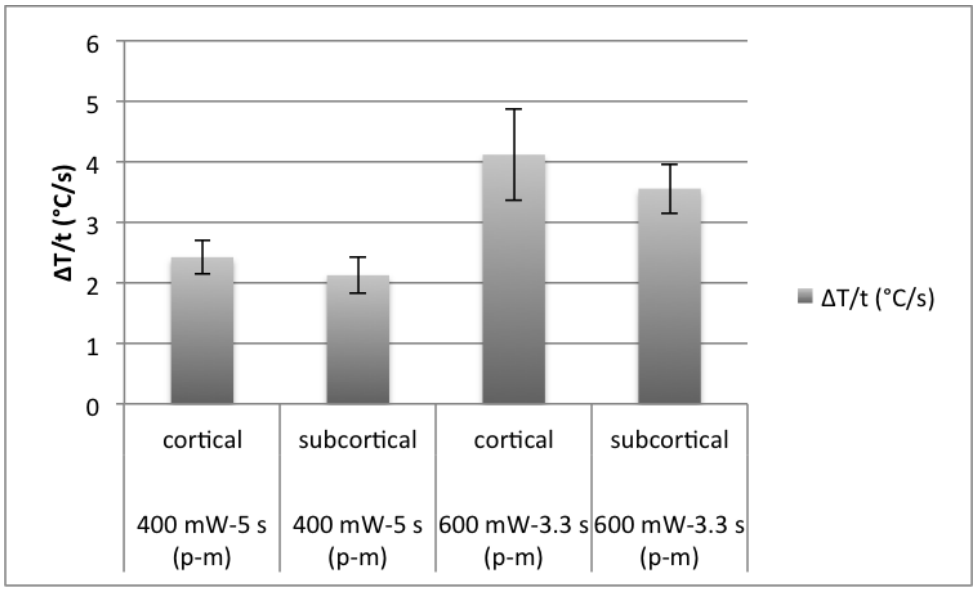

Figure 4.61 Rate of temperature change for the 1940-nm Tm:fiber laser in pulsed-modulated-mode study groups for cortical and subcortical tissues. Rate of temperature change in cortical tissues observed to be higher with respect to subcortical tissues ($p<0.05$). Increasing power resulted in a higher rate ($p<0.001$).

Figure 4.60 shows that the least change in temperature was achieved when the laser was applied for 5 s in 400 mW. Even though the amount of energy delivered to the tissue is same for both power outputs, we see that the temperature change is slightly higher for 600 mW applications. From Figure 4.61, we see that rates of temeperature change are remarkably higher for 600 mW applications. Both changes in temperature and the rates of temperature change was observed to be higher at cortical tissues.

Two-way ANOVA was performed, in order to investigate if the tissue type and the change in energy delivery via power and exposure time affect the change in temperature and the rate of temperature change. The results revealed that the tissue type and the change in energy delivery had a significant effect on temperature change ($p=0.014$ and $p=0.054$, respectively) and rate ($p=0.016$ and $p<0.001$, respectively). Table 4.16 shows the significance levels of the change in temperature and the rate of temperature change for both cortical and subcortical tissues when irradiated by 1940-nm Tm:fiber laser in pulsed-modulated-mode with varying energy delivery.

For the results of *in vivo* experiments with 1940-nm Tm:fiber laser in pulsed-modulated-mode, the Spearman's rank correlation coefficients and Pearson's correlation

Table 4.16
The significance levels of the change in temperature and the rate of temperature change with changing energy delivery for 1940-nm Tm:fiber laser in pulsed-modulated-mode applied on cortical and subcortical tissues.

Statistical Analysis \ Dependent Variable		p-values	
		ΔT	ΔT/t
ANOVA		0.024	<0.001
post-hoc tests	Cortical 400 mW-5 s - Cortical 600 mW-3.3 s	0.394	<0.001
	Cortical 400 mW-5 s - Subcortical 400 mW-5 s	0.351	0.599
	Cortical 400 mW-5 s - Subcortical 600 mW-3.3 s	0.970	<0.001
	Cortical 600 mW-3.3 s - Subcortical 400 mW-5 s	0.014	<0.001
	Cortical 600 mW-3.3 s - Subcortical 600 mW-3.3 s	0.196	0.110
	Subcortical 400 mW-5 s - Subcortical 600 mW-3.3 s	0.608	<0.001

coefficients were calculated to see if there is a correlation between rates of temperature change and ablation efficiencies and total damage and edematous area. Calculated Pearson's correlation coefficients, r and Spearman's rank correlation coefficient, ρ are given in Table 4.17. In Figure 4.62 those relations were presented.

Table 4.17
Pearson's correlation (r) and Spearman's rank correlation (ρ) coefficients for 1940-nm Tm:fiber laser in pulsed-modulated-mode.

Tissue Type	Exposure Time (s)	Power (mW)	AE		Total Damage		Edema	
			r	ρ	r	ρ	r	ρ
Cortical	5	400	0.873	0.857	-0.779	-0.762	-0.812	-0.857
	3.3	600	0.906	0.881	-0.742	-0.738	-0.604	-0.595
Subcortical	5	400	.838	0.762	-0.570	-0.714	-0.803	-0.619
	3.3	600	0.863	0.881	-0.879	-0.905	-0.880	-0.857

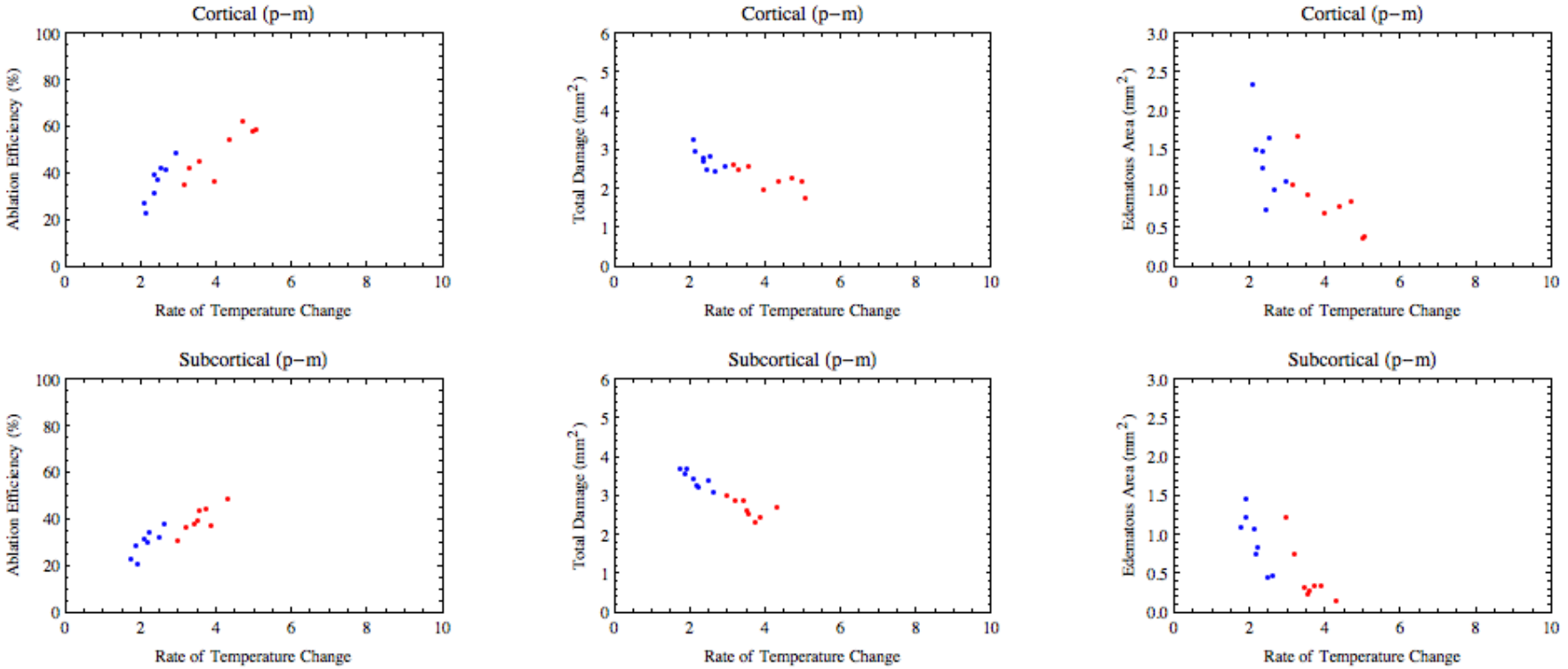

Figure 4.62 Ablation efficiency, total damage and edematous area versus rate of temperature change (from left to right) in 1940-nm Tm:fiber laser in pulsed-modulated-mode application for cortical (upper plots) and subcortical (lower plots) tissues. Red and blue dots represent 400 mW-5 s and 600 mW-3.3 s, respectively.

Irrespective of the tissue type, ablation efficiencies increased with increasing rate of temperature change, as it did for the *ex vivo* and previous *in vivo* studies. A negative correlation between edemous tissue and rate of temperature change was also observed. A similar correlation exists between total damage and rate of temperature change.

The behaviours of the ablation efficiency and the edematous area with varying rate of temperature change were combined in a single three-dimensional plot for 1940-nm Tm:fiber laser in pulsed-modulated-mode. In Figures 4.63 and 4.64, it is obvious that the ablation efficiency increases with the increasing rate of temperature change, where the edematous area decreases, for cortical and subcortical tissues, respectively. To make a reliable comparison, we calculated the normalized values for edema and presented them in Figures 4.65 and 4.66 for cortical and subcortical tissues, respectively. Normalization of edematous area did not change the behaviours explained above for cortical tissue. For subcortical tissue, even though there is a similar trend, it is not that strong.

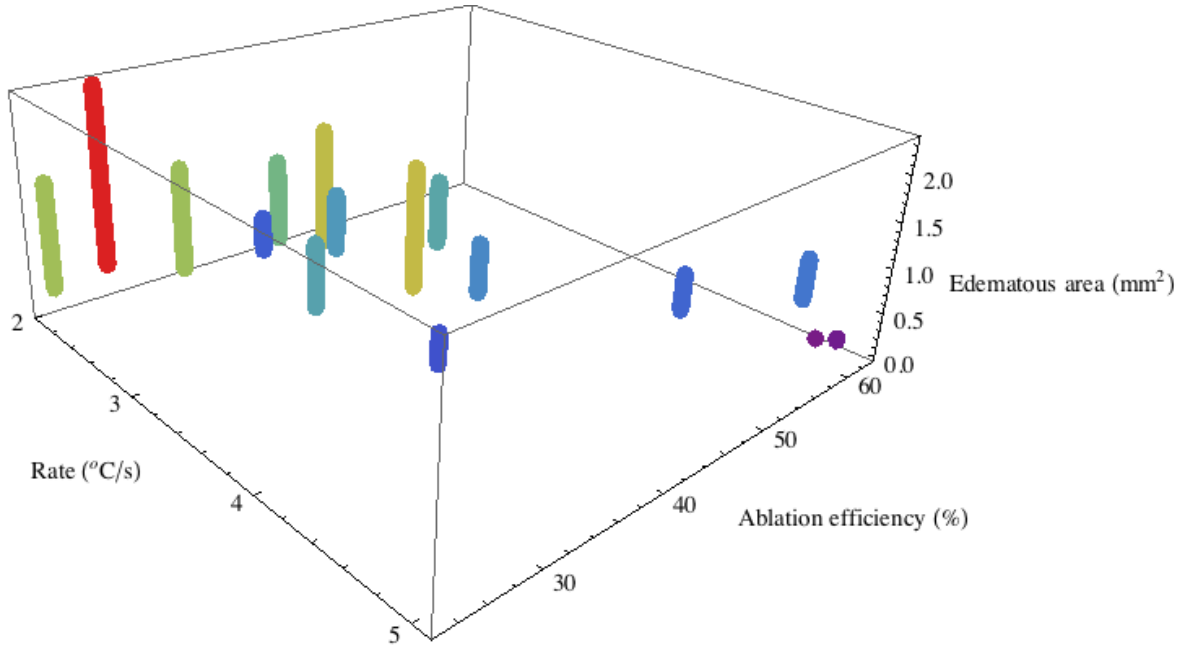

Figure 4.63 The ablation efficiency and the edematous area with varying rate of temperature change for 1940-nm Tm:fiber laser in pulsed-modulated-mode applied on cortical tissue. Color coding is proportional to the height of the bars.

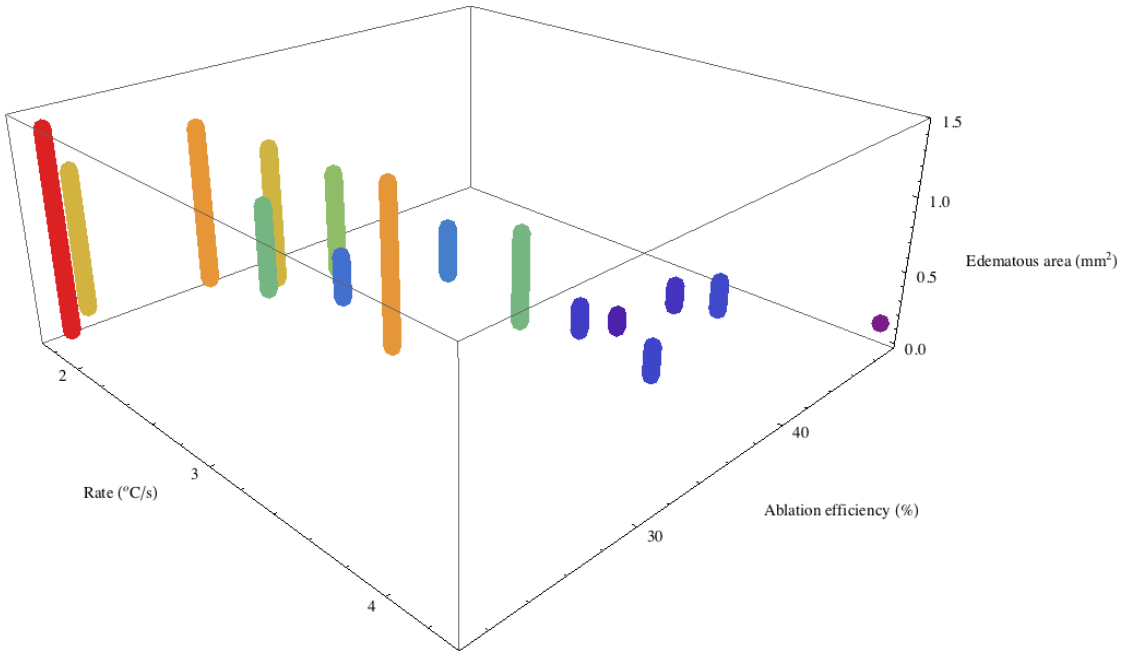

Figure 4.64 The ablation efficiency and the edematous area with varying rate of temperature change for 1940-nm Tm:fiber laser in pulsed-modulated-mode applied on subcortical tissue. Color coding is proportional to the height of the bars.

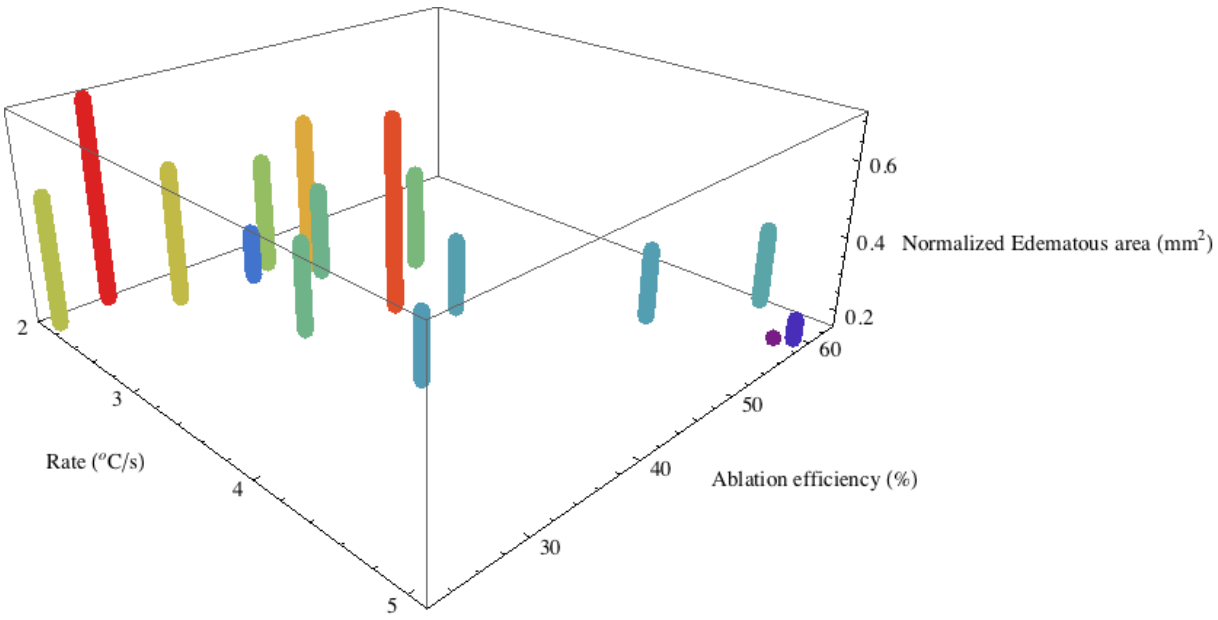

Figure 4.65 The ablation efficiency and the normalized edematous area with varying rate of temperature change for 1940-nm Tm:fiber laser in pulsed-modulated-mode applied on cortical tissue. Color coding is proportional to the height of the bars.

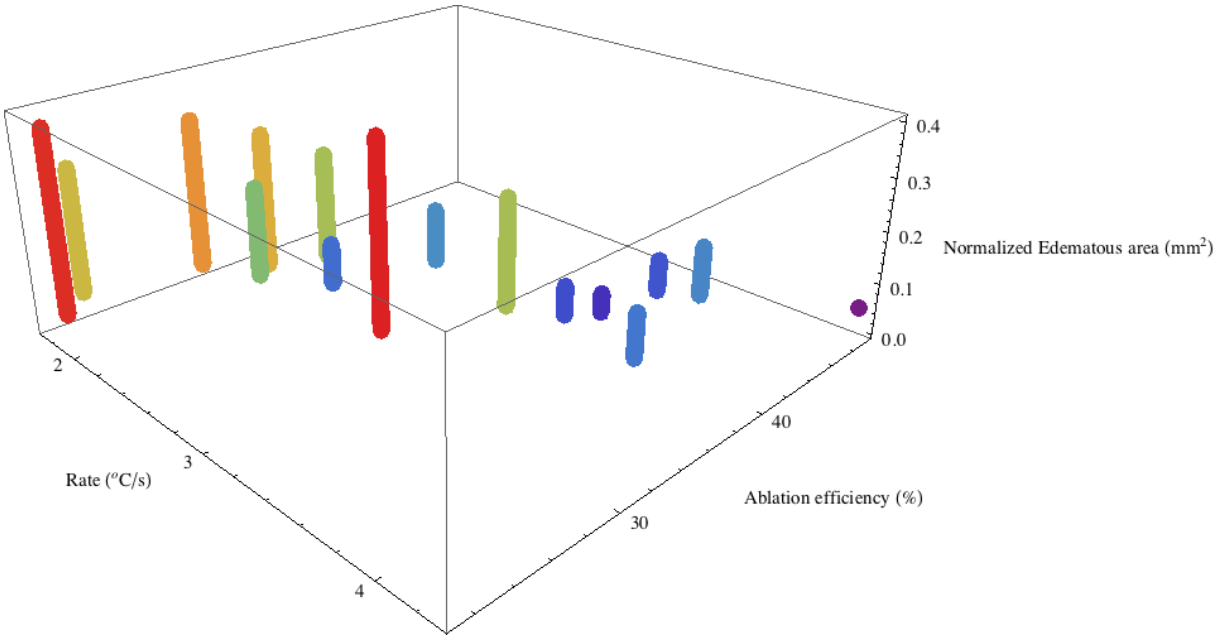

Figure 4.66 The ablation efficiency and the normalized edematous area with varying rate of temperature change for 1940-nm Tm:fiber laser in pulsed-modulated-mode applied on subcortical tissue. Color coding is proportional to the height of the bars.

4.5 Discussion

The 2-μm lasers have been proposed as potential ablators for soft tissues that are rich in water content and Tm:YAP laser emitting 1980-nm laser energy was presented as a new surgical tool for brain tissues previously by our group [149]. In the present study a new 1940-nm Tm:fiber laser was introduced for brain surgery, in addition to 980-nm diode laser. Ablation and coagulation were the expected photothermal effects but melting and carbonization could occur if the dose was not set properly. One way of proposing the laser as a convenient surgical tool is to carry out a well-defined dosimetry study and find a safe operating region. Ablation efficiency was a meaningful concept we defined previously [90, 149] and gave us an idea about the dose in terms of ablated tissue with respect to the thermal damage given. However dynamic changes with respect to the inhomogeneities can be crucial and can lead to a catastrophic carbonization and melting phase.

Tissue ablation and coagulation by laser irradiation is a complicated process, in-

volving many optical and thermodynamic processes. As laser light interacts with the tissue surface the photons energy is transformed into heat. Subsequent temperature increase in the tissue results in protein denaturation, coagulation, dehydration, carbonization and finally tissue ablation [6]. The conduction of this heat is directly related to laser parameters (such as laser type, wavelength, power, exposure time, pulse duration and pulse repetition), tissue parameters (such as tissue density, thermal conductivity and absorptivity) and environmental parameters [such as environmental medium (air, water), medium temperature] [19]. The dynamic variation of the optical properties with temperature alters the response of the tissue to the laser irradiation [150, 151]. In continuous wave laser irradiations, tissue is exposed to laser light for seconds, and the temperature of the tissue is continuously increasing, which causes a change in absorption coefficient. As the tissue is exposed to laser light, the temperature of the tissue increases and causes the tissue to dehydrate that is water content is changing dynamically [152, 153]. Individual differences as well as local inhomogeneities can undermine even the best dose estimation. real-time temperature monitoring can be an effective way to get rid of negative effects of the temporal and spatial irregularities. Therefore the laser-thermoprobe was designed for using the near-by tissue temperature as a real-time reference for the applicator. Laser-thermoprobe designed by our group lead us to understand and investigate basic laser-tissue interaction mechanism in a very cheap and easy way, without making a change in the experimental design.

In addition to investigating the ablative effects of three different laser sources and specifying the optimal parameters, another aim of the present study was to investigate the potential of a new laser thermoprobe, which consists of a laser and real-time thermocouple measurement system for brain surgery. Specifically, different parameters (laser power, energy density, exposure time, continuous-mode or pulsed-modulated-mode) were tested and the ablation efficiency (the amount of removed tissue with respect to the total photothermal damage) was investigated with reference to the real-time temperature measurements of nearby tissue in an *ex vivo* and *in vivo* study. Relationship between rate of temperature change over time and the thermal effects of the laser application was investigated. Although the primary emphasis in the study was on the relation between the rate of the temperature change and ablation efficiencies, some comparisons were also

made with 980-nm diode and 1940-nm Tm:fiber laser.

Three different laser sources with different application modes, powers and exposure times were investigated in this *ex vivo* and *in vivo* studies. For each parameter the ablated and coagulated areas were measured under light microscope, then the ablation efficiencies -to give us an insight about how much of the tissue was ablated with respect to the damage to the surroundings- and rates of temperature change were calculated. Laser light was transferred through an optical fiber. Both in *ex vivo* and *in vivo* studies lasers were applied in contact mode to reduce the amount of reflected laser light from tissue.

4.5.1 Laser Power

Ablated and coagulated areas increased with increasing power consistent with literature for both tissue types, laser types and modes of operation (c-m, p-m-m) and both *ex vivo* and *in vivo* studies [90, 154–156]. Ablation efficiencies, on the other hand, increased with increasing power up to 2 W for 980-nm *ex vivo* study and then reached a plateau. Beyond that threshold, there is a trend of decreasing in efficiencies due to the increase in coagulated areas at a higher rate than the ablated areas. For 1940-nm *ex vivo* studies, efficiencies increased with increasing power regardless of the mode of operation. But with the higher power applications, carbonization was also observed in addition to ablation and coagulation. Relatively higher ablation efficiencies were observed in studies with 1940-nm Tm:fiber laser compared to that of the 980-nm diode laser.

For the *in vivo* applications, there is an increasing trend in ablation efficiencies with increasing power for both modes of operation and tissue types. Efficiencies in *in vivo* applications ranged between 20% and 60% whereas efficiencies in *ex vivo* applications were observed to be higher. The main reason for this difference is that the measurements for *ex vivo* applications were done in terms of length but the measurements for *in vivo* studies were done in terms of area. The difference in application also may have caused this difference in efficiencies. In *ex vivo* studies laser was applied perpendicular to coronal sections whereas in *in vivo* studies it was applied coronally. Thus, we can not account for

the effects of the blood flow.

In addition to ablated and coagulated areas, edema was also observed in *in vivo* applications. It is observed that edematous areas showed a trend of decrease with increasing power.

In some experiments, even though the total energy delivered to the tissue was same, it was observed that ablation efficiencies varied with varying power outputs. This shows the importance of monitoring the increase in tissue temperature during laser irradiation.

4.5.2 Laser Wavelength

Absorbents in the tissue can be listed as water, porephyrine, haemoglobin, melanin, flavin, retinol and nucleic acids. Since biological tissues are made of 60-80% water, absorption in the infrared and near-infrared regions are made generally by water molecules. When the electromagnetic waves interact with the tissue, its energy is converted to heat. Absorption coefficient, μ_a, characterizes the absorption [6]. Right after penetration, light propagates in the tissue with its energy decreasing due to absorption and scattering, obeying the Beer's law,

$$I(l) = I_0 e^{-\sigma_a N_a l} = I_0 e^{-\mu_a l} \tag{4.1}$$

where I is the intensity of the light as a function of distance, l, I_0 is the initial intensity, σ_a is the interaction cross section and N_a is the concentration of the absorbent molecule.

Scattering characteristics of the tissue is important regarding the distribution of photons inside the tissue. Scattering becomes dominant in the tissue in visible and near-infrared region (400-1200 nm) [157]. Laser-tissue interaction begins with scattering followed by absorption and generation of heat.

Three different lasers were investigated in this study; 980-nm, 1070-nm and 1940-nm. 1070-nm laser did not have the ablation capability due to scattering domination

around that wavelength as explained above, therefore it was used for coagulation in *ex vivo* studies only. Even though the 980-nm is also in that scattering dominated range, its absorption by haemoglobin makes the applications of this wavelength interesting for medical use. Therefore, we compare 980-nm and 1940-nm lasers in this section.

When *ex vivo* studies are examined, it was observed that 1940-nm laser was more successful in terms of ablation efficiencies with respect to 980-nm laser for both tissue types. Similar lesions were obtained when the delivered energy has the same amount for both wavelengths, but vaporized tissue was bigger in 1940-nm laser. This can be explained by the absorption peak of water at 1940-nm which is higher than at 980-nm. Additionally, penetration depth for 1940-nm is lower than the one for 980-nm. The preference to use 980-nm lasers in medical surgeries is due to its high absorbance by haemoglobin, which is helpful to prevent bleeding. But in *ex vivo* studies, the structure of haemoglobin is degenerated due to protein denaturation and therefore its optical properties will change. So, the process is dominated by the water absorbance, which leads to a more efficient application of 1940-nm laser. Domination by water absorbance could be better understood when subcortical tissue applications were examined. In subcortical tissues both laser wave lengths created smaller lesion in comparison to cortical applications, because subcortical tissues are poorer in water content.

For *in vivo* studies, things are more complicated due to the presence of haemoglobin and blood flow. Existence of haemoglobin increases the absorption of 980-nm laser light, whereas blood flow in the tissue causes convection that may reduce ablation and increase coagulation. Blood flow rate is lower in the subcortical tissues, which means less absorption by haemoglobin. That can explain smaller subcortical lesions obtained with the 980-nm laser applications. On the other hand, on cortical tissues 1940-nm laser is more successful like it was in *ex vivo* studies. Although haemoglobin absorption increases the thermal effects of 980-nm laser, high blood flow rate in the cortical tissue may have contributed to coagulation through the dissipation of heat via convection. Additionally, lesions created by 1940-nm laser were bigger in subcortical tissues than the ones in cortical tissues and ablation efficiencies obtained were higher for subcortical tissues. This is in contradiction with the *ex vivo* results. The subcortical zones created in the *in vivo* studies

were deeper in the tissue, whereas zones in *ex vivo* studies were created on the surface of the cut sample. Therefore heat created in the *in vivo* studies was trapped in the tissue and this may be the reason for bigger lesions created in subcortical tissues. Another reason may be the difference in the blood flow rates between the cortical and subcortical tissues in *in vivo* studies. Higher blood flow rate in the cortical tissues may contributed more to coagulation rather than ablation, as it did for 980-nm laser via convection, which may explain the lower efficiencies for cortical tissues when 1940-nm laser was applied.

4.5.3 Mode of Operation

The effect of mode of operation was studied for Tm:fiber laser only. Regardless of the tissue type, a decrease was observed in ablated areas when switched mode of operation from c-m to p-m-m, in *ex vivo* studies ($p<0.001$). In addition to this, an increase in the coagulated areas was observed. This results in a dramatic decrease in ablation efficiencies ($p<0.001$).

For *in vivo* studies, a three-way ANOVA was performed to reveal if the tissue type, mode of operation and change in energy delivery via power and exposure time affect the measured quantities. The results revealed that the tissue type, mode of operation and change in energy delivery via power and exposure time affected ablated area ($p<0.001$, $p<0.001$ and $p=0.016$, respectively) and coagulated area ($p<0.001$, $p=0.019$ and $p<0.001$, respectively). On the other hand, edematous area was affected only by the change in energy delivery ($p=0.003$), whereas when the edematous area was normalized, values are affected by all three parameters ($p=0.004$, $p=0.025$ and $p=0.040$). Additionally, ablation efficiency was affected by the change in energy delivery and mode of operation ($p<0.001$ and $p=0.030$, respectively). The significance levels for the effects of mode of operation are given in Table 4.18.

Ablated areas were bigger for c-m applications in both types of tissues, whereas coagulated areas were bigger only in cortical tissues but were similar in subcortical tissues. Edematous areas turned out to be bigger for p-m-m applications in both types of tissues.

This can be explained by the reasoning that the low rate of energy delivery causes much more thermal damage to the surroundings instead of vaporizing the target. Ablation efficiencies were higher for c-m applications considering the subcortical tissues but they were in a similar range in cortical tissues for both modes of operation. However, the standard deviations for ablation efficiencies for p-m-m applications turned out to be bigger than for c-m applications.

Table 4.18
The significance levels of ablated area, coagulated area, edematous area, normalized edematous area and ablation efficiency with varying energy delivery for 1940-nm Tm:fiber laser (c-m vs. p-m-m) applied on cortical and subcortical tissues.

Statistical Analysis \ Dependent Variable		p-values				
		AA	CA	EA	NEA	AE
ANOVA		<0.001	<0.001	0.003	<0.001	<0.001
post-hoc tests	Cortical 400 mW-5 s (c-m) - Cortical 400 mW-5 s (p-m-m)	0.035	0.028	0.004	0.001	0.685
	Cortical 600 mW-3.3 s (c-m) - Cortical 600 mW-3.3 s (p-m-m)	0.048	0.001	0.398	0.041	0.156
	Subcortical 400 mW-5 s (c-m) - Subcortical 400 mW-5 s (p-m-m)	0.001	0.617	0.288	0.702	0.002
	Subcortical 600 mW-3.3 s (c-m) - Subcortical 600 mW-3.3 s (p-m-m)	0.091	0.171	0.166	0.245	0.012

4.5.4 Temperature increase

Our results revealed that irrespective of the tissue type, mode of operation, laser wavelength and laser power, there is a strong correlation between the rate of temperature change and ablation efficiency for both *ex vivo* and *in vivo* studies. A similar correlation between rate of temperature change and total damage and a negative correlation between the rate of temperature change and edematous area were found. The temperature increase itself does not give us an insight about the characteristics of laser-lesion. However, a fast and sudden increase in the temperature in the tissue results in less thermal damage to the surroundings, in terms of coagulation and edema, more vaporized tissue, whereas slow increase in the temperature results in more thermal damage to the surroundings and less vaporized tissue.

Strong correlations observed in the analysis tells us that temperature monitoring is crucial in laser surgery, in order to reduce the irreversible thermal damage and edema and avoid carbonization, which is a great medical concern. Therefore, we declare the rate

of temperature change as a key indicator for scientists and surgeons to understand what proportion of the tissue is vaporized and how efficient the operations were carried out.

5. CONCLUSION

The goal of this study was to investigate the ablative effect of three different laser sources and to propose a new thermoprobe in dose determination studies in order to estimate the ablation quality of laser doses. The motivation for this study was that with a better establishment of experiments for investigating photothermal effects of lasers, it may be possible to overcome the side effects of photothermal interactions and to specify optimal laser parameters in order to propose lasers in clinical use for laser-assisted medical surgeries.

Continuous wave laser irradiation of biological tissue is a highly dynamic process; when laser light interacts with the tissue, the light is distributed due to the optical parameters of the irradiated tissue. In order to achieve photothermal interaction, wavelength with high absorption coefficients are preferred. The effect of scattering of light is generally not concern due to this high absorption coefficient. The absorbed laser light is the source of energy to decompose the tissue. Generally, in laser studies absorption coefficient is assumed to be constant, however, Jansen *et al.* [150] showed that the absorption coefficient is changing with temperature. This dynamic property of the absorption coefficient is changing the laser-mediated lesions, that is, for same laser doses the thermal damage may be different. That's why it is extremely important to find the optimal laser parameters for photothermal interactions. The handicap of the photothermal interactions with continuous wave laser is that the heat diffusion takes place during laser irradiation, which will cause a thermal damage to the surrounding healthy tissue depending on the efficiency of the process. Some of the energy will be used for vaporization of the tissue and the remaining energy will diffuse to the cooler regions of the tissue and cells will be damaged reversibly or irreversibly depending on the energy deposited in the tissue. Therefore real-time temperature monitoring can be an effective way to get rid of these negative effects of the temporal and spatial irregularities. But in this study we showed that rather than the temperature increase, the rate of temperature change is more important. We found that if the temperature is changing in a short time interval, the extent of thermal damage

can be minimized. In this study, we focused on brain tissue only, but we strongly believe that the outcomes of this study will give an insight to other photothermal laser ablation studies of soft tissues. We can conclude that when the same amount of energy is delivered to the tissue, the most important issue is that to give this amount of energy in a shorter time of interval regardless of mode of delivery (continuous or pulsed-modulated mode) to achieve more efficient ablations with less edema around the lesion.

This study is a comprehensive comparative research which has accomplished the following tasks: 1)The proposal of new thermoprobe for real-time temperature monitoring in dose determination studies. 2)Comparison of the ablative effects of infrared lasers on brain tissue in *ex vivo* studies. 3)Investigation of the use of infrared lasers in brain surgery. 4)Comparison of the thermal effects of different modes of operation (c-m and p-m-m) with Tm:fiber laser on cortical and subcortical tissue.

In conclusion, the result of this comparative study supported the hypothesis that the change in temperature in the tissue during laser irradiation even though the laser source is different in terms of wavelength, can be a good indicator for the characteristics of lesion created by the laser.

REFERENCES

1. Van Way, C. W., "Electrosurgery 101," *Current surgery*, Vol. 57, no. 2, pp. 172–177, 2000.
2. Tataroğlu, Ö., A. Aksoy, A. Yılmaz, and R. Canbeyli, "Effect of lesioning the suprachiasmatic nuclei on behavioral despair in rats," *Brain research*, Vol. 1001, no. 1, pp. 118–124, 2004.
3. Anzai, Y., R. Lufkin, A. DeSalles, D. R. Hamilton, K. Farahani, and K. L. Black, "Preliminary experience with MR-guided thermal ablation of brain tumors.," *American journal of neuroradiology*, Vol. 16, no. 1, pp. 39–48, 1995.
4. Devaux, B., and F. Roux, "Experimental and clinical standards, and evolution of lasers in neurosurgery," *Acta neurochirurgica*, Vol. 138, no. 10, pp. 1135–1147, 1996.
5. Krishnamurthy, S., and S. K. Powers, "Lasers in neurosurgery," *Lasers in surgery and medicine*, Vol. 15, no. 2, pp. 126–167, 1994.
6. Welch, A. J., and M. J. Van Gemert, *Optical-thermal response of laser-irradiated tissue*, Vol. 2, Springer, 2011.
7. Sliney, D. H., and S. L. Trokel, *Medical lasers and their safe use*, Springer Science & Business Media, 2012.
8. Baxter, C. D., and G. W. Waylonis, "Therapeutic lasers: Theory and practice.," *American Journal of Physical Medicine & Rehabilitation*, Vol. 74, no. 4, p. 327, 1995.
9. Downing, E. F., P. W. Ascher, L. J. Cerullo, C. R. Neblett, J. H. Robertson, and J. M. Tew, *Lasers in neurosurgery*, Springer, 1989.
10. Crone, K. R., "Lasers in neurosurgery," *Journal of Clinical Laser Medicine & Surgery*, Vol. 11, no. 4, pp. 199–199, 1993.
11. Robertson, J. H., and W. C. Clark, *Lasers in neurosurgery*, Vol. 1, Springer Science & Business Media, 2012.
12. Mahapatra, A., "Lasers in neurosurgery," *Textbooks of Operative Neurosurgery (2 Vol.)*, p. 93, 2005.
13. Philipp, C. M., and M. A. Trelles, "Lasers in surgery," *Photonics & Lasers in Medicine*, Vol. 4, no. 3, pp. 207–209, 2015.
14. Niemz, M. H., *Laser-tissue interactions: fundamentals and applications*, Springer Science & Business Media, 2013.
15. Goldman, L., *The biomedical laser: technology and clinical applications*, Springer Science & Business Media, 2013.
16. Steiner, R., "Laser-tissue interactions," in *Laser and IPL Technology in Dermatology and Aesthetic Medicine*, pp. 23–36, Springer, 2011.
17. Boulnois, J.-L., "Photophysical processes in recent medical laser developments: a review," *Lasers in Medical Science*, Vol. 1, no. 1, pp. 47–66, 1986.
18. Fillerup, D. L., and J. F. Mead, "The lipids of the aging human brain," *Lipids*, Vol. 2, no. 4, pp. 295–298, 1967.

19. McKenzie, A., "Physics of thermal processes in laser-tissue interaction," *Physics in medicine and biology*, Vol. 35, no. 9, p. 1175, 1990.

20. Prasad, P. N., *Introduction to biophotonics*, John Wiley & Sons, 2004.

21. Sajjadi, A. Y., K. Mitra, and Z. Guo, "Thermal analysis and experiments of laser-tissue interactions: A review," *Heat Transfer Research*, Vol. 44, no. 3-4, 2013.

22. D'Arcangelo, C., F. D. N. Di Maio, G. D. Prosperi, E. Conte, M. Baldi, and S. Caputi, "A preliminary study of healing of diode laser versus scalpel incisions in rat oral tissue: a comparison of clinical, histological, and immunohistochemical results," *Oral Surgery, Oral Medicine, Oral Pathology, Oral Radiology, and Endodontology*, Vol. 103, no. 6, pp. 764–773, 2007.

23. Fried, N. M., B. Choi, A. J. Welch, and J. T. Walsh Jr, "Radiometric surface temperature measurements during dye-assisted laser skin closure," *Lasers in surgery and medicine*, Vol. 25, pp. 291–303, 1999.

24. Fried, N. M., and J. T. Walsh Jr, "Cryogen spray cooling during laser tissue welding," *Physics in medicine and biology*, Vol. 45, no. 3, p. 753, 2000.

25. Ben-David, M., R. Cantor, N. Balbul, M. Yehuda, and I. Gannot, "Measuring tissue heat penetration by scattered light measurements," *Lasers in surgery and medicine*, Vol. 40, no. 7, pp. 494–499, 2008.

26. Yaroslavsky, A., P. Schulze, I. Yaroslavsky, R. Schober, F. Ulrich, and H. Schwarzmaier, "Optical properties of selected native and coagulated human brain tissues in vitro in the visible and near infrared spectral range," *Physics in medicine and biology*, Vol. 47, no. 12, p. 2059, 2002.

27. Stolik, S., J. Delgado, A. Perez, and L. Anasagasti, "Measurement of the penetration depths of red and near infrared light in human *ex vivo* tissues," *Journal of Photochemistry and Photobiology B: Biology*, Vol. 57, no. 2, pp. 90–93, 2000.

28. Pearce, J., and S. Thomsen, "Rate process analysis of thermal damage," in *Optical-thermal response of laser-irradiated tissue*, pp. 561–606, Springer, 1995.

29. Zhou, J., J. Chen, and Y. Zhang, "Theoretical analysis of thermal damage in biological tissues caused by laser irradiation," *Molecular and Cellular Biomechanics*, Vol. 4, no. 1, p. 27, 2007.

30. Gulsoy, M., Z. Dereli, H. O. Tabakoglu, and O. Bozkulak, "Closure of skin incisions by 980-nm diode laser welding," *Lasers in Medical Science*, Vol. 21, no. 1, pp. 5–10, 2006.

31. Goldman, L., R. G. Wilson, P. Hornby, and R. G. Meyer, "Radiation from a q-switched ruby laser," *Journal of Investigative Dermatology*, Vol. 44, no. 1, pp. 69–71, 1965.

32. Goldman, L., "Laser history and theory," in *Biomedical Aspects of the Laser*, pp. 1–8, Springer, 1967.

33. Goldman, L., and R. Dreffer, "Laser treatment of extensive mixed cavernous and port-wine stains," *Archives of dermatology*, Vol. 113, no. 4, pp. 504–505, 1977.

34. Koester, C., E. Snitzer, C. J. Campbell, and M. Rittler, "Experimental laser retina photocoagulation," *J Opt Soc Am*, Vol. 52, p. 607, 1962.

35. Campbell, C. J., C. J. Koester, V. Curtice, K. S. Noyori, and M. C. Rittler, "Clinical studies in laser photocoagulation," *Archives of Ophthalmology*, Vol. 74, no. 1, pp. 57–65, 1965.

36. Campbell, C. J., K. S. Noyori, M. C. Rittler, and C. J. Koester, "Intraocular temperature changes produced by laser coagulation," *Acta Ophthalmologica*, Vol. 41, no. S76, pp. 22–31, 1963.

37. Noyori, K. S., C. J. Campbell, C. Rittler, and C. J. Koester, "The characteristics of experimental laser coagulations of the retina," *Archives of Ophthalmology*, Vol. 72, no. 2, pp. 254–263, 1964.

38. Kangasniemi, M., R. J. McNichols, J. A. Bankson, A. Gowda, R. E. Price, and J. D. Hazle, "Thermal therapy of canine cerebral tumors using a 980 nm diode laser with mr temperature-sensitive imaging feedback," *Lasers in surgery and medicine*, Vol. 35, no. 1, pp. 41–50, 2004.

39. Wendt-Nordahl, G., S. Huckele, P. Honeck, P. Alken, T. Knoll, M. S. Michel, and A. Häcker, "980-nm diode laser: a novel laser technology for vaporization of the prostate," *European urology*, Vol. 52, no. 6, pp. 1723–1728, 2007.

40. Mordon, S., A. F. Eymard-Maurin, B. Wassmer, and J. Ringot, "Histologic evaluation of laser lipolysis: pulsed 1064-nm Nd:YAG laser versus cw 980-nm diode laser," *Aesthetic Surgery Journal*, Vol. 27, no. 3, pp. 263–268, 2007.

41. Bozkulak, O., H. O. Tabakoglu, A. Aksoy, O. Kurtkaya, A. Sav, R. Canbeyli, and M. Gulsoy, "The 980-nm diode laser for brain surgery: histopathology and recovery period," *Lasers in medical science*, Vol. 19, no. 1, pp. 41–47, 2004.

42. Gulsoy, M., T. Celikel, O. Kurtkaya, A. Sav, A. Kurt, R. Canbeyli, and I. Cilesiz, "Application of the 980-nm diode laser in stereotaxic surgery," *IEEE Journal of selected topics in Quantum Electronics*, Vol. 5, no. 4, pp. 1090–1094, 1999.

43. Romanos, G., and G.-H. Nentwig, "Diode laser (980 nm) in oral and maxillofacial surgical procedures: clinical observations based on clinical applications," *Journal of clinical laser medicine & surgery*, Vol. 17, no. 5, pp. 193–197, 1999.

44. Genovese, W. J., M. T. B. R. dos Santos, F. Faloppa, and L. A. de Souza Merli, "The use of surgical diode laser in oral hemangioma: a case report," *Photomedicine and laser surgery*, Vol. 28, no. 1, pp. 147–151, 2010.

45. Convissar, R. A., *Principles and practice of laser dentistry*, Elsevier Health Sciences, 2015.

46. Elanchezhiyan, S., R. Renukadevi, and K. Vennila, "Comparison of diode laser-assisted surgery and conventional surgery in the management of hereditary ankyloglossia in siblings: a case report with scientific review," *Lasers in medical science*, Vol. 28, no. 1, pp. 7–12, 2013.

47. Beer, F., W. Körpert, H. Passow, A. Steidler, A. Meinl, A. Buchmair, and A. Moritz, "Reduction of collateral thermal impact of diode laser irradiation on soft tissue due to modified application parameters," *Lasers in medical science*, Vol. 27, no. 5, pp. 917–921, 2012.

48. Prescher, A., R. Poprawe, S. Gaus, S. Stanzel, N. Pallua, *et al.*, "Ablative targeting of fatty-tissue using a high-powered diode laser," *Lasers in surgery and medicine*, Vol. 40, no. 2, pp. 100–105, 2008.

49. Green, J., and J. Kaufman, "Long-pulsed 1,064 nm Nd:YAG lasers effective in vein, pws, other treatments," 2012.

50. Anderson, R. R., R. J. Margolis, S. Watenabe, T. Flotte, G. J. Hruza, and J. S. Dover, "Selective photothermolysis of cutaneous pigmentation by q-switched Nd:YAG laser pulses at 1064, 532. and 355nm," *Journal of Investigative Dermatology*, Vol. 93, no. 1, pp. 28–32, 1981.

51. Kilmer, S. L., M. S. Lee, J. M. Grevelink, T. J. Flotte, and R. R. Anderson, "The q-switched Nd:YAG laser effectively treats tattoos: a controlled, dose-response study," *Archives of dermatology*, Vol. 129, no. 8, pp. 971–978, 1993.

52. Latina, M. A., and C. Park, "Selective targeting of trabecular meshwork cells: in vitro studies of pulsed and cw laser interactions," *Experimental eye research*, Vol. 60, no. 4, pp. 359–371, 1995.

53. Kim, J. H., H. Kim, H. C. Park, and I.-H. Kim, "Subcellular selective photothermolysis of melanosomes in adult zebrafish skin following 1064-nm q-switched Nd:YAG laser irradiation," *Journal of Investigative Dermatology*, Vol. 130, no. 9, pp. 2333–2335, 2010.

54. Landthaler, M., D. Haina, R. Brunner, W. Waidelich, and O. Braun-Falco, "Neodymium-yag laser therapy for vascular lesions," *Journal of the American Academy of Dermatology*, Vol. 14, no. 1, pp. 107–117, 1986.

55. Rosenfeld, H., and R. Sherman, "Treatment of cutaneous and deep vascular lesions with the Nd:YAG laser," *Lasers in surgery and medicine*, Vol. 6, no. 1, pp. 20–23, 1986.

56. Rox Anderson, R., R. J. Margolis, S. Watenabe, T. J. Flotte, G. J. Hruza, and J. S. Dover, "Selective photothermolysis of cutaneous pigmentation by q-switched Nd: YAG Laser Pulses at 1064, 532. and 355 nm" *Journal of Investigative Dermatology*, Vol. 93, no. 1, pp. 28–32, 1989.

57. Tse, Y., V. J. Levine, S. A. McClain, and R. Ashinoff, "The removal of cutaneous pigmented lesions with the q-switched ruby laser and the q-switched neodymium: Yttrium-aluminum-garnet laser," *The Journal of dermatologic surgery and oncology*, Vol. 20, no. 12, pp. 795–800, 1994.

58. Goldberg, D. J., "Laser treatment of pigmented lesions," *Dermatologic clinics*, Vol. 15, no. 3, pp. 397–407, 1997.

59. Weiss, R. A., and M. A. Weiss, "Early clinical results with a multiple synchronized pulse 1064 nm laser for leg telangiectasias and reticular veins," *Dermatologic surgery*, Vol. 25, no. 5, pp. 399–402, 1999.

60. Yang, M. U., A. N. Yaroslavsky, W. A. Farinelli, T. J. Flotte, F. Rius-Diaz, S. S. Tsao, and R. R. Anderson, "Long-pulsed neodymium: yttrium-aluminum-garnet laser treatment for port-wine stains," *Journal of the American Academy of Dermatology*, Vol. 52, no. 3, pp. 480–490, 2005.

61. Bencini, P. L., A. Luci, M. Galimberti, and G. Ferranti, "Long-term epilation with long-pulsed neodimium: YAG laser," *Dermatologic surgery*, Vol. 25, no. 3, pp. 175–178, 1999.

62. Fournier, N., N. Aghajan-Nouri, G. Barneon, and S. Mordon, "Hair removal with an athos Nd:YAG 3.5 ms pulse laser: a 3-month clinical study," *Journal of cutaneous laser therapy*, Vol. 2, no. 3, pp. 125–130, 2000.

63. Alster, T. S., H. Bryan, and C. M. Williams, "Long-pulsed Nd: YAG laser-assisted hair removal in pigmented skin: a clinical and histological evaluation," *Archives of dermatology*, Vol. 137, no. 7, pp. 885–889, 2001.

64. Tanzi, E. L., and T. S. Alster, "Long-pulsed 1064-nm Nd:YAG laser-assisted hair removal in all skin types," *Dermatologic surgery*, Vol. 30, no. 1, pp. 13–17, 2004.

65. Kilmer, S. L., and R. Anderson, "Clinical use of the q-switched ruby and the q-switched nd: Yag (1064 nm and 532 nm) lasers for treatment of tattoos," *The Journal of dermatologic surgery and oncology*, Vol. 19, no. 4, pp. 330–338, 1993.

66. Jones, A., P. Roddey, I. Orengo, and T. Rosen, "The q-switched Nd:YAG laser effectively treats tattoos in darkly pigmented skin," *Dermatologic surgery*, Vol. 22, no. 12, pp. 999–1001, 1996.

67. Goldberg, D. J., and S. Silapunt, "Histologic evaluation of a q-switched Nd:YAG laser in the nonablative treatment of wrinkles," *Dermatologic surgery*, Vol. 27, no. 8, pp. 744–746, 2001.

68. Trelles, M., X. Alvarez, M. Martin-Vazquez, O. Trelles, M. Velez, J. Levy, and I. Allones, "Assessment of the efficacy of nonablative long-pulsed 1064-nm Nd:YAG laser treatment of wrinkles compared at 2, 4, and 6 months," *Facial plastic surgery*, Vol. 21, no. 02, pp. 145–153, 2005.

69. Hong, J. S., S. Y. Park, K. K. Seo, B. L. Goo, E. J. Hwang, G. Y. Park, and H. C. Eun, "Long pulsed 1064 nm Nd:YAG laser treatment for wrinkle reduction and skin laxity: evaluation of new parameters," *International journal of dermatology*, Vol. 54, no. 9, pp. e345–e350, 2015.

70. White, J. M., H. E. Goodis, and C. L. Rose, "Use of the pulsed Nd:YAG laser for intraoral soft tissue surgery," *Lasers in surgery and medicine*, Vol. 11, no. 5, pp. 455–461, 1991.

71. Powell, J. L., C. L. Bailey, A. T. Coopland, C. N. Otis, J. L. Frank, and I. Meyer, "Nd:YAG laser excision of a giant gingival pyogenic granuloma of pregnancy," *Lasers in surgery and medicine*, Vol. 14, no. 2, pp. 178–183, 1994.

72. Bradley, P. F., "A review of the use of the neodymium YAG laser in oral and maxillofacial surgery," *British Journal of Oral and Maxillofacial Surgery*, Vol. 35, no. 1, pp. 26–35, 1997.

73. Costello, A., W. Bowsher, D. Bolton, K. Braslis, and J. Burt, "Laser ablation of the prostate in patients with benign prostatic hypertrophy," *British journal of urology*, Vol. 69, no. 6, pp. 603–608, 1992.

74. Costello, A. J., D. E. Johnson, and D. M. Bolton, "Nd:YAG laser ablation of the prostate as a treatment for benign prostatic hypertrophy," *Lasers in surgery and medicine*, Vol. 12, no. 2, pp. 121–124, 1992.

75. Fried, N. M., and K. E. Murray, "High-power thulium fiber laser ablation of urinary tissues at 1.94 μm," *Journal of endourology*, Vol. 19, no. 1, pp. 25–31, 2005.

76. Keller, M. D., J. A. Stafford, B. P. Schmidt, and J. D. Wells, "*In vitro* testing of dual-mode thulium microsurgical laser," in *SPIE BiOS*, pp. 820711–820711, International Society for Optics and Photonics, 2012.

77. Sroka, R., T. Pongratz, M. Havel, E. Englert, T. Kremser, C. S. Betz, and A. Leunig, "Comparison of 1470nm diode laser vs. $C0_2$-laser for tonsillotomy and a clinical feasability trial on the use of 1940nm in ent," in *SPIE BiOS*, pp. 85652O–85652O, International Society for Optics and Photonics, 2013.

78. Kang, H. W., J. Kim, and J. Oh, "Effect of wavelength on laser-assisted surgical techniques," *Optics and Lasers in Engineering*, Vol. 51, no. 2, pp. 104–110, 2013.

79. Khoury, J. G., R. Saluja, D. Keel, S. Detwiler, and M. P. Goldman, "Histologic evaluation of interstitial lipolysis comparing a 1064, 1320 and 2100 nm laser in an *ex vivo* model," *Lasers in surgery and medicine*, Vol. 40, no. 6, pp. 402–406, 2008.

80. Abelow, S. P., "Use of lasers in orthopedic surgery: current concepts," *Orthopedics*, Vol. 16, no. 5, pp. 551–556, 1993.

81. Anderson, R. R., W. Farinelli, H. Laubach, D. Manstein, A. N. Yaroslavsky, J. Gubeli, K. Jordan, G. R. Neil, M. Shinn, W. Chandler, *et al.*, "Selective photothermolysis of lipid-rich tissues: a free electron laser study," *Lasers in surgery and medicine*, Vol. 38, no. 10, p. 913, 2006.

82. Bach, T., G. Wendt-Nordahl, M. Michel, T. Herrmann, and A. Gross, "Feasibility and efficacy of thulium:YAG laser enucleation (vapoenucleation) of the prostate," *World journal of urology*, Vol. 27, no. 4, pp. 541–545, 2009.

83. El-Sherif, A., and T. King, "Soft and hard tissue ablation with short-pulse high peak power and continuous thulium-silica fibre lasers," *Lasers in medical science*, Vol. 18, no. 3, pp. 139–147, 2003.

84. Minaev, V. P., "Laser apparatus for surgery and force therapy based on high-power semiconductor and fibre lasers," *Quantum Electronics*, Vol. 35, no. 11, p. 976, 2005.

85. Wendt-Nordahl, G., S. Huckele, P. Honeck, P. Alken, T. Knoll, M. S. Michel, and A. Häcker, "Systematic evaluation of a recently introduced 2-μm continuous-wave thulium laser for vaporesection of the prostate," *Journal of Endourology*, Vol. 22, no. 5, pp. 1041–1046, 2008.

86. Chen, W. R., K. E. Bartels, H. Liu, and R. E. Nordquist, "Laser-photothermal effect on skin tissue–damage and recovery," *Journal of X-Ray Science and Technology*, Vol. 14, no. 3, pp. 207–215, 2006.

87. Saccomandi, P., E. Schena, and S. Silvestri, "Techniques for temperature monitoring during laser-induced thermotherapy: An overview," *International Journal of Hyperthermia*, Vol. 29, no. 7, pp. 609–619, 2013.

88. Manns, F., P. J. Milne, X. Gonzalez-Cirre, D. B. Denham, J.-M. Parel, and D. S. Robinson, "In situ temperature measurements with thermocouple probes during laser interstitial thermotherapy (litt): quantification and correction of a measurement artifact," *Lasers in surgery and medicine*, Vol. 23, no. 2, pp. 94–103, 1998.

89. Anvari, B., M. Motamedi, J. H. Torres, S. Rastegar, and E. Orihuela, "Effects of surface irrigation on the thermal response of tissue during laser irradiation," *Lasers in surgery and medicine*, Vol. 14, no. 4, pp. 386–395, 1994.

90. Tunc, B., and M. Gulsoy, "Tm:Fiber laser ablation with real-time temperature monitoring for minimizing collateral thermal damage: *ex vivo* dosimetry for ovine brain," *Lasers in surgery and medicine*, Vol. 45, no. 1, pp. 48–56, 2013.

91. Agha, H. Z., and M. Gülsoy, "Photothermal ablation of liver tissue with 1940-nm thulium fiber laser: an *ex vivo* study on lamb liver," *Journal of biomedical optics*, Vol. 21, no. 1, pp. 015007–015007, 2016.

92. Launay, Y., S. Mordon, A. Cornil, J. Brunetaud, and Y. Moschetto, "Thermal effects of lasers on dental tissues," *Lasers in Surgery and Medicine*, Vol. 7, no. 6, pp. 473–477, 1987.

93. Torres, J. H., T. A. Springer, A. J. Welch, and J. A. Pearce, "Limitations of a thermal camera in measuring surface temperature of laser-irradiated tissues," *Lasers in surgery and medicine*, Vol. 10, no. 6, pp. 510–523, 1990.

94. Cilesiz, I., "Controlled temperature photothermal tissue welding," *Journal of Biomedical Optics*, Vol. 4, pp. 327–336, 1999.

95. Shenfeld, O., E. Ophir, B. Goldwasser, and A. Katzir, "Silver halide fiber optic radiometric temperature measurement and control of CO_2 laser-irradiated tissues and application to tissue welding," *Lasers in surgery and medicine*, Vol. 14, no. 4, pp. 323–328, 1994.

96. Lobel, B., O. Eyal, N. Kariv, and A. Katzir, "Temperature controlled CO_2 laser welding of soft tissues: Urinary bladder welding in different animal models (rats, rabbits, and cats)," *Lasers in surgery and medicine*, Vol. 26, no. 1, pp. 4–12, 2000.

97. Ishihara, M., T. Arai, S. Sato, Y. Morimoto, M. Obara, and M. Kikuchi, "Measurement of the surface temperature of the cornea during arf excimer laser ablation by thermal radiometry with a 15-nanosecond time response," *Lasers in surgery and medicine*, Vol. 30, no. 1, pp. 54–59, 2002.

98. Dibaji, S. A. R., J. Wansapura, M. R. Myers, and R. K. Banerjee, "*In vivo* monitoring of hifu induced temperature rise in porcine liver using magnetic resonance thermometry," *Journal of Medical Devices*, Vol. 8, no. 3, p. 030937, 2014.

99. Quesson, B., C. Laurent, G. Maclair, B. D. de Senneville, C. Mougenot, M. Ries, T. Carteret, A. Rullier, and C. T. Moonen, "Real-time volumetric mri thermometry of focused ultrasound ablation in vivo: a feasibility study in pig liver and kidney," *NMR in biomedicine*, Vol. 24, no. 2, pp. 145–153, 2011.

100. McNichols, R. J., A. Gowda, M. Kangasniemi, J. A. Bankson, R. E. Price, and J. D. Hazle, "Mr thermometry-based feedback control of laser interstitial thermal therapy at 980 nm," *Lasers in surgery and medicine*, Vol. 34, no. 1, pp. 48–55, 2004.

101. Carpentier, A., R. J. McNichols, R. J. Stafford, J.-P. Guichard, D. Reizine, S. Delaloge, E. Vicaut, D. Payen, A. Gowda, and B. George, "Laser thermal therapy: Real-time MRI-guided and computer-controlled procedures for metastatic brain tumors," *Lasers in surgery and medicine*, Vol. 43, no. 10, pp. 943–950, 2011.

102. Carpentier, A., J. Itzcovitz, D. Payen, B. George, R. J. McNichols, A. Gowda, R. J. Stafford, J.-P. Guichard, D. Reizine, S. Delaloge, *et al.*, "Real-time magnetic resonance-guided laser thermal therapy for focal metastatic brain tumors," *Neurosurgery*, Vol. 63, no. 1, pp. ONS21–ONS29, 2008.

103. Chen, L., J. P. Wansapura, G. Heit, and K. Butts, "Study of laser ablation in the *in vivo* rabbit brain with mr thermometry," *Journal of Magnetic Resonance Imaging*, Vol. 16, no. 2, pp. 147–152, 2002.

104. Breen, M. S., M. Breen, K. Butts, L. Chen, G. M. Saidel, and D. L. Wilson, "MRI-guided thermal ablation therapy: Model and parameter estimates to predict cell death from mr thermometry images," *Annals of biomedical engineering*, Vol. 35, no. 8, pp. 1391–1403, 2007.

105. Kateb, B., V. Yamamoto, C. Yu, W. Grundfest, and J. P. Gruen, "Infrared thermal imaging: a review of the literature and case report," *Neuroimage*, Vol. 47, pp. T154–T162, 2009.

106. Noguchi, M., E. Aoki, D. Yoshida, E. Kobayashi, S. Omori, Y. Muragaki, H. Iseki, K. Nakamura, and I. Sakuma, "A novel robotic laser ablation system for precision neurosurgery with intraoperative 5-ala-induced ppix fluorescence detection," in *International Conference on Medical Image Computing and Computer-Assisted Intervention*, pp. 543–550, Springer, 2006.

107. Liao, H., K. Shimaya, K. Wang, T. Maruyama, M. Noguchi, Y. Muragaki, E. Kobayashi, H. Iseki, and I. Sakuma, "Combination of intraoperative 5-aminolevulinic acid-induced fluorescence and 3-d mr imaging for guidance of robotic laser ablation for precision neurosurgery," in *International Conference on Medical Image Computing and Computer-Assisted Intervention*, pp. 373–380, Springer, 2008.

108. Earle, K., S. Carpenter, U. Roessmann, M. Ross, J. Hayes, and E. Zeitler, "Central nervous system effects of laser radiation.," in *Federation proceedings*, Vol. 24, pp. SUPPL–14, 1965.

109. Fine, S., E. Klein, W. Nowak, R. Scott, Y. Laor, L. Simpson, J. Crissey, J. Donoghue, and V. Derr, "Interaction of laser radiation with biologic systems. i. studies on interaction with tissues," in *Federation proceedings*, Vol. 24, pp. SUPPL–14, Federation of American Societies for Experimental Biology, 1965.

110. Fox, J., J. Hayes, M. Stein, and R. Green, "Effects of laser radiation on intracranial structures.," tech. rep., Veterans Administration Hospital, Washington, DC, 1967.

111. Fox, J. L., "The use of laser radiation as a surgical "light knife"," *Journal of Surgical Research*, Vol. 9, no. 4, pp. 199–205, 1969.

112. Fox, J. L., J. R. Hayes, M. N. Stein, R. C. Green, and R. Paananen, "Experimental cranial and vascular studies of the effects of pulsed and continuous wave laser radiation*," *Journal of Neurosurgery*, Vol. 27, no. 2, pp. 126–137, 1967.

113. Fox, J., M. Stein, J. Hayes, and R. Green, "Effects of laser irradiation on the central nervous system. ii. the intracranial explosion.," *Journal of Neurology, Neurosurgery & Psychiatry*, Vol. 31, no. 1, pp. 43–49, 1968.

114. Liss, L., and R. Roppel, "Histopathology of laser-produced lesions in cat brains.," tech. rep., Ohio State Univ., Columbus, 1966.

115. Rosomoff, H., and F. Carroll, "Effect of laser on brain and neoplasm.," in *Surgical forum*, Vol. 16, p. 431, 1965.

116. Brown, T. E., C. True, R. L. McLaurin, P. Hornby, and R. J. Rockwell, "Laser radiation acute effects on cerebral cortex," *Neurology*, Vol. 16, no. 8, pp. 730–730, 1966.

117. Brown, T. E., C. True, R. L. McLaurin, R. Rockwell Jr, and P. Hornby, "Laser radiation. ii. long-term effects of radiation on certain intracranial structures.," tech. rep., Children's Hospital Research Foundation, Cincinnati, 1967.

118. Patel, C. K. N., "Continuous-wave laser action on vibrational-rotational transitions of CO_2," *Physical review*, Vol. 136, no. 5A, p. A1187, 1964.

119. Stellar, S., T. Polanyi, and H. Bredemeier, "Experimental studies with the carbon dioxide laser as a neurosurgical instrument," *Medical and biological engineering*, Vol. 8, no. 6, pp. 549–558, 1970.

120. Stellar, S., T. G. Polanyi, and H. C. Bredemeier, "Lasers in surgery," in *Laser applications in medicine and biology*, pp. 241–293, Springer, 1974.

121. Polanyi, T. G., H. Bredemeier, and T. Davis Jr, "A CO_2 laser for surgical research," *Medical and biological engineering*, Vol. 8, no. 6, pp. 541–548, 1970.

122. Ascher, P. W., and F. Heppner, "CO_2-laser in neurosurgery," *Neurosurgical review*, Vol. 7, no. 2-3, pp. 123–133, 1984.

123. Heppner, F., "The laser scalpel in the nervous system" *Wiener medizinische Wochenschrift (1946)*, Vol. 128, no. 7, pp. 198–201, 1978.

124. Ascher, P., "Use of CO_2-laser in neurosurgery," in *Acta Neurochirurgica*, Vol. 84, pp. 140–140, Springer-Verlag Wien Sachsenplatz 4-6, PO BOX 89, A-1201 Vienna, Austria, 1987.

125. Andrews, A. H., and T. G. Polanyi, *Microscopic and endoscopic surgery with the CO_2 laser*, Butterworth-Heinemann, 1982.

126. Takizawa, T., T. Yamazaki, N. Miura, M. Matsumoto, Y. Tanaka, K. Takeuchi, Y. Nakata, O. Togashi, M. Nagai, T. Ariga, *et al.*, "Laser surgery of basal, orbital and ventricular meningiomas which are difficult to extirpate by conventional methods," *Neurologia medico-chirurgica*, Vol. 20, no. 7, pp. 729–737, 1980.

127. Ascher, P., and L. Cerullo, "Chapter 9: Laser use in neurosurgery," *Surgical Applications of Lasers*, pp. 163–174, 1983.

128. Strait, T. A., J. H. Robertson, and C. W. Clark, "Use of the carbon dioxide laser in the operative management of intracranial meningiomas: a report of twenty cases.," *Neurosurgery*, Vol. 10, no. 4, pp. 464–467, 1982.

129. Gropper, G. R., J. H. Robertson, and G. McClellan, "Comparative histological and radiographic effects of CO_2 laser versus standard surgical anterior cervical discectomy in the dog.," *Neurosurgery*, Vol. 14, no. 1, pp. 42–47, 1984.

130. Robertson, J. H., C. W. Clark, J. T. Robertson, G. L. Gardner, and C. M. Shea, "Use of the carbon dioxide laser for acoustic tumor surgery.," *Neurosurgery*, Vol. 12, no. 3, pp. 286–290, 1983.

131. Robertson, J., "Carbon-dioxide laser in neurosurgery," in *Neurosurgery*, Vol. 10, pp. 780–780, 1982.

132. Welch, A., M. Motamedi, S. Rastegar, G. L. LeCarpentier, and D. Jansen, "Laser thermal ablation," *Photochemistry and photobiology*, Vol. 53, no. 6, pp. 815–823, 1991.

133. Peavy, G. M., "Lasers and laser–tissue interaction," *Veterinary Clinics of North America: Small Animal Practice*, Vol. 32, no. 3, pp. 517–534, 2002.

134. Wieliczka, D. M., S. Weng, and M. R. Querry, "Wedge shaped cell for highly absorbent liquids: infrared optical constants of water," *Applied optics*, Vol. 28, no. 9, pp. 1714–1719, 1989.

135. Cubeddu, R., C. Sozzi, P. Taroni, G. Valentini, G. Bottiroli, and A. Croce, "Study of mechanical and thermal damage in brain tissue after ablation by erbium-YAG laser," *Lasers in Medical Science*, Vol. 12, no. 1, pp. 21–30, 1997.

136. Gülsoy, M., T. Celikel, A. Kurt, R. Canbeyli, and I. Cilesiz, "Er:YAG laser ablation of cerebellar and cerebral tissue," *Lasers in medical science*, Vol. 16, no. 1, pp. 40–43, 2001.

137. Takizawa, T., "The carbon dioxide laser surgical unit as an instrument for surgery of brain tumours—its advantages and disadvantages," *Neurosurgical review*, Vol. 7, no. 2-3, pp. 135–144, 1984.

138. Nishioka, N. S., and Y. Domankevitz, "Comparison of tissue ablation with pulsed holmium and thulium lasers," *IEEE journal of quantum electronics*, Vol. 26, no. 12, pp. 2271–2275, 1990.

139. Paxinos, G., and C. Watson "The rat brain in stereotaxic coordinates," *Academic, San Diego*, 2007.

140. Popov, S., "Fiber laser overview and medical applications," *Tunable laser applications*, pp. 197–226, 2009.

141. McKenzie, A. L., "A three-zone model of soft-tissue damage by a CO_2 laser," *Physics in medicine and biology*, Vol. 31, no. 9, p. 967, 1986.

142. Sagi-Dolev, A., A. Shitzer, A. Katzir, and S. Akselrod, "Heating of biological tissue by laser irradiation: theoretical model," *Optical engineering*, Vol. 31, no. 7, pp. 1417–1424, 1992.

143. Gijsbers, G. H., F. M. Selten, and M. J. van Gemert, "Cw laser ablation velocities as a function of absorption in an experimental one-dimensional tissue model," *Lasers in surgery and medicine*, Vol. 11, no. 3, pp. 287–296, 1991.

144. Wharen Jr, R. E., R. E. Anderson, B. Scheithauer, and T. M. Sundt Jr, "The Nd:YAG laser in neurosurgery: Part 1. laboratory investigations: dose-related biological response of neural tissue," *Journal of neurosurgery*, Vol. 60, no. 3, pp. 531–539, 1984.

145. Beck, O., "The use of the Nd:YAG and the CO_2 laser in neurosurgery," *Neurosurgical review*, Vol. 3, no. 4, pp. 261–266, 1980.

146. Burke, L., R. Rovin, L. Cerullo, and J. Brown, "Thermal effects of the Nd:YAG and carbon dioxide lasers on the central nervous system," *Lasers in surgery and medicine*, Vol. 5, no. 1, pp. 67–71, 1985.

147. Svennerholm, L., and M. T. Vanier, "The distribution of lipids in the human nervous system. ii. lipid composition of human fetal and infant brain," *Brain research*, Vol. 47, no. 2, pp. 457–468, 1972.

148. O'Brien, J. S., and E. L. Sampson, "Lipid composition of the normal human brain: gray matter, white matter, and myelin," *Journal of lipid research*, Vol. 6, no. 4, pp. 537–544, 1965.

149. Bilici, T., S. Mutlu, H. Kalaycioglu, A. Kurt, A. Sennaroglu, and M. Gulsoy, "Development of a thulium (Tm:YAP) laser system for brain tissue ablation," *Lasers in medical science*, Vol. 26, no. 5, pp. 699–706, 2011.

150. Jansen, E. D., T. G. van Leeuwen, M. Motamedi, C. Borst, and A. J. Welch, "Temperature dependence of the absorption coefficient of water for midinfrared laser radiation," *Lasers in surgery and medicine*, Vol. 14, no. 3, pp. 258–268, 1994.

151. Lange, B. I., T. Brendel, and G. Hüttmann, "Temperature dependence of light absorption in water at holmium and thulium laser wavelengths," *Applied optics*, Vol. 41, no. 27, pp. 5797–5803, 2002.

152. Spells, K., "The thermal conductivities of some biological fluids," *Physics in Medicine and Biology*, Vol. 5, no. 2, p. 139, 1960.

153. Cooper, T., and G. Trezek, "Correlation of thermal properties of some human tissue with water content," *Aerospace medicine*, Vol. 42, no. 1, pp. 24–27, 1971.

154. Guney, M., B. Tunc, and M. Gulsoy, "Investigating the ablation efficiency of a 1940-nm thulium fibre laser for intraoral surgery," *International journal of oral and maxillofacial surgery*, Vol. 43, no. 8, pp. 1015–1021, 2014.

155. Merigo, E., F. Clini, C. Fornaini, A. Oppici, C. Paties, A. Zangrandi, M. Fontana, J.-P. Rocca, M. Meleti, M. Manfredi, *et al.*, "Laser-assisted surgery with different wavelengths: a preliminary ex vivo study on thermal increase and histological evaluation," *Lasers in medical science*, Vol. 28, no. 2, pp. 497–504, 2013.

156. Youn, J.-I., and J. D. Holcomb, "Ablation efficiency and relative thermal confinement measurements using wavelengths 1,064, 1,320, and 1,444 nm for laser-assisted lipolysis," *Lasers in medical science*, Vol. 28, no. 2, pp. 519–527, 2013.

157. Ritz, J.-P., A. Roggan, C. Isbert, G. Müller, H. J. Buhr, and C.-T. Germer, "Optical properties of native and coagulated porcine liver tissue between 400 and 2400 nm," *Lasers in surgery and medicine*, Vol. 29, no. 3, pp. 205–212, 2001.